Nanofabrication and its Effect on Electrical and Optical Properties of Gallium Nitride

Bifeng Rong ME

A thesis presented for the degree of Doctor of Philosophy
In
Electrical and Electronic Engineering
At the
University of Canterbury
Christchurch, New Zealand
December 2001

Abstract

GaN and related materials keep drawing attention because of their successful application in light emitter diodes (LEDs) and laser diodes (LDs) and their high potential application in high power and high temperature electric devices. Lots of efforts have been devoted to dry etching of GaN due to ongoing device size minimization and chemical inertness of the material. The first goal of this research is to develop a procedure for fabricating GaN patterns in the nanometer scale. To achieve this goal, the dose of electron beam lithography and plasma parameters have been varied. The effort has concentrated on obtaining the fine patterns with steep sidewall and smooth etched surface for the device applications. Scanning electron microscopy has been used to inspect the pattern profile and atomic force microscopy has been employed to monitor the surface roughness. Nano-wires and dots have been fabricated in gallium nitride using electron beam lithography and reactive ion etching (RIE). The developed nanofabrication procedure has been successfully implemented in nano-dots fabrication in Si/Si_xN_y superlattice.

High density plasma (HDP) has been recommended for etching GaN, because of high reactive species and ion density, predominately controllable ion energy and easier scale-up for production (inductively coupled plasma (ICP)). Thus, study ICP for etching GaN has become the second goal. A Langmuir probe has been used to quantify the amount of ion bombardment during plasma etching by measuring the ion flux, while optical emission spectroscopy has been employed to monitor atomic F radical. ICP etching of GaN is highly ion induced. The etch condition has been optimised, resulting in an almost vertical pattern profile and a etch rate of 67nm/min. This is about 5 times more of that obtained in RIE by using the same gas composition (SF_6+N_2). To achieve higher etch rate, ICP chlorine plasma etching of

GaN has been investigated. The fastest etch rate of 314nm/min has been obtained with good vertical nature of pattern profile.

However dry etch induced damage may affect material properties and deteriorate device quality. Thus, the study of dry etch-induced damage effects at the microscopic scale and optimisation of the etch conditions to obtain fast etch rate, smooth surface morphology, anisotropic profile and minimal etch damage is the final goal of this project. We achieved this goal by correlating the plasma characteristics to etch behaviour, diodes properties to photoluminescence (PL) properties for studying the top surface damage, and quantum device conductivity for the sidewall damage.

Our data show that $SF_6 + N_2$ ICP plasma with high ion energy improves diodes properties with reasonable etch rate, almost vertical profile and smooth surface morphology. However, it reduces PL D^oX intensity dramatically. While, $25\%Cl_2 + 75\%Ar$ ICP plasma produces a fast etch rate and does not reduce the PL intensity significantly. However, it deteriorates the diodes properties. These results suggest that a $SF_6 + N_2$ (1:1) plasma with high ion energy should be appropriate for GaN transistor gate recessing, subjecting to mobility investigation. A 75% Ar + 25% Cl_2 plasma is suitable for the fabrication of optical devices, such as light emitting diodes and laser diodes. The preliminary result of quantum wire devices shows that sidewall depletion in quantum wire structures is about 65 nm at the given $SF_6 + N_2$ plasma conditions. This gives an indication that length scale of the depth of defects introduced by etching is about 52 nm in our GaN. However, the defects may propagate deeper.

Preface

This dissertation describes research undertaken at the Electrical and Electronic Engineering and Physics and Astronomy Department of Canterbury University, New Zealand and Delft Institute of Microelectronics and Submicron-technology (DIMES), Technical University of Delft (TUD), Netherlands from March 1999 to December 2001. I am grateful to my original supervisor Dr Rebecca Cheung for the topic of research and consistent supervision after her leave. She had come to DIMES to discuss work for three times during I worked there. I am very glad of having Dr E. van der Drift, Dr M. M. Alkaisi, Dr R. J. Reeves (alphabetically ordered) as supervisors for sharing me their valuable knowledge with me.

I have enjoyed working on this wide topic, from nano wire and dots to device fabrication, from electrical to optical characterization.

This dissertation is the result of my original work and includes nothing that is the work done in collaboration, except where specifically acknowledged. This dissertation has not been submitted in whole, or in part for any degree, diploma, or other qualification at any other university.

Aspects of the work described in this dissertation are going to be published and have been published as following:

1) B. Rong, E. van der Drift, M. A. Blauw, R. J. Reeves, M. M. Alkaisi and R.Cheung *"ICP chlorine plasma etching of GaN and etch induced damage characterization"* draft made for submitting to J. Appl. Phys.

2) B. Rong, E. van der Drift, R. J. Reeves and R. Cheung "*Dry etching of GaN and etch-induced damage in an inductively coupled plasma*" J. Vac. Sci. Technol. B Nov./Dec. 2001

3) B. Rong, R. J. Reeves, S. A. Brown, M. M. Alkaisi, E. van der Drift and R. Cheung "*A study of Reactive ion Etching Effects on Optical properties in GaN*" Microelectron. Eng. Vol. 57-58, 2001, pp 585-591

4) B. Rong, R. Cheung, W. Gao, M. M. Alkaisi and R. J. Reeves '*Effects of Reactive Ion Etch-Induced Damage on the Electrical Characteristics in GaN*' J. Vac. Sci. Technol. B 18, 2000, pp 3467-3470

5) B. Rong, R. Cheung, W. Gao and M. kamp '*Fabrication of Nanostructures in GaN*' Microelectron. Eng. 53(1-4), 2000, 419-422

6) R. Cheung, R. J. Reeves, B. Rong, S A Brown, E J M Fakkeldij, E van der Drift and M Kamp; *High resolution reactive ion etching of GaN and etch-induced effects*" J. Vac. Sci. Tech. B 17, 1999, pp 2759-2763

7) R. J. Reeves, O Dickie, B. Rong, R Cheung, and S A Brown, '*Photoluminescence and Photoconductivity Studies of Reactive-Ion-Etched GaN on SiC Substrates*' Proc. of the International Workshop on Nitride Semiconductors (IWN2000), at Nagoya, Japan, September 2000, (IPAP) CS1, pp 774-777

8) S. A. Brown, R J Reeves, B. Rong, R. Cheung, M. Seyboth, C. Kirchner and M. Kamp, '*Argon plasma etching of gallium nitride: spectroscopic surprises*', Nanotechnology, 11, 2000, pp 363-269

9) R. Cheung, B. Rong, W. Gao and M. kamp '*Nanostructure pattern transfer in GaN by Reactive Ion Etching*' Presented at Electron New Zealand, national conference proceeding in Auckland, New Zealand, 1999.

Acknowledgement

First of all, I want to express my sincere gratitude to my original supervisor Dr Rebecca Cheung of EEE Department, Edinburgh University, United Kingdom, who supervised the main line work, suggested the topic of this research and guide through the thesis. Special thanks to Dr Emile van de Drift of DIMES, TUD, Netherlands. I have been there for 10 months doing research, and learned a lot from his knowledgeable and strict supervision and had a very pleasant time due to his kindness. I appreciate of their highlighting the positive and leading me through.

Many thanks to Dr Roger J. Reeves for supervision of optical characterization part, reading through the first draft of the thesis and lots of valuable comments. Many thanks to Dr Maan. M. Alkaisi, who became my supervisor after Rebecca moved to Edinburgh. He reminded me to record all experimental detail for thesis writing in advance, and gave good suggestions for thesis structure and valuable comments on writing. Also thanks to Dr Richard. J. Blaikie for his kind helps and training to use HP 4155 and Dr Simon A. Brown for discussion on photoluminescence and photoconductivity of GaN.

I would like to say great thanks to my colleagues in DIMES, Michiel. A. Blauw for the introducing me to fluorine ICP and optical emission spectroscopy, Tony Zijlstra for all the etchers and Scanning Electron Microscopy, Diederik. Rep for the four-probe measurement, Anja van Langen-Suurling for the electron beam pattern generator 5, Mischa S. P. Andriesse for the chlorine ICP and langmuir probe measurement, Arja van Zuuk for the optical lithography, and Mark Zuiddam for the Atomic Force Microscopy.

Great attitudes to Dr Ching-Hui Chen of Lumileds Lighting, USA for valuable discussions of diode characterization, Dr Yong Chen of Hewlett Packard, USA, David Peyrade of L2M-CNR, France for material support.

Thanks go to my colleagues in Canterbury University, Olive Dickie and Monica Schulze in Physics and Astronomy Department for assistance in photoconductivity and photoluminescence experiments, respectively. Thanks to Sharee McNab, Tim Drysdale, Helen Devereux in Electrical and Electronic Engineering Department for all kinds of topic discussions and lots of fun in computer games and sports.

Thanks to Professor E. L. Hu in California University for providing a clean room tour from GaN growth to characterization, from optical to electrical aspects and discussing of my work.

I would like to acknowledge the Marsden Fund of Royal Society of New Zealand provided the financial support in the form of the student fellowship. I was awarded Huygens scholarship (NIFFIC) during I was working in DIMES, Technical University of Delft, Netherlands. I gratefully acknowledge their kind selection.

Many thanks to my business partner J. Su. With his honest and successful management, my business keeps running and growing in those three years.

Very special thanks to my son for his mature and understanding. Also thanks to my parents for taking care of him when I was in Europe. The deepest thank to Tony for his love, patience and comments.

This dissertation is dedicated to my father, who suggested me to make this step forward. I always remember his word,

"You could do more things after you finish your Ph.D"

List of Figures

List of Tables

Contents

Chapter 2 Experimental Techniques

Chapter 3 Nanostructure Pattern Fabrication

Chapter 4 Reactive Ion Etching Induced Damage Effects on Electrical Properties

Chapter 1

Introduction

1.1 Applications and potential of GaN material

GaN and related compound semiconductor materials have been very popular in the last decades [1-3], because of their successful applications in light emitting diodes (LED) and short wavelength laser diodes (LD), and other optoelectronic devices. The need for blue LEDs has been acute for a long time for full color displays. Red LEDs with efficiencies greater than 10% have been commercially available for some years, but efficiencies of green and blue diodes fell a long way short, seriously restricting the possibilities for LED full color display panels. The attempt to achieve high efficiencies from blue LEDs using IV-VI compound semiconductor has been partially successful. However, the problem of operating lifetime needs to be solved, this leaves the field open to III-V alternatives. Blue InGaN LEDs with efficiencies around 5 to 10% developed by Nichia Chemical Company in Japan in 1994/1995 led to the development of large outdoor full colour displays and opens up other display possibilities, such as traffic lights and white light sources. Solid state white light emitting devices would be more durable with less power consumption than conventional incandescent bulbs or fluorescent lamps [4]. Even more promising is a recent report on a high brightness GaN based blue LED that shows the quantum efficiency approaching 38% [5].

Semiconductor LDs have a wide range of application, from optical communication systems to compact disk (CD) players. The shorter wavelength means that the light can be focused more sharply, which would increase the storage capacity of optical disks. Digital versatile disks (DVDs), which entered production in

1996, rely on red wavelength aluminum indium gallium phosphide (AlInGaP) semiconductor lasers and have a data capacity of about 4.7 gigabytes, compared with 0.65 gigabytes for CDs, which use infrared aluminum gallium arsenide (AlGaAs) laser diodes. By moving to violet wavelengths using InGaN-based compound semiconductors, the capacity can be increased to more than 15 gigabytes. Thus, these semiconductors are indispensable for next generation DVDs. The ultra-violet InGaN may also improve the performance of laser printers and undersea optical communication.

The applications of GaN and related material for light emitting devices lie in full colour displays, optical data storage, white-light sources and communications, while their applications in electronic devices are suitable for high power and high temperature. Such electronic devices, for example, heterostructure field effect transistors (FETs), heterojunction bipolar transistors (HBTs), metal oxide semiconductor field effect transistors (MOSFETs) and diode rectifiers, have all been realized in the AlGaInN system, with very promising performance at high temperature (beyond 300°C) and high voltage [6].

Furthermore, a very recent report on GaN has demonstrated the potential of this material for micro-electronic-mechanical systems (MEMS), such as cantilever structure [7]. This is because GaN and its related material have good mechanical, high piezoelectric, optically transparent properties, and the possibility of integration of MEMS with optical and electronic devices.

In many of these applications, the ability to transfer high resolution patterns in GaN is a critical step towards the fabrication of a real device. At the time when this project started, there were not many papers about GaN and related material device fabrication. Thus, nanostructural pattern fabrication has become one of the aspects of this work.

The growing interests in GaN and related materials for all of the above mentioned applications are based on the nitride unique electronic properties such as direct and wide band gap (3.50 eV), good thermal conductivity (1.3 W/cm. K), chemical stability and physical hardness [8]. In addition, possible technological advantages, such as easier doping of n-type GaN, easier cleaving (for laser facets)

and easier contacting and high electron mobilities (4000 cm^2 /Vs). The following sections will discuss some basic properties of GaN and related issues.

1.2 Properties of GaN and related issues

1.2.1 Crystal structure

The principle concern of this work is the electrical and optical properties of GaN and its alloys, however these can never be fully understood without referring to the structural properties. Therefore, a brief description of structural aspects, which have relevance to the optoelectronic and electrical application are presented here.

The most important structures for nitrides are the wurtize and zinc blende. GaN usually crystallizes in the hexagonal wurtzite (WZ) structure, as shown in figure 1.1 [9]. In the WZ structure of GaN, like in diamond, each atom has a tetrahedral coordination of the nearest neighbors. The GaN WZ structure has two formular units per unit cell (4 atoms per cell) and a molecular weight of 83.728 g/mol. Strains and defects could distort the crystal structure and therefore, change the lattice constants from their intrinsic value. This is believed to be the reason for a wide dispersion in reported values [10]. For WZ-GaN at room temperature, the following lattice parameters are generally accepted [11].

$$a_0 = 3.1892 \pm 0.0009 \text{Å}$$

$$c_0 = 5.1850 \pm 0.0005 \text{Å}$$

Crystal parameters of zinc blende polytype [12] and rocksalt structure [13, 14] of GaN also have been reported.

Structural aspect of real GaN films, such as dislocation density is of interest for the understanding of the electrical and optical properties. Transmission electron microscopy (TEM) [15] studies found high dislocation densities in even good quality GaN films and bulk crystals. In contrast to other materials systems [16-18], GaN based devices are highly efficient and show little degradation in spite of an extremely

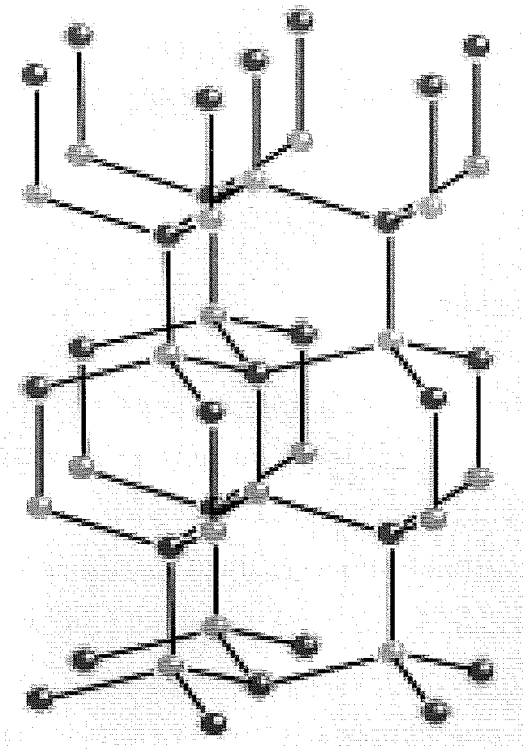

Figure 1. 1 The hexagonal wurtzite structure of GaN. Like in diamond, each atom has tetrahedral coordination of the nearest neighbours.

high (10^8-10^{11}cm^{-2}) dislocation density [19]. This fact is surprising and anomalous in view of experience with other materials of light emitting devices.

The reason why the existence of the extremely high density of dislocation does not affect the optical properties and lifetime remains unknown.

1.2.2 Band gap

It was found that gallium nitride is a semiconductor material having a direct band gap in both wurtzite and zinc blende structure, see figure 1.2 [20]. The figure shows the calculated band structure near the Γ point of WZ GaN. At k = 0, the top of valence band is split by crystal field and spin orbit coupling into the A (Γ_9), B (Γ_7) and C (Γ_7) states. The conduction band is shifted upwards. The exciton binding energies are denoted as E_A^b, E_B^b, and E_C^b for all the A, B and C excitons [21-23],

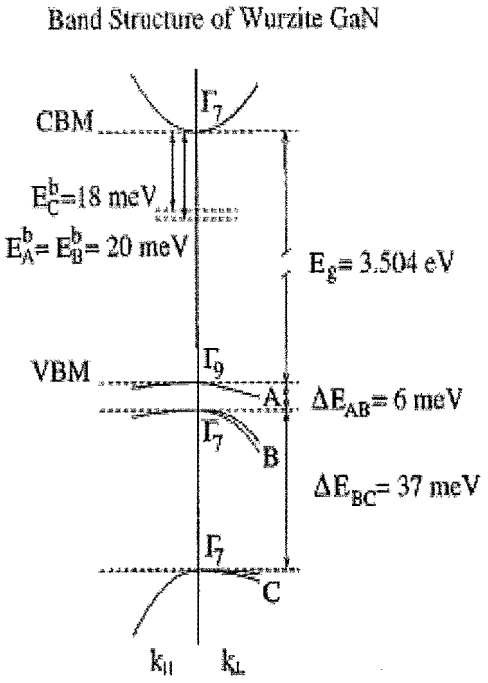

Figure 1. 2 Calculated band structure near the Γ point of WZ GaN. At k = 0, the top of valence band is split by crystal field and spin orbit coupling into the A (Γ_9), B (Γ_7) and C (Γ_7) states. The conduction band is shifted up wards. The exciton binding energies are denoted as E_A^b, E_B^b and E_C^b for all the A, B and C excitons, respectively.

respectively. The most important reason for the wide spread use of GaN and related materials is direct and wide band gap (~3.5 eV), which produces a higher efficiency during energy transfer or emission. A related nitride compound AlN has an even wider band gap, however AlN is predicted to be an indirect band gap semiconductor material.

Several groups have calculated the band structure of GaN and results have been reviewed [24-25]. The measurement of band structure parameter is complicated by the existence of residual strain in most available GaN samples. This is because the majority of epitaxial films have been grown on non-lattice matched substrates, which not only possess different lattice parameters, but also different thermal expansion coefficients. The energies of A, B and C excitons are quite sensitive to the heteroepitaxial strain in the thin layers [26]. The band gap has been measured on many occasions. Temperature dependence of band gap has been reported. It is found

that $E_{g\ (330K)} = 3.39$ eV and $E_{g\ (1.6k)} = 3.50$ eV for WZ structure. The early data of Monemar [22, 27, 28] has been recommended to be the most reliable. The strain in the GaN film will affect the exciton energies [29], and broaden the exciton lines [30].

Obviously, strain affects the wavelength of the emitted light. Annealing can release the thermal strain in total, or partly by a slow cool-down cycle. So far, there is no report about this aspect and not much research on strain effects on optical and electrical properties. It is interesting indeed that annealing as-grown material exhibits excellent Schottky characteristics and shifts up the near band gap emission of GaN grown on SiC [31].

More dislocations have been found on GaN grown on sapphire rather than on SiC substrate [32, 33].

1.2.3 Substrate issue

The electrical and optical properties of GaN have many advantages over other semiconductors, as mentioned before. However, to develop a high performance GaN device, first of all, it is important to obtain high quality material and to control the doping level. A key limiting issue for the growth of high quality GaN has been the lack of an ideal substrate with minimal lattice mismatch.

In most work, thin film GaN has been grown on sapphire or SiC substrates. For sapphire $a_0 = 4.758$ Å, $c_0 = 12.991$ Å and for 6H-SiC $a_0 = 3.08$ Å, $c_0 = 15.12$ Å. Commonly WZ GaN films grown on basal plane sapphire grow with their c-axes parallel to the sapphire c-axis but rotated in-plane so that $[2110]_{GaN} \parallel [1100]_{Sapphire}$ and $[1100]_{GaN} \parallel [1210]_{Sapphire.}$ In this configuration, the mismatch turns out to be 16%, much less than the 49% discrepancy in a_0, although still very large in epitaxy terms [34]. Apart from this, applications with sapphire are limited by its lack of electrical conductivity and high cost.

As an alternative, SiC has been used as a substrate to grow GaN on. An attractive point of silicon carbide is the possibility to combine power devices on silicon carbide and optoelectronic compounds in the GaN based layers. Furthermore, the lattice mismatch on SiC substrate is less and causes tensile strain. The defect

density can be brought below a value of 10^9 cm^{-2}, which is better by one order of magnitude in comparison to layers grown on sapphire substrates [35]. However, SiC substrate is expensive. Besides, surface cleaning has been a problem until the recent use of hydrogen plasma for surface deoxidization.

In addition, Si, ZnO and $LiAlO_2$ have been investigated to be a possible substrate [36-39]. However, these substrates are still in experimental testing stage. To relax strain in GaN, a porous GaN sublayer has been tried, as well as AlN buffer layer [40].

Until today, the main substrates for GaN growth are sapphire and SiC. Lots of research work have been done on GaN grown on sapphire due to the fact that this material has been used as substrate first. There are not many studies of GaN grown on SiC yet.

1.2.4 Growth technologies

The melting point of GaN is approximately 2000 °C. Thus, the growth of GaN crystals from a melt is difficult. Hence, for the growth of GaN, an equilibrium mixture of nitride and Ga-containing gas has been used, instead of normal growing process using the halide vapor phase epitaxy method (HVPE). New growth methods such as molecular beam epitaxy (MBE) and metal organic chemical vapor phase epitaxy (MOVPE) have recently resulted in rapid improvements in the methodology of GaN crystal growth. Prior to the growth of the GaN film, a thin AlN buffer layer has been deposited, yielding GaN films with carrier concentrations of 2 - 5 x 10^{17} cm^{-3} and hall mobility in the range of 350 - 430 $cm^2/(Vs)$. However, without the AlN buffer layer, the carrier concentration is around 2 x $10^{19}cm^{-3}$ and the hall mobility is only around 50 $cm^2/(Vs)$ in MOVPE growth without any intentional doping. These values have to be improved in order to form a high quality film for the fabrication of optical and electrical devices [41]. The development of a growth procedure, including the buffer layers grown at low temperature to gain high quality GaN on sapphire substrates, has been very successful. The highest electron mobility reported is 900 $cm^2/(Vs)$ at 300 K and 4000 $cm^2/(Vs)$ at 77 K [42].

P-doped GaN is one of the issues in GaN applications. Demonstration of p-type GaN using low energy electron beam irradiation solves the problem by using thermal annealing and two gases for growth.

Nowadays GaN films have good morphology, low carrier concentration and high mobility, and are ready for application. Free standing bulk GaN is under development by lucent technology. These progresses in developments have kept GaN to be popular for last decades and speeded up the commercialization. This has ensured this project to start.

1.2.5 Chemical property

GaN has a bonding energy of 8.92 eV/atom, which explains the somewhat inert chemical nature. This property is beneficial for device durability and high temperature applications.

In addition, because of the high bonding energy, there are limited wet chemical etching recipes for GaN [43]. Therefore, a significant amount of effort has been devoted to develop dry etch processes of GaN.

However there is no systematic study on dry etching of GaN and its mechanism when this project started. Therefore, it is necessary to study the dry etching mechanism of GaN and to optimize the etch conditions for device fabrication. However, exposure of GaN to a reactive gas discharge can also be deteriorative to device perforamnce.

The following section will describe the general introduction of dry etching and etch induced damage.

1.3 Dry etching and etch induced damage

1.3.1 General introduction

Dry etching has become increasingly important in electronic device manufacturing. As design rules, decrease feature size to sub-micron dimensions (0.13 μm) and junction depths are limited to hundreds of Angstroms, the anisotropic nature of dry

etching becomes critical. However, the dry etching process introduces defects into substrate surfaces. For example, during ion-enhanced dry etching, point defects and defect clusters are introduced into the substrate, which may affect the device characteristics [44]. Dry etching induced damage may have serious effects on electrical characteristics [45-47] and optical properties [48-51]. Thus, studying the etch induced damage, understanding the implications for the optical and electrical properties of the resulting devices, and hence optimizing the process parameters emerges as an important area of research.

1.3.2 RIE etching GaN and its damage

Dry etch techniques such as reactive ion etching (RIE) have found wide applicability in the fabrication of optoelectronic devices [52]. RIE utilizes the chemical and physical components of an etch mechanism to achieve an anisotropic profile, combined with a fast etch rate and a good dimensional control. RIE plasma is typically generated by applying radio frequency (rf) power e. g. at 13.56 MHz between two parallel electrodes in a reactive gas. The substrate is placed on the powered electrode where a potential is induced with respect to the plasma. Ion energies, defined as ions cross the plasma sheath, are typically a few hundred eV. RIE is operating at pressures, ranging from a few mTorr up to 200 mTorr, which promotes anisotropic etching due to few collisional scattering of ions during acceleration in the plasma sheath.

There are a large number of papers reporting on GaN etching, using different etch gases [53-55]. Cl-based chemicals, such as BCl_3/Ar, CCl_2F_2/Ar, Cl_2/CH_4/Ar or CF_3Br/Ar are commonly used [56]. The fluorine based plasmas sometimes suffer from polymerisation of fluorocarbons, which deposit on the sample leading to a grassy surface morphology due to micromask effects [57].

Adesida et al [58] reported the RIE etching of GaN in $SiCl_4$ based plasma. It is found that the etch rate increased with dc bias, and reached 500 Å/min at a 400 V dc bias. Fricke et al [59] used Cl_2/N_2 based reactive ion etching to etch GaN and found that the high etch rates and almost vertical profile can be obtained at low N_2

content. Other RIE results have been reported using HBr, CHF_3 and CCl_2F_2 based plasmas.

The fastest etch rate has been obtained in a chlorine-based plasma under high ion energy conditions. At these conditions the Ga-N bond breaks and the sputter desorption of etch products from the surface are most efficient. Under these conditions, plasma damage can occur and degrade both electrical and optical device performance [60] compared to unetched material. This change on electrical and optical properties is described as dry etch induced damage. Lowering of the ion energy or increasing the chemical activity in the plasma to minimize the damage, often results in slower etch rates or less anisotropic profiles, which significantly limit the critical dimensions.

Thus, etch induced damage attracts attention. There are some papers on etch induced damage, where top surface damage was evaluated by the electrical characterization of diodes [61-62] and surface analysis [63-64]. General finding indicates that dry etching degrades the device performance. When defects are generated, the diodes become more leaky with a decrease in barrier height, breakdown voltage, and intercept voltage while ideality factor increases.

Most dry etching process incorporate both a chemical and a physical component: the chemical component generally provides rapid etch rates and material selectivity, while the physical component, such as ion bombardment, provides controlled directionality and can itself enhance the chemical etch rate. RIE is the commonly used dry etching technique. However, sensitive, separate control of chemical and physical components, which are important in etching GaN for its chemical inertness properties, is difficult to achieve in RIE. But it is possible in other dry etching techniques, such as high density plasma (HDP), chemically assisted ion beam etching (CAIBE) and radical beam/ion beam etching (RBIBE).

Many different types of dry etching methods have been used to etch GaN. Ping et al. used ion beam etching of GaN [65]. High etch rates have been achieved using electron cyclotron resonance etching (ECR), magnetron reactive ion etching (MIE) and inductively coupled plasma etching (ICP) [66-68]. HDP has been recommended for etching GaN because of high reactive species content and predominately controllable ion energy.

1.3.3 ICP etching GaN and its damage

Among HDP, ICP has been most commonly used because of easier scaling up and adjustable chuck position. The ICP plasma is formed in a dielectric vessel encircled by an inductive coil into which rf power is applied. The alternating electric field between the coils induces a strong alternating magnetic field, trapping electrons in the center of the chamber and generating a high density plasma. Since ion energy and plasma density can be effectively decoupled, uniform ion density and energy distributions are transferred to the sample while keeping ion and electron energy low. Thus, ICP etching can result in low damage while maintaining fast etch rates.

Fast etch rate of GaN in ICP chlorine based plasma has been reported [69]. Lee et al [70] investigated magnetized ICP etching of GaN in Cl_2/BCl_3. Khan et al [71] used ICP-RIE to etch GaN and optimized etch condition for fast etch rate. Smith et al [66] reported fast etch rate of 980nm/min. The fastest etch rate published is 1.3μm/min from M. E. Ryan et al [43] using surface technology System (STS) ICP system.

The ICP plasma is well known for its low electron energy, high density, and ease of scaling to large diameter wafer processing. Unfortunately, these plasma sources still induce a certain amount of damage [72]. Recently there has been increasing concern regarding the intrinsic damage associated with many dry etch techniques. Such issues become especially important for small dimension structures. Generic process-induced damage includes degradation of integrity of dielectric layers [73], structure damage, contamination [74] and other kinds. Pearton et al [6] reported HDP etching of GaN resulted in improved etch characteristics compared to RIE. This is attributed to plasma densities, which are 2 to 4 orders of magnitude higher than RIE. Eddy Jr [54] reported that chlorine based plasma discharges minimize the stoichiometry problem by improving the rate of gallium removal from the surface. This mechanism provides an excellent surface for ohmic contacts on n-type GaN, but presents a major obstacle for Schottky contacts or ohmic contacts on p-type GaN. Cao et al [75] reported dry etch induced damage in etching GaN and the recovery by annealing in N_2 atmosphere. Lee et al [63] reported dry etch induced damage in n–type GaN and its recovery by treatment in an N_2 plasma. Khan et al [71] found low

damage in ICP-RIE plasma etching of GaN regarding to mobility, carrier concentration, breakdown voltage, and forward turn on voltage.

However, there are no systemic studies on the dry etch behavior of RIE and ICP SF_6 + N_2 plasma, and the comparison of ICP fluorine plasma and chlorine plasma etching of GaN and their effects. It would be of great interest to understand the etch mechanisms, and optimize the etch conditions to obtain high etch rate, vertical etch profile, smooth surface, high mask selectivity and minimal etch induced damage for GaN and its related material-device fabrication.

1.4 Dry etch induced damage assessment

Although the consequences of etch-induced damage on device performance may be all too apparent, one must nevertheless carefully choose the appropriate set of analytical tools in characterizing damage. Analytical techniques that are sensitive to modifications of the substrate surface may not reveal information about structural damage to etched material.

A variety of techniques have been used to evaluate dry etch damage. For surface effects, one can use surface science methods, such as XPS [76], auger spectroscopy and low angle X-ray scattering; electrical methods, which are based on the characteristics of semiconductor-metal junctions and optical methods, such as photoluminescence [77] and Raman spectroscopy. The comparison of a Schottky junction formed on the etched and unetched surfaces of a III-V semiconductor gives a great deal of useful information [78], such as ideality factor, the reverse breakdown voltage, barrier height, forward turn-on voltage and reverse leakage current [79].

Photoluminescence (PL) intensity, which is helpful information as a measurement of one of the optical properties, can be measured in III-V materials. The variation in photoluminescence intensity due to etch induced damage could be correlated to etch conditions.

Sidewall damage can be measured by creating a Schottky contact on the sidewall [80], but this is not an easy technique. Another method is to measure the electrical conductance of the wire as a function wire width. The wire would be

expected to show zero conduction when the width of the wire is just equal to twice the sidewall depletion depth [79].

It would be very useful for industrial application if one can set up effective characterization of the electrical and optical properties to monitor the etch induced damage during device fabrication. For the time being, there are not many reports on etch induced damage characterization on GaN and no research on sidewall damage of GaN to determine the limitations of narrow wire on device fabrication. Thus, we started the "Nanofabrication and its effect on electrical and optical properties of GaN" research from early 1999.

1.5 GaN devices

1.5.1 Ohmic contact on GaN

To evaluate the electrical properties, ohmic and Schottky contacts are essential. Thus, before measuring the damage, it is necessary to develop suitable ohmic and Schottky contacts.

Semiconductor devices and specimens used for the measurement of semiconductor parameters require ohmic contacts to which connections can be made. The important feature of such contacts is that voltage drop across them must be negligible, compared with the voltage drop across the device or specimen, so that the contacts do not affect the I/V characteristic. In principle, ohmic contacts can be made by using a metal with a work function less than the work function of an n-type semiconductor or greater than the work function of a p-type semiconductor. However, there are very few metal-semiconductor combinations, which satisfy this condition. The vast majority of ohmic contacts involve a thin layer of very heavily doped semiconductor immediately adjacent to the metal, so that the depletion layer is so thin that the carriers can readily tunnel through it [81].

During the last few years' significant progress has been made in the growth and characterisation of GaN and its alloys with AlN and InN. This progress led to the realization of several electronic and optoelectronic devices including metal-semiconductor field-effect transistors (MESFETs), modulation doped field-effect

transistors (MODFETs), metal-insulator field-effect transistors (MISFETs), and light-emitting diodes (LEDs). Lower resistance ohmic contacts are imperative in the successful implementation of all these devices, particularly high power devices, which require high power conversion efficiency and heat management. Owing to the very wide band gaps of nitrides, these ohmic contacts must be quite different from those of GaAs, InP and Si.

Thus, ohmic contact technology remains an important part of the progress of wide–band gap semiconductors. Further improvements are still necessary in order to enhance the performance of current GaN based materials in blue and UV optoelectronics, such as LEDs and LD, as well as for device application in high-temperatures and high-power microwave electronics. According to the Schottky-Mott mode, it is especially difficult for p-type doped wide- band gap semiconductors, such as ZnSe or GaN to find suitable metallisation which leads to low specific contact resistance in order to withstand high current flows and high temperature.

During the past years, many attempts have been made to obtain low resistance ohmic contacts to GaN [82-83]. Ruvimor et al [84] tried Ti/Al and Ti/Al/Ni/Au ohmic contact, Lester et al [85] tried non-alloyed Ti/Al ohmic contact. Z. Fan et al [86] made ohmic contact on GaN by depositing Multiple layers Ti/Al/Ni/Au on n - type GaN with a reactive ion etching process and obtained very low resistivity of $\rho = 8.9 \times 10^{-8}\ \Omega\ cm^2$. The development of ohmic contact formation using Al and TiAl contact to n-GaN and the analysis in terms of interfacial layer AlN in Ti/Al and Pd/Al to n - GaN were made by Luther et al [87].

For industrial applications, it is desirable to have a simple process giving reliable reproducible low resistance ohmic contacts for minimum cost.

1.5.2 Schottky contact on GaN

The Schottky [88] model of metal-semiconductor barrier is shown in figure 1.3. The assumption here is intimate contact between the metal and semiconductor with no interfacial layer. The barrier height after contact is formed is given by

$$\Phi_o = \Phi_M - \chi$$

where Φ_M the metal work function, χ is the electron affinity of the semiconductor, defined as the potential difference between the bottom of conduction band and the vacuum level at the semiconductor surface. ϕ_S is the work function of the semiconductor. In the theoretical analysis, we assume that the barrier height depends only on the metal work function to a particular semiconductor.

To get good Schottky contacts, one should use metals having large work functions. In practice, even with the same metal, different techniques can result in different diode properties. Auret et al [89] found Au Schottky contact exhibited excellent rectification properties when using resistive evaporation. In contrast, sputter deposited Au contacts had poor characteristics.

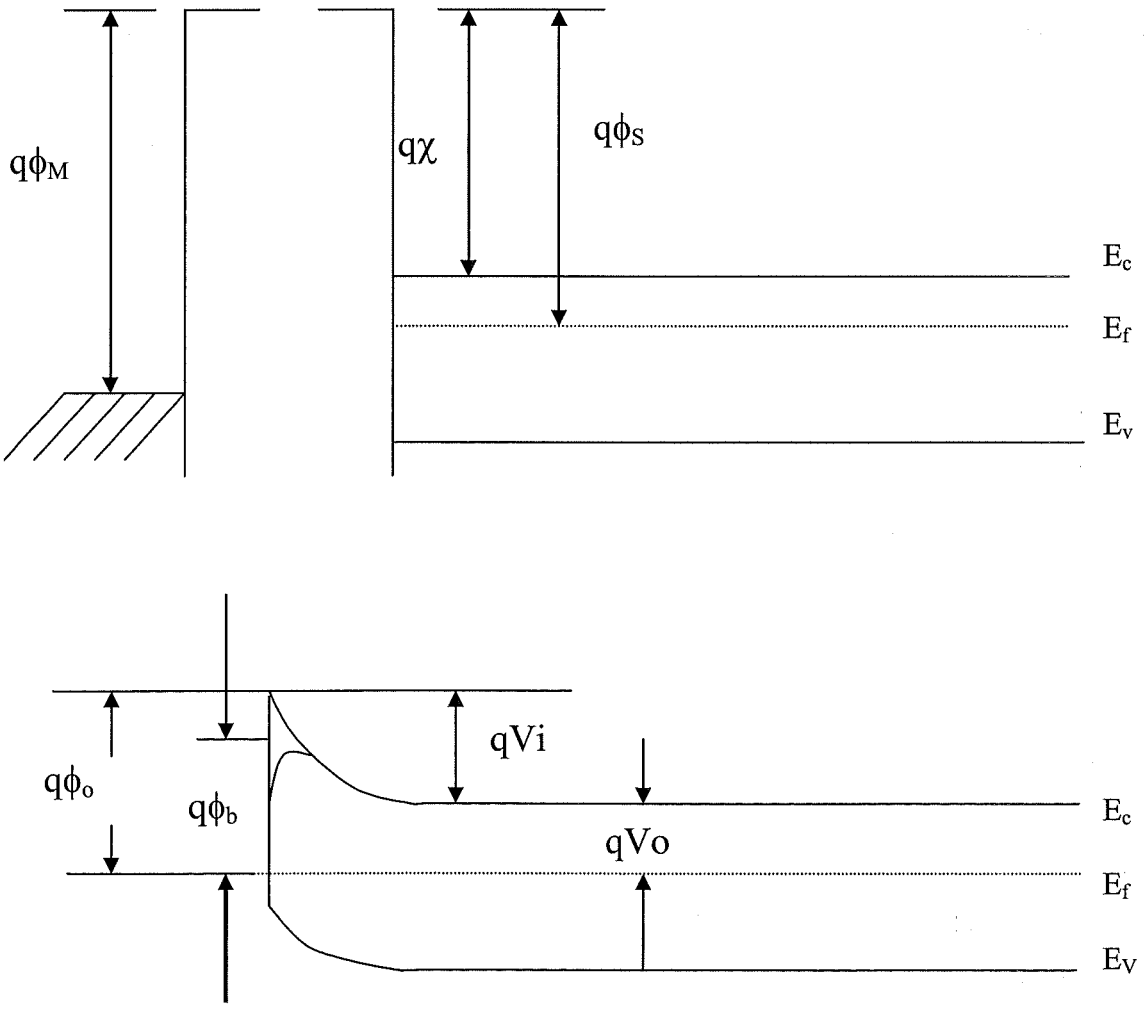

Figure 1. 3 Upper, lower parts are metal and semiconductor system before and after contact, respectively. Lower part shows Schottky barrier energy band diagram.

In practice, the actual barrier height ϕ_b is always less than ideal barrier height ϕ_o due to image force barrier lowering and other factors. The built-in potential is V_i, and V_o is the potential of the semiconductor Fermi level with respect to the conduction band. Bardeen was the first to point out the importance of surface states in determining the barrier height [90]. Such surface states may be dangling bonds at surface or some other types of defects [91-92].

Dry etching can be used to make good ohmic contacts because many defects serve as recombination centres. However, dry etching will deteriorate Schottky barrier height by changing the surface states and the introduction of other type of defects. A. P. Zhang et al [93] reported an Ar/Cl_2 discharge deteriorated diodes properties by reducing reverse breakdown voltage and Schottky barrier height. Mistele et al [94] pointed out that using N_2 as etching gas could obtain rectifying characteristics (Schottky) of metal-n-type GaN, while conventional etching gas produced linear (ohmic) behaviour such as Ar or $Ar + Cl_2$.

Therefore, diodes fabricated on dry etched GaN are good monitor for plasma-induced surface damage as manifested by Schottky barrier height and ideality factor extract from the I-V behaviour.

1.6 Outline of this thesis

In chapter two, main experimental techniques, which have been used in this work, will be described and discussed. All the results will be presented and discussed in the sequence of category.

Chapter three describes the GaN etch behaviour of RIE and nanofabrication into GaN by using RIE and electron beam lithography, and the successful implementation of the developed nanofabrication procedure in Si/Si_xN_y. The EBL (at Canterbury University) dose optimisation will be presented. The effects of the N_2 percentage in the etching gas mixture of the etch rate, vertical nature of profile and surface roughness has been examined and discussed.

In Chapter 4, results of successful fabrication of ohmic contacts without annealing, Schottky contacts, and further characterization of the RIE etch-induced damage effects on diode properties will be presented. Different power densities of Ar

plasma pre-exposure effects on ohmic contact properties of GaN grown on SiC have been investigated. Different metals have been investigated for making good Schottky contacts. The effects on electrical properties of the diode by changing the nitrogen percentage in the RIE fluorine plasma have been investigated. Effect on electrical diode properties of annealing as grown material will be presented.

Chapter five describes the RIE etch induced damage effects on optical properties, such as photoluminescence and photoconductivity. Surface composition analysis by XPS will be correlated to the observed results. To optimise the etch condition with minimal damage on optical and electrical properties, different gas mixture in etching of GaN grown on SiC has been investigated. The result of annealing effect on photoluminescence spectra will be presented and discussed.

Chapter six outlines a fundamental study of the etch mechanism of GaN using an inductively coupled plasma (ICP) with Fluorine and Chlorine gases respectively. A basic starting point has been set according to preliminary results. Then the dc bias, temperature, ICP source power and pressure around the starting point have been varied. The etching conditions for fast etch rate and vertical profile in both fluorine plasma and chlorine plasma have been optimised. The etch mechanisms of fluorine RIE plasma and ICP plasma etching GaN have been compared and discussed.

In chapters seven and eight, ICP etch induced damage effects on electrical diodes properties and photoluminescence characteristics using fluorine plasma and chlorine plasmas will be presented. The etch mechanism will be correlated to etch induced damage effects on both electrical and optical properties. The comparison of RIE and ICP fluorine plasma effects will be discussed. The ICP fluorine plasma etch induced damage on electrical and optical properties will be compared with that of ICP chlorine plasma.

Chapter nine describes the quantum wire (QW_r) device principle, device design, fabrication, and the characterization of the sidewall damage. The problems we had during device design and fabrication, and the steps we took to solve these problems will be presented.

Chapter ten gives a coherent overview the work. Conclusions are made and suggestions for additional research are given.

Chapter 2

Experimental Techniques

2.1 Dry etch technologies

2.1.1 General introduction

Dry etching covers a family of methods, by which a solid state surface is etched in the gas phase, physically by ion bombardment, chemically by a chemical reaction with reactive species at the surface, or combined physical and chemical mechanism.

Most dry etch systems find their common base in plasma or gas discharges, the area of high energy electrical and magnetic fields that will effectively dissociate any gases present to form energetic ions, photons, electrons, and high reactive radicals and molecules [95]. A common definition of the plasma state has been postulated by Chen [96].

A plasma is a quasi-neutral gas of charged and neutral particles, which exhibits collective behavior .

The plasma etching is predominately caused by or assisted by ions from the discharge. The ions bombard the substrate at normal incidence, which causes directional or anisotropic etching. This anisotropy is a demand to overcome the problem of under-etching and to make it possible to produce patterns with (sub)-micron dimensions.

Another demand in plasma etching is a high selectivity between etch rates of different materials to avoid unwanted etching (etch mask). This selectivity can be achieved by applying chemical processes in the etch mechanism. Therefore, different concentrations of gas mixture are used in discharges. Then the surfaces of the substrates are exposed simultaneously to energetic ions and to chemically active

molecules and radicals. By adjusting the gas mixture, one expects to get fast etch rates, anisotropic profiles, smooth surfaces and high selectivities.

In the plasma, only about 1 : 10^4 molecules or atoms are ionized. Thus, it is clear that the flux of ions, which bombard a substrate, is small in comparison with the flux of neutrals. It has been suggested that the dominant etching mechanism is caused by synergistic effects of the exposure to neutrals and energetic ions [97].

Dry etching has become the dominant patterning technique for GaN and its related materials, such as InGaN and AlGaN, due to the chemical inertness of the material and high resolution demands for the minimization of device size.

There are many types of plasmas sources such as those based on discharges created by direct current (dc), capacitively coupled radio frequency (rf) (RIE), inductively coupled rf (ICP) and microwaves (ECR) [98]. This chapter describes the conventional RIE etching system and high density plasma ICP techniques used for etching GaN in this project. Plasma diagnostics, like Langmuir probe and optical emission spectroscopy will be presented for unraveling the etching mechanism.

2.1.2 Reactive ion etching (RIE)

Figure 2.1(a) is a schematic drawing of a RIE reactor. RIE is a conventional etch system. It consists of a high-vacuum chamber, in which two parallel electrodes are normally horizontally positioned. The chamber wall and the top electrode (anode) are electrically grounded. The lower electrode (cathode) and substrate holder is connected via a dc-blocking capacitor and matching network to an rf generator (mostly 13.56 MHz).

The gases are supplied from the top of the reactor. The rf discharge introduces, apart from the parent gas, a multitude of neutral and positively or negatively charged, excited and fragmented molecules [99]. These species are generated mostly by the collision processes between electrons and the neutral gas molecules. The electrons have a dominant role, as they are the hottest particles in the cold plasma.

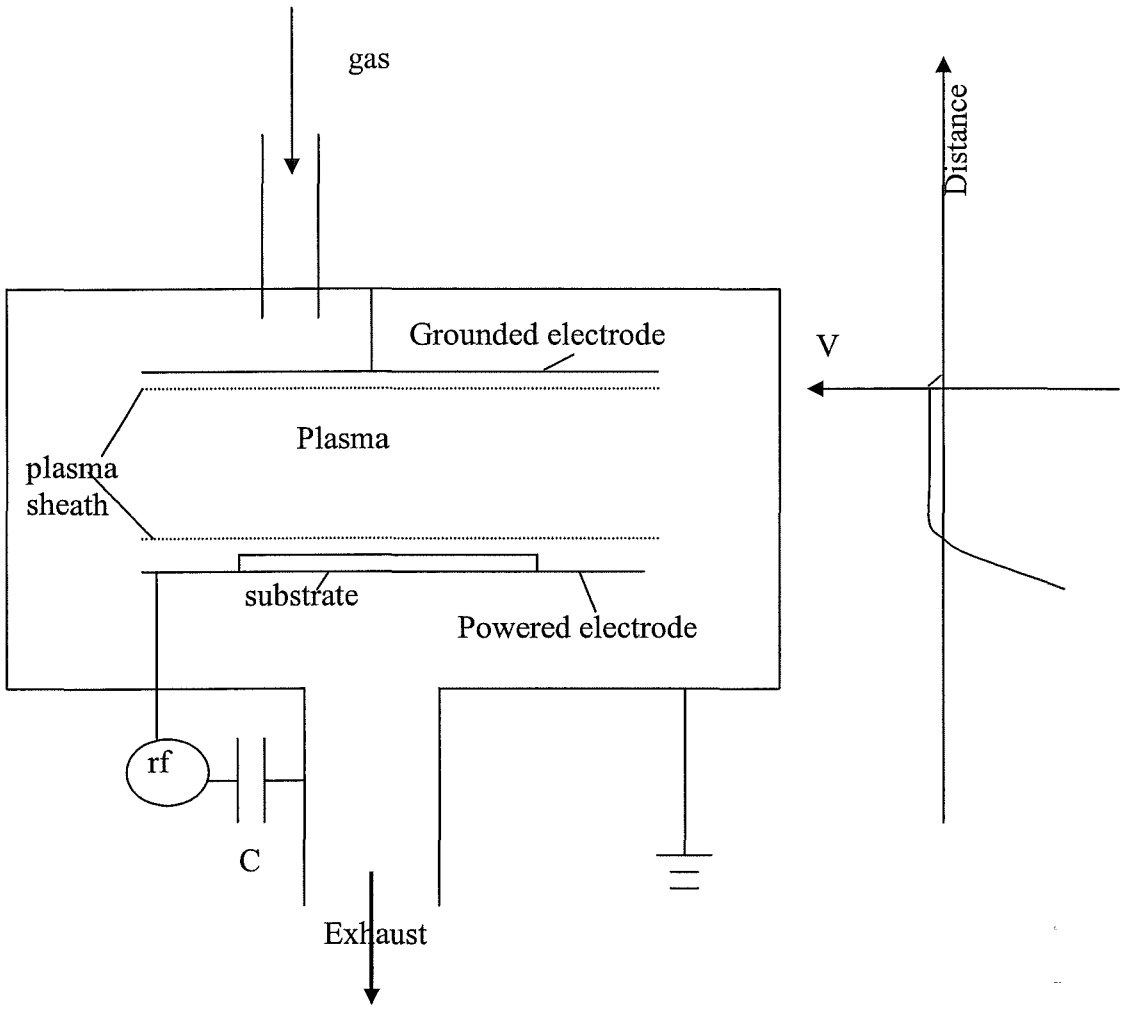

Figure 2.1 Schematic drawing of a) reactive ion etching. RIE consists of a high-vacuum chamber, in which two parallel electrodes are normally horizontally positioned. The chamber wall and the top electrode (anode) are electrically grounded. The lower electrode (cathode) and substrate holder is connected via a dc-blocking capacitor and matching network to an rf generator (mostly 13.56 MHz). b) dc bias distribution in chamber. Most of dc bias drops over the plasma sheath.

The movement of electrons in gases is a situation quite different from that of ions. The mobility of the electrons in an electric field is much higher than that of ions because of the smaller mass. In an electrical field, a charge experience of a force (F), which is given by:

$$F = q\,E \qquad 2.1$$

in which: q is the electrical charge, E is the electrical field. If work is done on a charge, it gains energy as following,

$$\frac{1}{2}\,m\,v^2 = q\,V \qquad 2.2$$

where v is the drift velocity. qV is the energy that is gained by moving a distance. In the same electrical field, energy will be identical. So, the velocity of an ion to that of an electron can be expressed as

$$\frac{v_e}{v_{ion}} = \frac{\sqrt{m_{ion}}}{\sqrt{m_e}} \qquad 2.3$$

where v_e and v_{ion} are the velocities of electron and ion, respectively. m_e and m_{ion} are the masses of electron and ion. Since the mass of ion is very much larger than that of an electron. The electron gains a larger velocity.

As a consequence, any surface in contact with plasma will get negatively charged. Thus, a negative potential develops. Consequently, any surface in contact with the plasma is subject to ion bombardment. At the powered electrode, the potential drop (commonly named dc bias) is the highest, and so the ions hit the cathode surface [100].

The dc bias resulted from external alternating voltage to a substrate, can be accurately predicate by a simple calculation [101].

$$V_{dc} \approx -V_F - V_{rf} + V_e \ln\left(\frac{2\pi V_{rf}}{V_e}\right)^{1/2} \quad 2.5$$

$$\text{Where } V_F = V_e \ln\left(\frac{2m_i}{\pi m_e}\right)^{1/2} \quad 2.6$$

is the floating potential, V_{rf} is the peak applied radio frequency voltage. V_e is the electron temperature expressed in volts. Most of dc bias drops over the plasma sheath. See figure 2.1(b).

Ions play an important role in dry etching. Although, many processes have to be considered simultaneously. The synergetic effect of having fluxes of reactive neutrals and ions at the same time is the key factor determining many dry etch processes.

Primary processes occurring in a plasma etch processes are the following;

1.Partial dissociation of the process gas into radicals and charged particles.

2.Radicals diffusion to surface.

3.Adsorportion of radicals or reactive gas at the substrate surface.

4. Chemical reaction taking place on the surface.

5. Removal of etch products by desorption and/or sputtering.

6. The etch products diffusion into to bulk gas.

Ions may enhance the adsorption, reaction and/or desorption step, as shown in figure 2.2. If etch reaction proceeds without ion bombardment (spontaneous etching), isotropic etch profiles are obtained. If ion bombardment is the driving force and the ions collide on the substrate at normal incidence, the etch profiles are anisotropic [102].

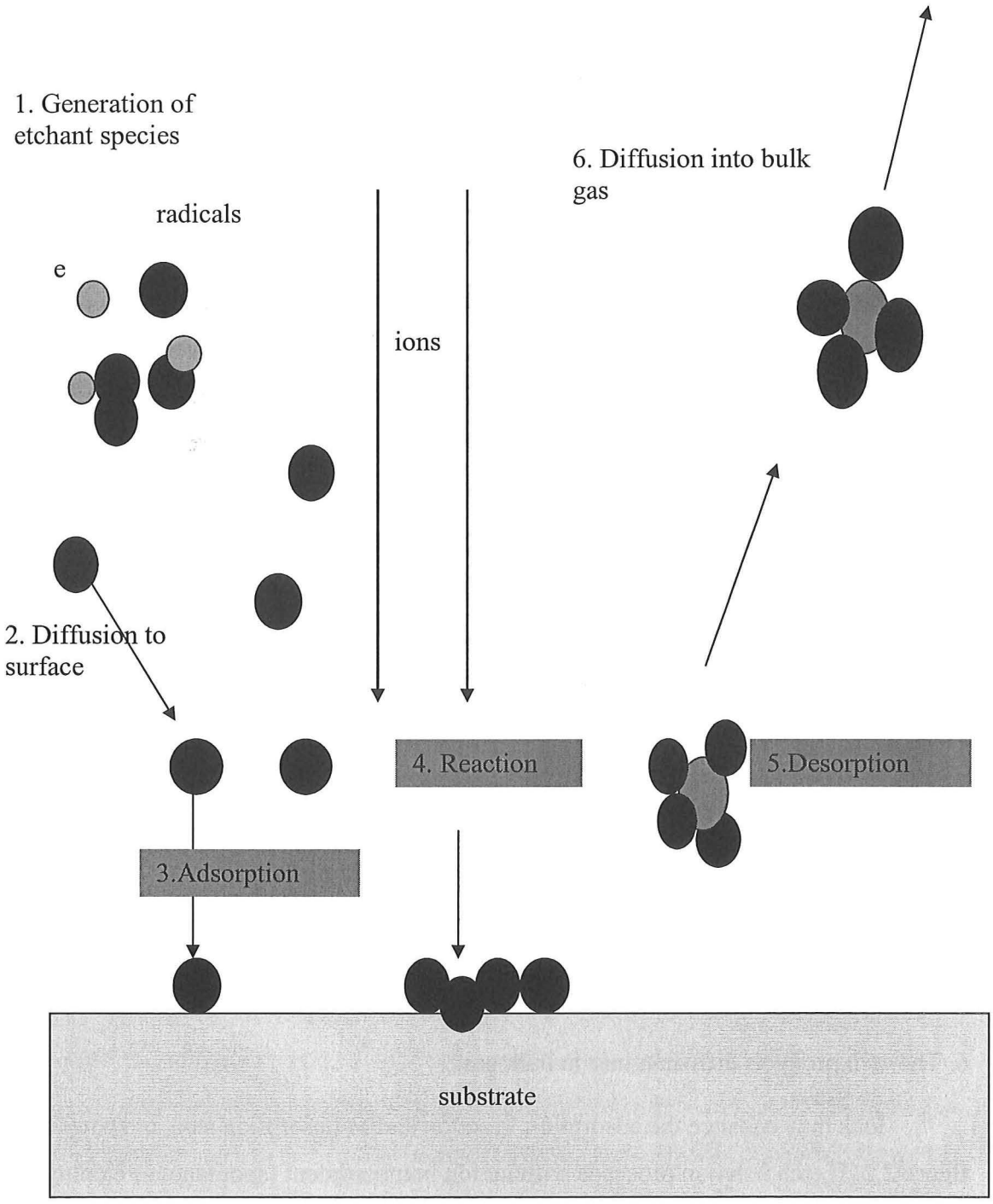

Figure 2.2 Primary process occurring in plasma etch process. 1) Partial dissociation of the process gas into radicals and charged particles. 2) Radicals and reactive particles diffusion to surface. 3) Adsorportion of radicals or reactive gas at the substrate surface. 4) Chemical reaction taking place on the surface. 5) Removal of etch products by desorption and/or sputtering. 6) The etch products diffusion down to bulk gas.

In RIE, the ion density is about 10^9 to 10^{10} per cm^3 for an Ar plasma. The specified RIE equipment employed in this project is an Oxford Plasma 80 plus in our laboratory, which has a maximum rf power of 220 W.

2.1.3 Inductively coupled plasma (ICP)

The drawback of RIE system is that the energy of the bombarding ions is coupled to the dissipated power, which hampers control of ion bombardment. A way to overcome this is changing the frequency of the source power [100], at high frequencies, a low voltage is required at the same power. A more conventional method is decoupling the source and chuck powers. This results in independent bias control. An important advantage of rf discharge over other discharges is that they are relatively easy to scale up to larger dimensions [100].

Another disadvantage of RIE is the relatively low plasma density. Source configuration like ECR and ICP shows high plasma densities. However, ECR source configuration is much more complex than that of ICP. Thus, people commonly used ICP to etch GaN instead of ECR.

Figure 2.3 is the schematic drawing of an ICP reactor assembled with a Langmuir probe and an optical emission spectroscope. The technical differences between RIE and ICP are listed in table 2.1. The main difference is that ICP has source power separately from chuck power. The ICP plasma can create low energy ions, which is expected to cause less damage and at the same time has high ion current density. Secondly, the magnetic field of ICP plasma reflects electrons to plasma, which collide with gas molecules to generate high density of charged radicals and high ion current density, and confines the plasma by keeping it away from the chamber wall. All these facts make sure that ICP has a high ion density and high reactive species content.

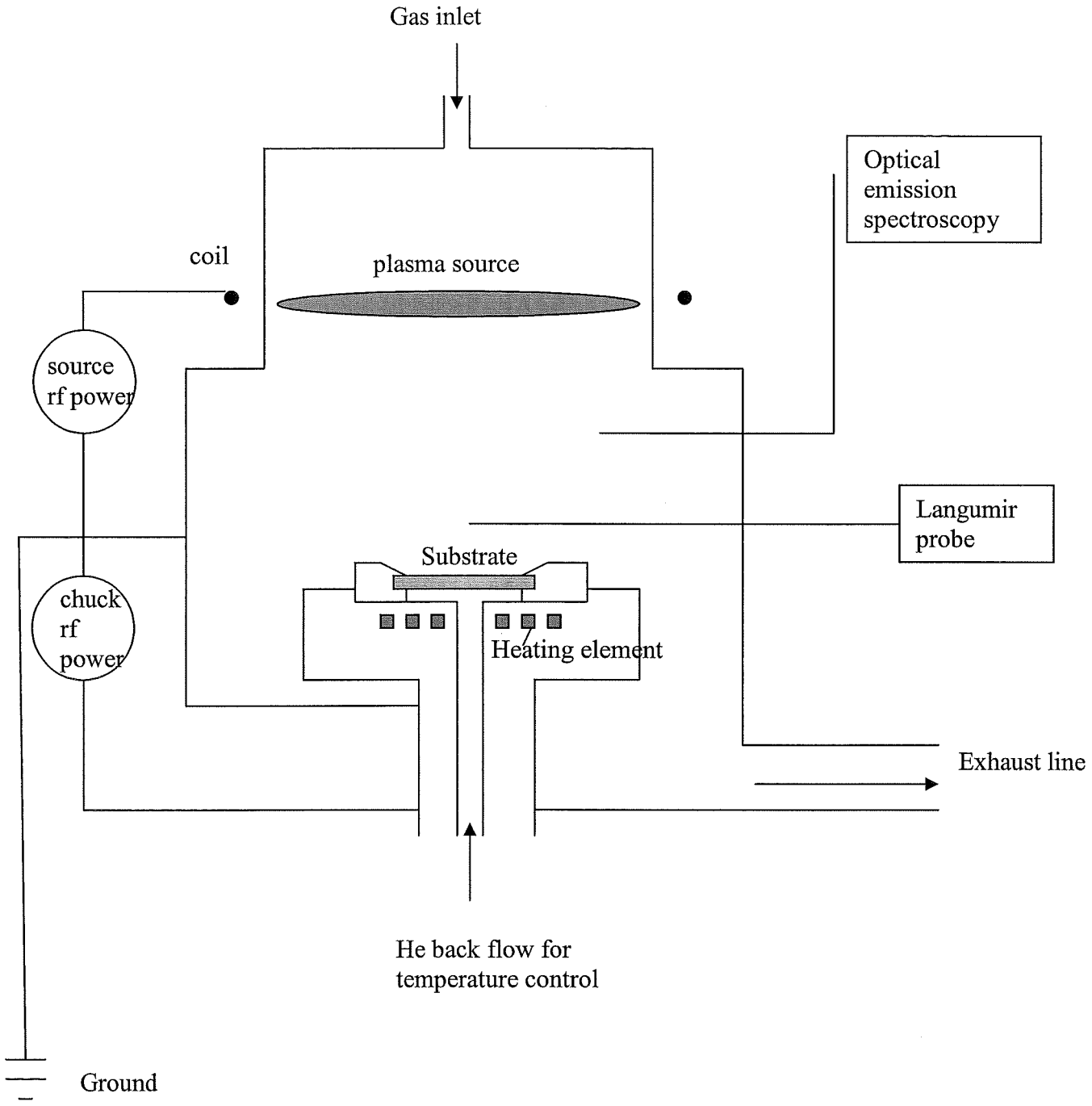

Figure 2. 3 Schematic drawing of inductively coupled plasma reactor assembled with a Langmuir probe and an optical emission spectroscope. The main advantage is that ICP has source power separately from chuck power.

Table 2. 1 Main differences between ICP and RIE systems

Type of etcher	Number of rf power	Ion density	Magnetic field	Ion current density
ICP	2	High	Yes	High
RIE	1	Low	No	Low

The specific ICP we used for this project is an Alcatel micromachining etch tool (MET lab). The basic system consists of a single wafer vacuum load lock system connected to a process chamber. This chamber is fitted with a proprietary high density, low pressure plasma source and temperature controlled cryo chuck. The process module consists of the process chamber, substrate holder, plasma source, power suppliers, gas lines and pumping package. We will focus at the process module, which is more related to our research work.

The substrate is introduced into the process module through the single substrate load lock chamber by an automatic loading and unloading system. The chamber is equipped with a magnetic multipolar confinement system, which reflects electrons back into plasma. The mechanical clamping is to improve the thermal exchange between the wafer and substrate holder. The helium gas flow at the back of the wafer for adequate heat transfer to the cooled chuck.

The distance of the substrate to the plasma is adjustable by changing the chuck position. In the highest chuck position, one can get the highest ion density and radical density. In the low position one can get relatively low ion density and high radical density because radicals have relatively a longer lifetime than ions. The highest position, 13 cm from the plasma source, has been used for GaN etching to meet the high ion current density demand. More detail about the ICP system can be found in reference [103].

2.1.4 Plasma diagnostic

The study of plasma-material interactions has evolved into an important dynamic field of research. An understanding of the basic physical and chemical process underlying these interactions is vital to the development of optimal process for IC

technology, surface modification, satellite of space and other key technologies. Diagnostics and characterization techniques are prerequisites for understanding plasma and solid surfaces exposed to the plasma [104-105]. Langmuir probe measurement and optical emission spectroscopy techniques have been employed in this project to quantify ion and radical content in the plasma, respectively.

2.1.4.1 Langmuir probe measurement (LP)

A Langmuir probe is an electrically conducting electrode of "negligibly small area" inserted into a plasma. The potential of the probe may be variable with respect to the plasma. Because of the large difference in electron and ion mobilities, a much larger flux of electrons is incident on the probe. The plasma compensates for the loss of electrons to the probe by developing a sheath between the plasma and the probe tip. The applied voltage across the probe is varied and the resultant current through the tip is measured. A current (I) -voltage (V) characteristics is measured and the analysis of this characteristics yields the following plasma parameters, plasma floating potential, plasma potential, electron temperature, electron density, ion density, electron energy distribution function, Debye length and ion current density.

Measuring the ion current density has been crucial in our experiments to determine the ion yield in a given dry etch process. Ion current density is defined as the ion flux towards the probe at strong negative bias, divided by tip surface area, with corrections made for the sheath. This parameter is determined at default ion voltage of –50 Volts. So there are very few electrons attracted to the probe, because the electrons are repelled. Only positive ions are collected.

The specific Langmuir probe we used is the Smart probe set up, which is a computerised electronic system for measuring Langmuir probe current-voltage characteristics. It contains the following components, smart probe acquisition electronics unit, PC and software, and Langmuir probe. Smart probe system is operated using the Smart soft program. This program allows the users to acquire and automatically analyse Langmuir probe data. For more details about the system are given in [106].

2.1.4.2 Optical emission spectroscopy (OES)

Optimisation of plasma parameters has successfully produced etching and deposition recipes for industrial applications. However, with advent of increasingly sophisticated diagnostics techniques and computer modelling, it is possible to obtain very detailed information on the chemistry and physics of these processing plasma and their interaction with surface. Optical probes are particularly well suited for in situ plasma diagnostics studies because they are non-intrusive, species-selective, and can yield both space- and time- resolved information. The identification of the spectrally resolved feature establishes the presence of radicals and ions formed by reactions in the discharge.

The apparatus required for this technique is one of the least complicated. It requires a monochromator to disperse the plasma emission, a set of optics to image light from the discharge onto the detector, and a photo-detector to measure the dispersed fluorescence. Light from the discharge can be imaged onto the monochromator entrance slit with UV-grade fused silica lenses and UV-coated aluminium mirrors for the best average response between 200 – 900 nm.
The plasma – induced emission can arise from electron impact excitation,

$$A + e \rightarrow A^{*} + e$$

Electron impact dissociaction,

$$AB + e \rightarrow A^{*} + B + e$$

Or an ion impact process

$$A^{+} + e\,(+M) \rightarrow A^{*}\,(+M)$$

where A and B are atoms or molecules, * indicates the excited, emitting species, and e (+M) may be neutral species, a negative ion, an electron plus a third body, or a surface.

Molecular species can also be excited by chemiluminescence recombination reactions,

$$A + BC \rightarrow AB^{*} + C$$

The excited molecules subsequently emit photons. The peak of 751.4 nm for Ar and 704.2 nm for F have been used in this study. The photons are detected by the photo-detector. This produces the spectrum of the plasma.

During the plasma etching, not only a qualitative description of the plasma is desirable, but also quantitative estimate of concentration of the reactive species. To measure the fluorine radical concentration, Ar actinometry has been employed [107]. Thus, from an optical emission spectrum, one can calculate species concentration with respect to the reference. In practice, a certain amount of Ar has been induced into plasma as actinometer. We assume the intensity of spectroscopy is given as following.

$$I(Ar) = f(T_e, n_e) = \alpha\, h(T_e)\, n_e P(Ar) \qquad 2.7$$

$$I(F) = g(T_e, n_e) = \beta\, h(T_e)\, n_e P(F) \qquad 2.8$$

Where T_e is the electron temperature, n_e is the electron density. P is the partial pressure. α, β are constants. Thus, by combining equations 2.7 and 2.8, we can get,

$$\frac{I(Ar)}{I(F)} = (\alpha / \beta)\, \frac{P(Ar)}{P(F)} \qquad 2.9$$

A well-defined amount of Ar is added to the overall gas flow, so the concentration of Ar (P(Ar)) is known. From detected spectra, I (Ar)/I (F) can be extracted. Then the particle fluorine pressure P (F) can be calculated. An essential condition is that the excitation energies of detected particle and Ar should not differ more than several eV and the transition should be the same type.

2.2 Pattern definition

2.2.1 Optical photolithography (OL)

The most widely used form of lithography is optical lithography. In the integrated circuits (IC) technology industry, pattern transfer from masks onto thin films is accomplished almost exclusively via photolithography. Photolithography, matured rapidly and has become better and better at resolving smaller and smaller features. The optical lithography can be divided into contact lithography and projection lithography (stepper and scanner). The contact lithography is faster than the stepper, because the stepper exposes the substrate for a few square centimetres per exposure. Stepper resolution is limited by diffraction, while contact lithography is limited by exposure wavelength and mask contamination. In our experiments, contact lithography has been employed.

The stencil used to generate a desired pattern in resist-coated wafers repeatedly is called photo-mask. A photo-mask is a nearly optically flat glass (transparent to near UV) or quartz plate (transparent to deep UV) with a metal (e. g. a 800 Å thick chromium layer) absorber pattern. It is placed into direct contact with photo resist coated wafer surface. The resist is exposed with ultra-violet radiation. The absorber pattern on the photo mask is opaque to ultraviolet light, whereas glass or quartz is transparent. A light field or dark field image is transferred to the resist. When the photo-mask makes direct physical contact (hard contact) to the substrate, we call it hard contact photolithography. This kind of approach has been employed in this project. It offers the highest lateral resolution. Unfortunately photo masks degrade faster through wear than they do in non-contact or soft contact lithography, where the masks are slightly raised about 10 to 20 μm above the substrate.

A broadband exposure system has been employed for ohmic and Schottky contact pattern definition. The pattern size is 200 μm X 200 μm, shown in figure 2.4. The image has been taken by using optical microscopy with a magnification of 330. By using undiluted Shipley photo resist S1813, a perfect uniform pattern definition has been obtained.

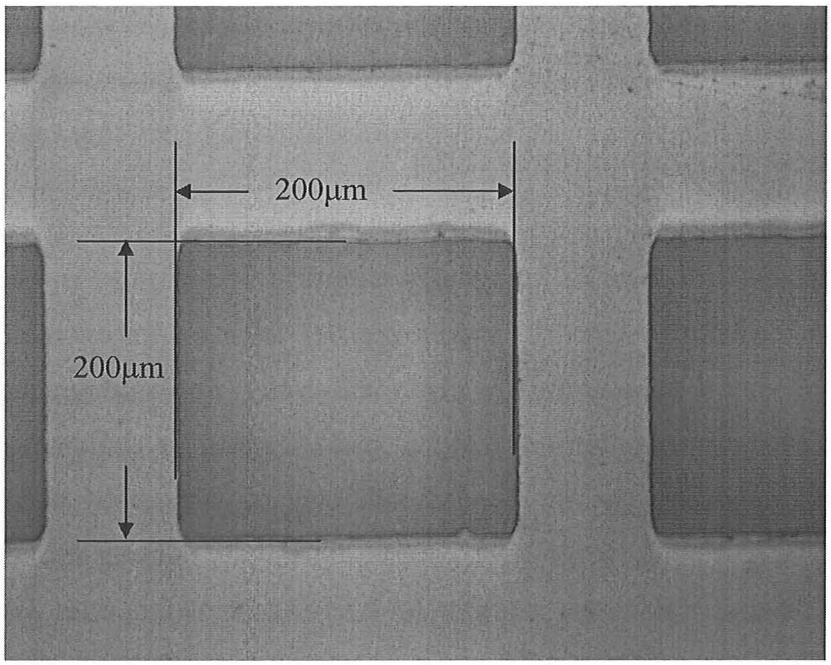

Figure 2. 4 Optical microscopy image of mask pattern with magnification 330.

2.2.2 Electron beam lithography (EBL)

With the requirement of decreasing device size, electron beam lithography (EBL) [108] and ion beam lithography have been developed to define the patterns in parallel with deep UV optical photolithography [109] and X-ray lithography [110]. In this project, a scanning electron microscope converted EBL at Canterbury University and a commercial electron beam pattern generator at the Delft Institute of Micro-Electronics and Sub-micron-technology (DIMES) have been employed to write nanoscale patterns. The principles in both electron beam exposue tools are the same. But the setups have different characteristics, e. g. beam energy, scan field and beam size etc..

In EBL, a high energy electron beam (primary electron beam) is focused on a substrate, which is coated with electron beam sensitive resist material, polymer e. g. PMMA. Elastic and inelastic scattering changes the direction of the beam (broadening of the beam) and causes energy loss of the primary electrons, thus

generating secondary electrons (SE), backscattered electrons (BSE), auger electrons (AE), and X-ray quanta (X). This is illustrated in figure 2.5 [111]. PE stands for primary electronic beam. The secondary electrons are responsible for the actual exposure.

In analogy to photo-resist, two types of EBL resists exist, see figure 2.6. The principle of positive resist is bond scission on exposed area. The principle of negative resist is cross linking on exposed area. Therefore, after development, positive resist remains in non-exposed area, while negative resist remains in exposed area. Negative resist shows swelling, positive resist shows better contrast and resolution. Bilayer positive resist PMMA with 2.5% high molecule weight (950K

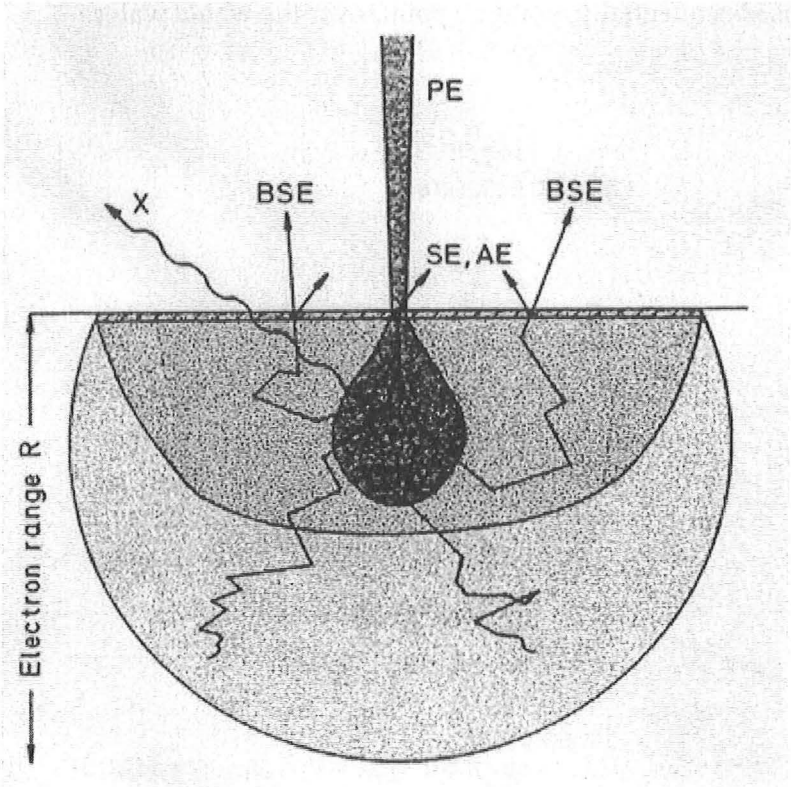

Figure 2. 5 High energy electronic beam and its effects in EBL. Elastic and inelastic scattering changes the direction and broadening of the beam and causes energy loss of primary electrons, thus generate secondary electron, backscattered electron, auger electrons and X-ray quanta. The secondary electrons are responsible for actual exposure.

dissolved in xylene) as first layer and 7% low molecule weight (180K dissolved in chlorobenzene) as second layer has been employed in quantum wire device fabrication. A 4% low molecular weight PMMA dissolved in chlorobenzene and 2.5% high molecular weight PMMA dissolved in xylene has been used for nanoscale wires and dots fabrication in our project.

The main differences between optical photolithography and EBL process are exposure time, mask and resolution. EBL has the longer exposure time because it is a sequential process. Optical contact lithography is a parallel process. The mask fabrication process is significantly simpler in case of electron beam lithography compared to flood exposure-based photon and x-ray lithography. The computer – stored pattern is directly converted to address the writing electron beam, enabling the pattern to be exposed sequentially, point by point, over the whole wafer.

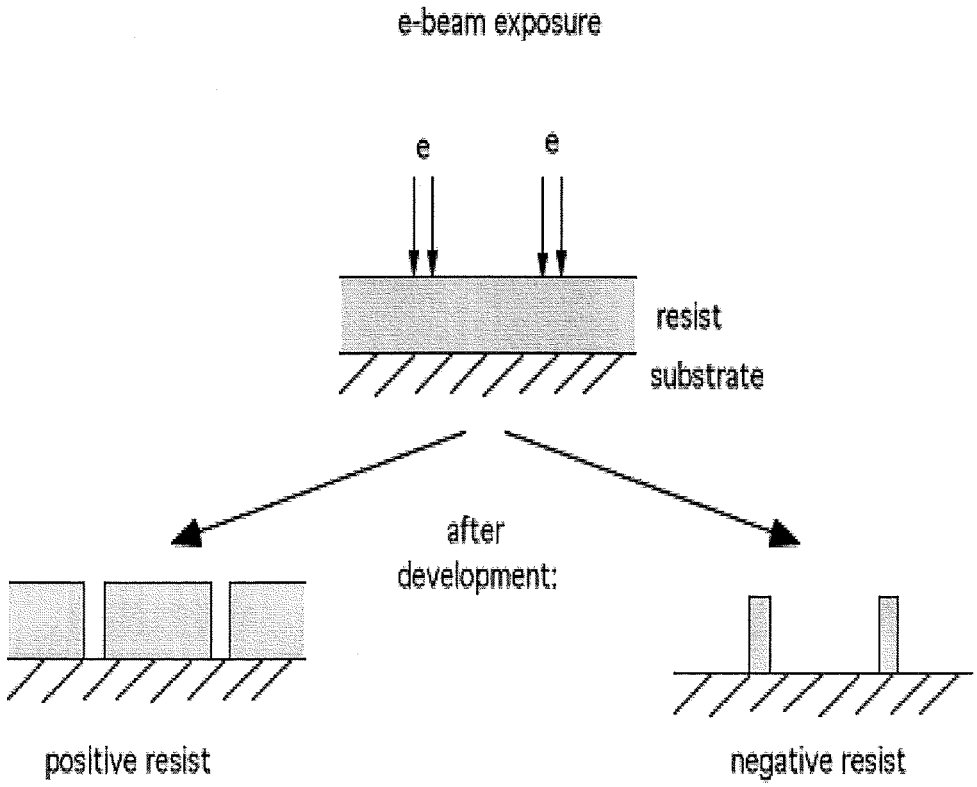

Figure 2. 6 Two types of resist. The principle of positive resist is bond scission on exposed area. The principle of negative resist is cross linking on exposed area.

In EBL, the smaller the beam size, the higher the resolution, but the high resolution mode takes more time to write the pattern. Exposure dose is defined by [112-113]:

$$D=\frac{It}{A} \qquad 2.10$$

D is the maximum dose (in coulombs per cm^2) delivered by a particular beam. I is the maximum current (in mA) of particular beam. A is the pixel area (in cm^2). t is dwell time per pixel (in second). Nowadays, the best resolution of an electron beam lithography is 5 nm, while that of optical photolithography is around 130 nm.

The advantages of EBL are high resolution, maskless, precise control of the energy and dose delivered to resist-coated substrate, ability to register accurately over small areas of a wafer, lower defect densities and a large depth of focus.

The disadvantages of EBL are that flood exposure is limited by chip size field due to difficulties in obtaining broad, collimated, charged-particle beams. Electrons scatter quickly in solids, limiting practical resolution to dimensions greater than 5 nm. Electrons need to be held in a vacuum, making the apparatus more complex than for photolithography, slower writing speed and high system cost. For more detail about the EBL can be found in reference [113].

The main EBL system has been used in this project is EBPG5, which has Gaussian shaped beam, vector scan writing strategy. Figure 2.7 [111] is schematic drawing of field emission gun of EBPG5 configuration and the electron optics. The system is under control of an Alpha computer. EBPG5 is the state-of-the-art e-beam lithography tool.

The main differences between a SEM converted EBL machine and an EBPG5 are that EBPG5 has higher acceleration voltage, bigger writing field and an alignment system.

The procedure for patterns generating in the EBPG5 are described in appendix A. Details of the computer process to operate the beam writing are given in reference [111].

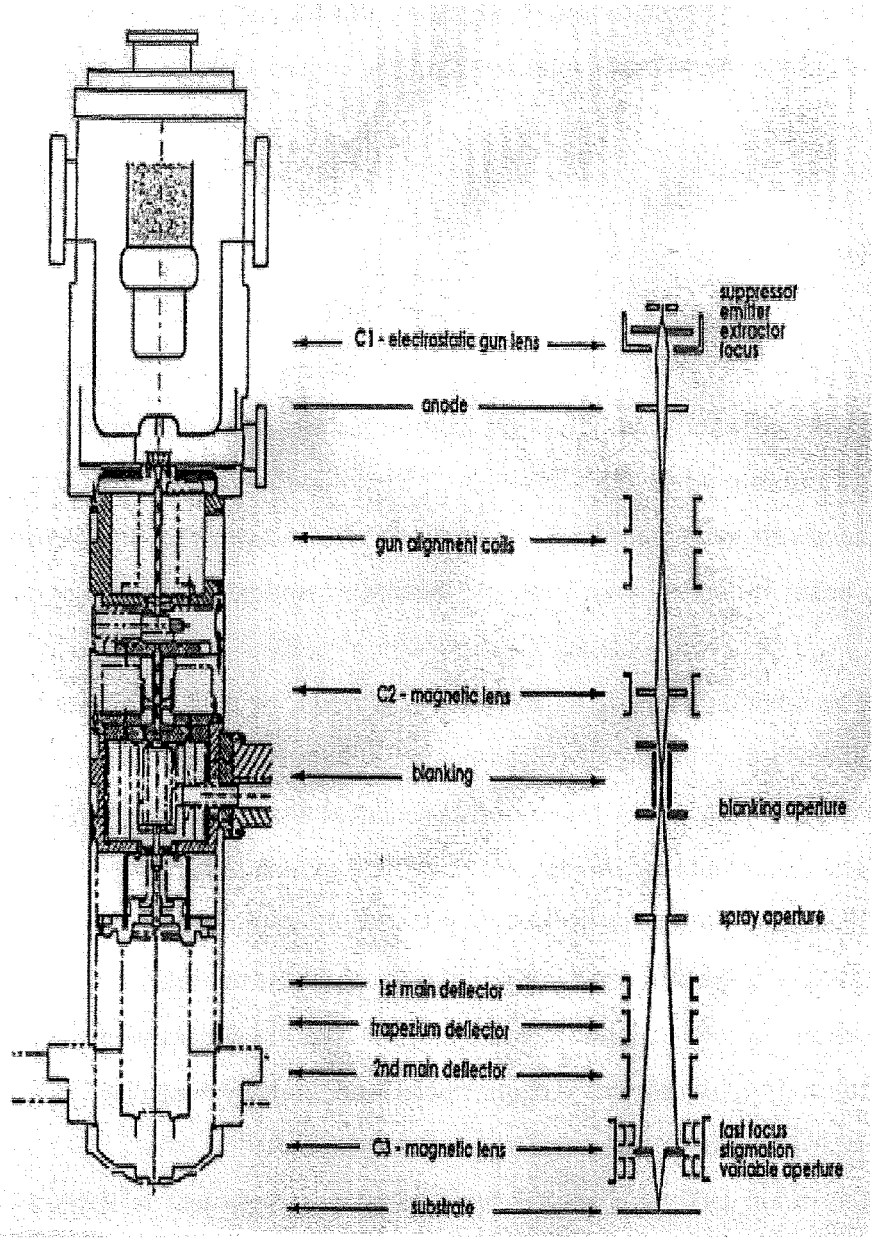

Figure 2. 7 Schematic drawing of field emission gun of EBPG5 configuration and electron optics.

It should be pointed out that the wafer must be pre-aligned. To align a pattern with respect to a previous layer, markers are required to measure the translation, rotation and keystone deformation of the wafer. The maximum correction of rotation is 0.2 °.

Precautions against contamination e.g. cracking of organic compounds, and external influences e.g. mechanical vibrations, electro-magnetic fields and thermal stability must be taken into account.

2.3 Inspection techniques

2.3.1 Profilometry (alpha-step)

The Alpha-step 500 surface profiler made by Tencor instruments has been used for etch depth measurements (from a few nanometres to a few micron). It measures the step-heights by scanning a surface with a stylus. The stylus is a part of a capacitor. A change in capacitance value is correlated to the change in step-height. As the stylus moves up and down, the instrument records its variation along the length measurement. It is a computerized, high-sensitivity surface profiler that measures roughness, waviness, and step height in a variety of applications. It features the ability to measure micron roughness, with up to 1 Å resolution over short distances as well as waviness over a full, 10 mm scan. The 80486 DX computer offers powerful measurement control, data storage, and analysis.

It is a very reliable, reasonable precision and useful instrument. Several factors could affect the measurements, such as environmental interference as well as stylus geometry and filtering. More details about the alpha-step 500 are give in reference [114].

2.3.2 Atomic force microscopy (AFM)

Atomic force microscopy is a family member of scanning probe microscopy (SPM), which is used to study surface properties with high resolution. Contact mode AFMs at DIMES of Technical University of Delft, Netherlands and Auckland University of New Zealand, have been employed. The principle of contact model AFM [115-116] is following. A tip attached to the end of a cantilever scans the sample surface while

the trace of tip is recoded in three dimension. Detail about installation and operation refer to reference [117].

The root mean square roughness (rms) and max height or relative peak to valley (r p-v) data extracted from AFM measurement, have been used to aid GaN damage analysis. The explanation of these values are as following.

$$rms_{(R_q)} = \sqrt{\frac{\Sigma(Z_i - Z_{ave})^2}{N}} \qquad 2.11$$

where Z_i is the particular point height, Z_{ave} is the average of all the Z values. N is the number of the point measured. The mean can have a negative value because the Z values are measured relative to the Z value when microscope is engaged. Maximum height (R_{max}) or r p-v is the difference in height between the highest and lowest point on the surface relative to the mean plane.

The data has been processed such that flatness is in the 1st order for whole image in two dimension x and y. Then the needed data is extracted.

2.4 Photoluminescence (PL) excitation spectroscopy

Photoluminescence is the radiative recombination of a sample excited by an optical source, typically a laser with energy $h\nu > E_g$, generating electron-hole pairs.

PL can provide simultaneous information on many types of impurities in a sample. However, only those impurities that can contribute to a radiative recombination process can be detected.

In our experiments, photoluminescence is excited by a 300 nm line of an argon laser. The absorption coefficient at this wavelength is about 10^5 cm^{-1} [118], which results a e^{-1} penetration depth of about 100 nm into the GaN material. The laser light with incident power of 2.5 mW is focused normally on to the sample plane in a back-scattering geometry. Luminescence is collected by quartz optics and focused to the entrance of a 0.75 m SPEX model 1700 spectrometer. The signal is detected by a thermo-electrically cooled photo-multiplier tube. The samples are

mounted in a closed cycle helium cryostat. Variable temperature experiments are performed between 20K and 250K.

According to Hovel [119], the PL intensity can be written by,

$$\Phi_{PL} = \frac{\Phi(1-R)\cos(\theta)}{\pi n(n+1)^2} \frac{L}{\tau_{rad} S_r} \qquad 2.12$$

where ϕ is the incident photon flux density, R the reflectivity, θ the emission angle, n the index of refraction, L the minority carrier diffusion length, τ_{rad} the radiative lifetime, and S_r the surface recombination velocity, which is related to surface states.

In our project, the as grown GaN sample has been compared with samples subjected to different etching processes. PL intensity is a measure of both surface and bulk. In this case, we keep using a series of sample from one wafer for a designed experiments to avoid other interference. Details refer to chapter 5 and chapter 7.

2.5 Electrical characterization

Many parameters can be used for semiconductor electrical characterization, such as resistivity, carrier and doping density, Schottky barrier, carrier lifetime and mobility. However, carrier and doping concentration, lifetime of carrier, mobility are more related to the bulk material, while Schottky diode properties and contact resistance are more related to semiconductor surface states, as manifesting from the dry etching process. So ohmic contact and Schottky diode properties have been selected to monitor top surface damage, and wire conductance to study sidewall damage in our project.

Ohmic contacts have linear or quasi-linear current-voltage characteristics. The contacts must be able to supply the necessary device current, and the voltage drop across the contact should be small compared to the voltage drops across the active device regions. It should not inject minority carriers. In addition, such ohmic contacts should be reproducible. An ideal I-V characteristics of ohmic contacts is

shown in figure 2.8a. While Schottky contacts should have rectifying behavior with distinctly nonlinear current-voltage characteristics. An ideal I-V characteristics of Schottky contact is shown in figure 2.8b. A Schottky contact only allows current to flow in the positive direction. In practice, a Schottky diode has a barrier and a leakage current, When the reverse voltage is big enough, the Schottky diode always breaks down, see figure 2.8c.

For ohmic contact and Schottky diode characterization, nominally undoped GaN on highly doped SiC substrate material has been used. Therefore, it is reasonable to assume current from one metal contact has gone through GaN film to SiC substrate and then pass the thickness of GaN film to another metal contact. A HP 4145 parameter analyzer has been employed to record the current by the varying input voltage. The resistance (R) consists of the resistance of two contacts (R_c) and the substrate (R_{sub}).

$$R = 2R_C + R_{sub} \qquad 2.13$$

Substrate resistance can be calculated by

$$R_{sub} = \frac{\rho l}{A} \qquad 2.14$$

$$\text{where } \rho = \frac{1}{ne\mu} \qquad 2.15$$

n is the semiconductor carrier density, e is the charge of electron, u is the mobility, l is the double thickness of GaN film (in this project), and A is the contact area.

R can be extracted from V/I measurement, the contact resistance can be obtained from equation 2.13.

The principle of data process for the Schottky barrier characterization will be presented in Chapter 4. The conductance measurement for sidewall depletion region will be presented in chapter 8.

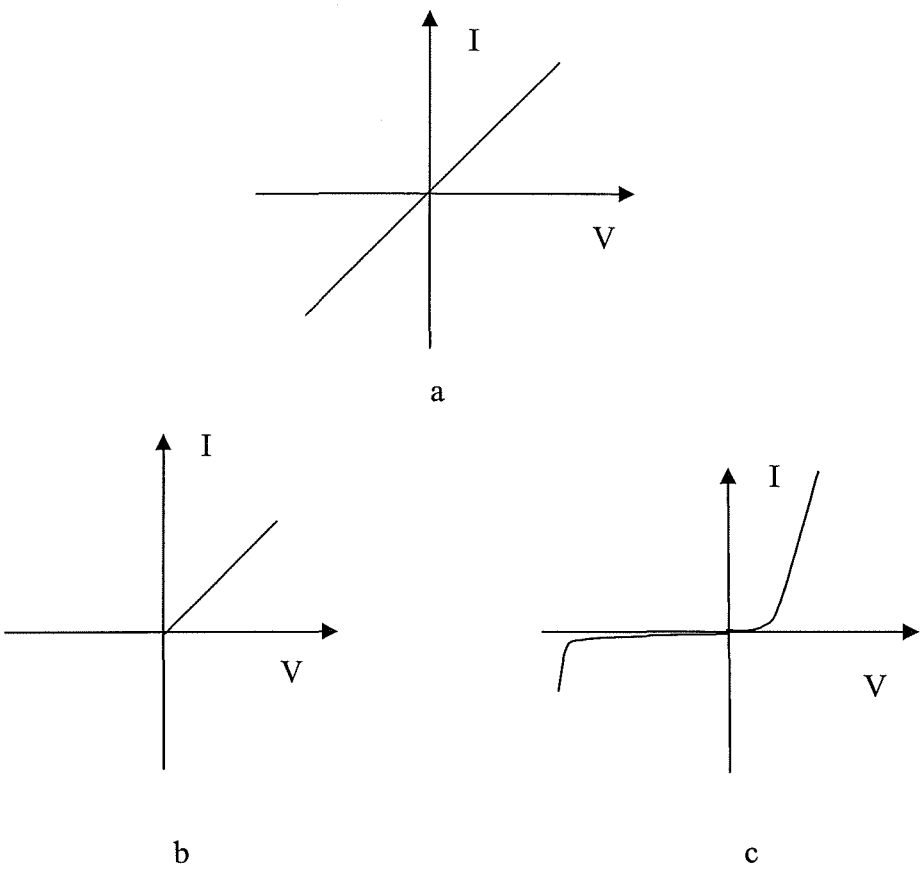

Figure 2. 8 Ideal I-V characteristics of a) ohmic contact, b) Schottky contact. An ideal Schottky contact only allows current to flow in the positive direction. c) A practical Schottky diode has a barrier and a leakage current.

2.6 X-ray photoelectron spectroscopy (XPS)

X-ray photoelectron spectroscopy (XPS) has been shown to be particularly useful in investigating plasma-surface interactions underlying dry etch behaviour [120]. XPS experiments are performed using a PHI 5400 ESCA instrument equipped with a dual anode (Mg / Al) X-ray source, a hemispherical analyzer and a precision angle substrate stage. Al Kα is used for spectra of Ga2p3/2, Ga3s, Cl2p, F1s and Mg Kα is used to detect the spectra of Ga3s, N1s, F1s. The Ga auger line overlaps with the N peak using Al radiation and overlaps with the Cl peak using Mg radiation. Thus, both

of radiation sources detect Ga peaks as a control. During experiments, the instrument was set at constant analyser pass energy of 71.55 eV, using unmonochromatised incident X-ray radiation. The electrons emitted from the specimen were detected at an angle of 45^{0} with respect to the specimen surface.

In this project, XPS has been used to analyze the chemical composition of dry etched surfaces. Samples have been transferred from the etchers to XPS strictly under nitrogen atmospheric ambient to avoid sample deterioration by air contamination [121]. The control sample follows the same procedure except the dry etching. The XPS spectra were obtained using the equipment at Material science department, Technical University of Delft, Netherlands with assistance of Dr Wim. Sloof.

2.6 Summary

The principle of dry etching has been explained in detail. RIE Oxford 80 plus and ICP (MET Lab) systems have been separately discussed and compared. There dry etch systems are used for pattern transfer, while EBL and optical lithography are used for pattern definition. For metallisation, thermal evaporation has been used. We did not discuss this technique because this is a standard method. A profilometer, so called Alpha–step, is used for etch depth measurement and AFM for surface roughness inspection, while scanning electron microscopy (SEM), has been employed for profile inspection and X-ray photoelectron spectroscopy has been used for surface composition analysis. All these techniques are important for characterization of nanofabrication technology, while plasma diagnostic equipments, like LP and OES, are used for correlating plasma and etch characteristics.

I-V characteristics of ohmic and Schottky diode are used to monitor the material surface states induced by etching process. The detailed description of GaN the diodes will be presented in Chapter 4. These methods are used for detecting top surface properties, while quantum wire device was designed to indicate the sidewall damage caused by etching process. The quantum wire device principle and device fabrication will be presented in chapter 9. Photoluminescence has been employed to detect the effects of etching process on optical properties by studying the changes in

PL intensities and the shifting of peak positions, which will be presented in chapter 5 and chapter 8.

Chapter 3

Nanostructure Pattern Fabrication•

3.1 Introduction

The fabrication and characterization of semiconductor nanostructure are essential because of the important role played by such structures in the development of new electronic and optoelectronic devices [122]. In many applications, the ability to transfer high resolution patterns in the nitride semiconductor is a critical step towards the fabrication of the final device [123]. Generally, etching techniques have been employed to transfer the pre-defined patterns into the underlying substrate. However, it is difficult to develop reliable processes and to obtain a controllable profile in the nanometer-scale using wet etching. Thus, dry etching techniques are highly desirable for fine pattern transfer [65].

In the past, high etch rates of GaN have been achieved using electron cyclotron resonance etching (ECR), magnetron reactive ion etching (MIE) and inductively coupled plasma etching (ICP) [54, 66, 67, 68]. While high etch rate techniques have been applied for the fabrication of optical devices, low etch rate techniques are desirable for electronic devices such as gate recessing in transistors.

This chapter describes the development of a SF_6+N_2 plasma process that allows fine lines and dots of nanometer dimension to be fabricated uniformly in GaN, as well as the optimization of profile with smooth surfaces. This has been achieved by varying the EBL dose and the etch gas mixture concentration of SF_6 and

• This chapter is based on the published papers " Fabrication of nanostructure" Microelectronic Eng. 54(1-4), (2000), pp 419-422 and "High resolution reactive ion etching of GaN and etch induced effects" J. Vac. Sci. Technol. B 17, (2000), pp 2759-2763.

N_2. The developed procedure has been applied for the fabrication of nano wires and dots into Si/Si_xN_y superlattices.

3.2 Fabrication process

The samples used in this study are nominally undoped 2.5 micron thick GaN with good surface morphology grown by metal organic vapor phase epitaxy (MOVPE) on c-plane sapphire substrate.

The wafer is scribed into a series of 5 X 5 mm^2 pieces, then cleaned in acetone in an ultrasonic bath, followed by rinsing in methanol and isopropanol alchohol (IPA). The samples are then blown dry with nitrogen gas and pre-baked in an oven at 85 °C to clean the surface from moisture.

The pattern has been designed as in figure 3.1 for one electron beam lithography (EBL) writing field. In a particular pattern block, for example, 50 nm x 200 nm means wires of 50 nm width and 200 nm length with a spacing of 200 nm. For the pattern design, L-edit software has been used.

A double layer of electron sensitive resist, polymethylmethacrylate (PMMA) with 4% low molecule weight (LMW 120K) PMMA dissolved in chlorobenzene and 2.5% high molecular weight (HMW 996K) PMMA dissolved in xylene, has been spun on the GaN substrate resulting in a total thickness of 120 nm. PMMA is one of the first materials developed for e-beam lithography. It is a standard positive e-beam resist and remains one of the highest resolution resist available. So, PMMA has been used for all e-beam pattern writing in this project. The spinning speed used is 3000 rpm and spinning time is 1 minute for every layer.

Chlorobenzene is a good solvent and used to form a thick bottom PMMA layer (~ 80 nm here). Xylene is a poor solvent, this prevent the bottom layer to be dissolved in the top layer during the top layer spinning. The high molecular weight PMMA on top of the low molecular weight PMMA leads to an enhanced undercut profile during developing, thus greatly improves the reliability and quality of the lift-off lines.

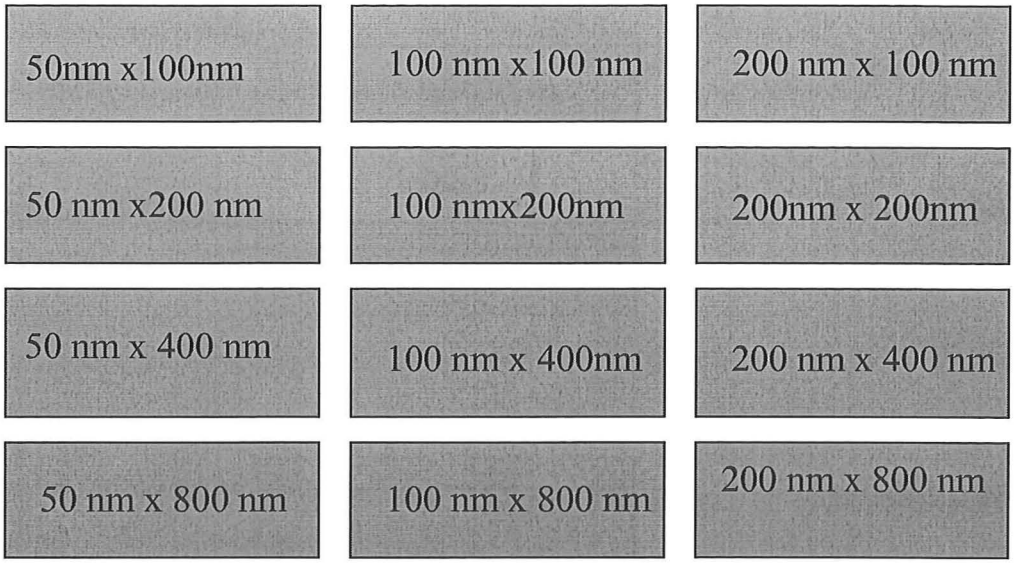

Figure 3. 1The pattern designed for one EBL field writing. In a particular pattern block, for example, 50 nm x 200 nm means wires of 50 nm width and 200 nm length with a spacing of 200 nm.

The electron beam lithography is performed using a converted Phillips PSEM 500 scanning electron microscope, which is operated at 50 kV. A beam size of 16 nm in diameter has been used to achieve proper line width, the exposure doses have been varied over a wide range from 300 $\mu C/cm^2$ to 3000 $\mu C/cm^2$. The exposed samples are developed in MIBK : IPA = 1 : 3, which dissolves the exposed resist, leaving unexposed resist behind.

Subsequently, the samples are coated with 80% Ni - 20% Cr alloy, which acts as the etching mask. The NiCr is deposited by thermal evaporation to a thickness of 30 nm. It is worth pointing that before evaporation, the evaporator chamber should be cooled down for about an half hour to achieve a better background pressure and film adhesion.

The lift-off technique is applied to reveal the etching mask. The samples are immersed in acetone, which is a strong solvent of PMMA, to remove the unwanted metal (lift-off). For the fine wires and dots, a plastics squeeze mouth has been used to promote the lift off process.

Sample clean and pattern design

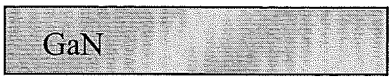

e beam exposure

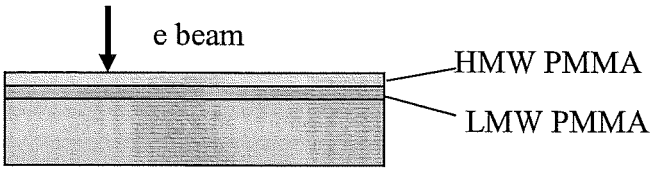

Development

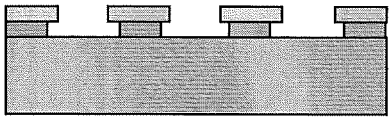

Metallization by thermal evaporator

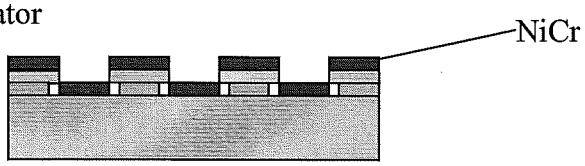

Additive pattern transfer by lift off process

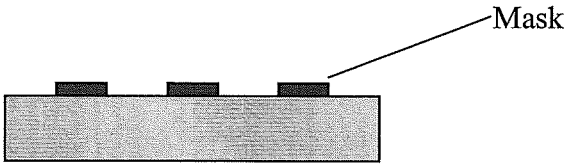

Subtractive pattern transfer by RIE

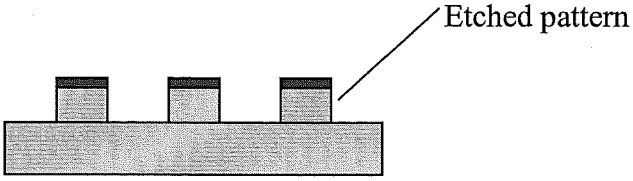

Wet etch to remove residual mask

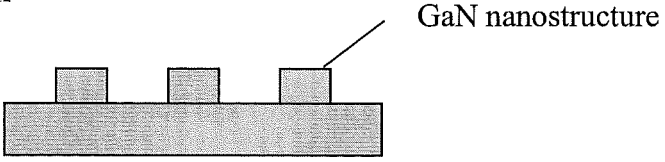

Figure 3. 2 Fabrication process of nanometer structure on GaN and Si/Si_xN_y.

The reactive ion etching process has been carried out using an Oxford Plasmalab 80 plus system with the following etching conditions: rf power density, 0.45 W/cm^2, etching pressure, 19.5 μbar, substrate temperature, 50 °C, variation of N_2, from 0% to 75% and total gas flow rates, 40 sccm (SF_6 + N_2). The fabrication process is shown in figure 3.2.

The etch profiles have been inspected using scanning electron microscopy. The etch depth has been measured using a Dektak II surface profiler. To determine the degree of the sloped profiles, the angles between the inner sidewall and substrate surface are calculated from $\tan^{-1}$ D/S = α, where D is the etched depth and S is the distance between the actual profile compared to the anisotropic one, (see figure.3.3b). Figure 3.3a will be discussed later.

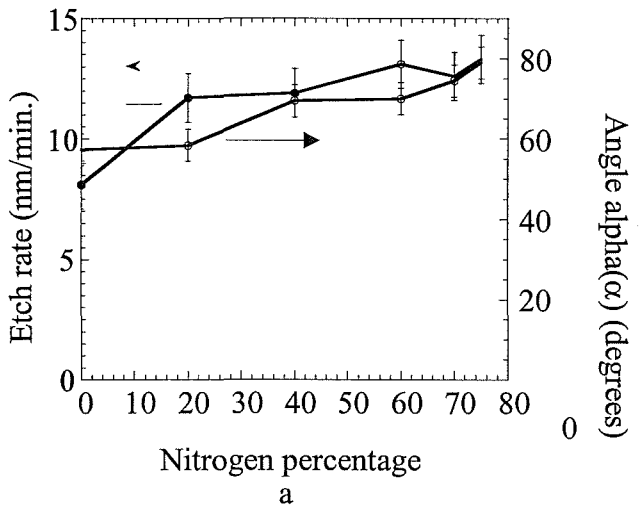

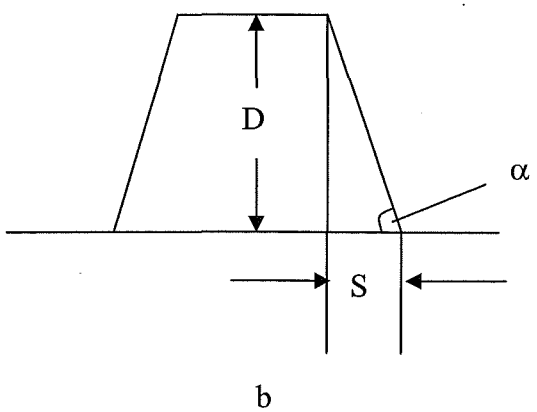

Figure 3. 3 a) Etch rate and profile dependence on %N_2 in SF_6 plasma, b) Schematic drawing of profile and the angle α.

To assess the microscopic roughness of the GaN surfaces before and after etching, atomic force microscopy (at Auckland University) has been employed. A 4 μm x 4 μm dimension of the surface area has been selected for random verification the surface roughness.

3.3 Results and discussion

3.3.1 Dose optimization for GaN EBL

In EBL, dose optimization plays an important role, thus dose optimization for nanostructure pattern fabrication has been focused on first. Other workers have performed much experimental work on resist and dose [113, 124]. If one exposes a positive resist to a range of doses and then develop the pattern, ideally, the film thickness of resist exposed, would drop abruptly to zero at the critical dose. The bigger the dose used, the cleaner the exposed surface. In practice, in order to minimize bias and proximity effects, positive resists should be exposed and/or developed as lightly as possible while still fulfilling the conditions of a clean surface.

For the given double layers PMMA, the doses from 300 $\mu C/cm^2$ to 3000 $\mu C/cm^2$ with a step of 100 $\mu C/cm^2$ have been verified. For narrow wires, such as 50 nm, 100 nm or 200 nm wide, doses smaller than 1000 $\mu C/cm^2$ do not give good result in the EBL system at Canterbury university. Average estimation from experiments, the doses between 2000 $\mu C/cm^2$ and 2500 $\mu C/cm^2$ are the optimum for 100 nm and 200 nm wires and dots writing in this EBL system. 50 nm wires or dots could not be successfully fabricated. It is under exposed if small doses are used, while it has been washed away if high dose, such as 3000 $\mu C/cm^2$, is used.

Figure 3.4 shows SEM images of GaN gratings using doses of 1200 $\mu C/cm^2$, 1400 $\mu C/cm^2$ and 2100 $\mu C/cm^2$ respectively. The numbers on the patterns, are related to the dose for easy distinguishing. All these images are from one sample, which means that the etching conditions are the same for all structures.

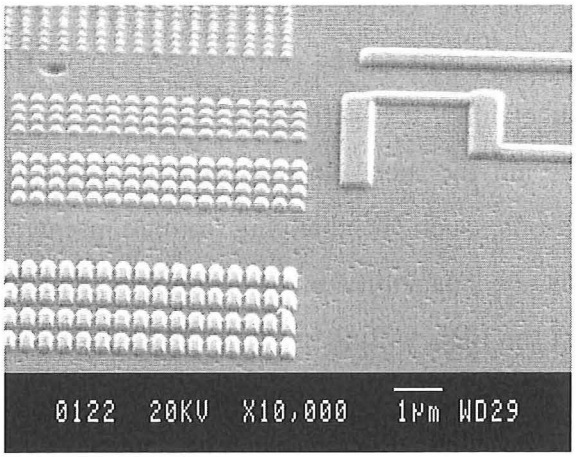

a

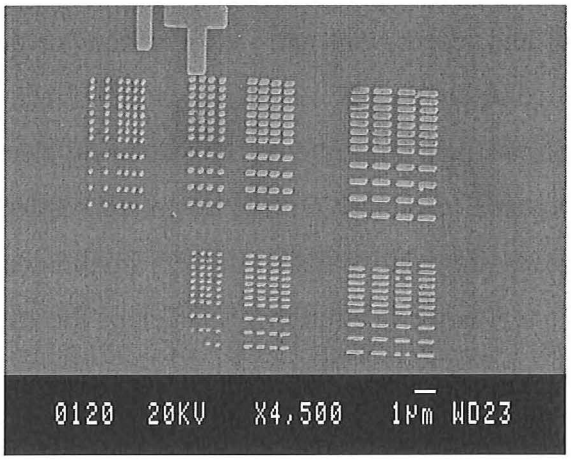

b

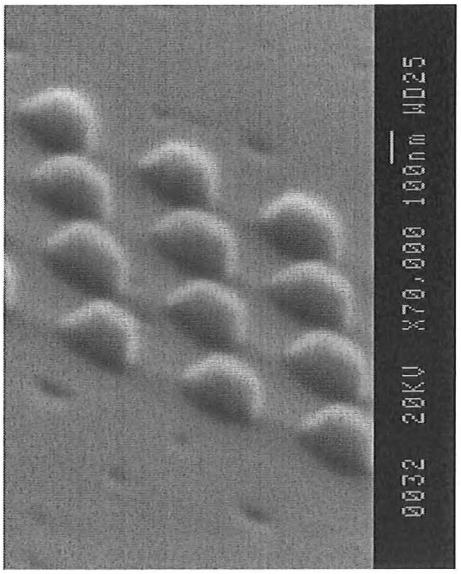

c

Figure 3. 4 a) SEM images of GaN wires and dots after subtractive pattern transfer using dose a) 1400 $\mu C/cm^2$, b) 1200 $\mu C/cm^2$ and c) 2100 $\mu C/cm^2$.

Figure 3.4a shows 200 nm wires clearly. Figure 3.4b shows that 200 nm wires and 100 nm wires and dots can be resolved. However, 100 nm x 100 nm dots have disappeared after etching. It is difficult to determine the absolute value of the dose, since PMMA is not the most electron sensitive resist, however it has high resolution. Other reasons, such as changing sample preparation conditions and instrumental functions, i.e. instability in beam current, and focusing to the same degree etc., will affect the EBL writing as well. Figure 3.4c shows the nano dots by using a dose of 2100 $\mu C/cm^2$.

The dose needs to be more accurately determined for high-density patterns. Over exposure or exposure with high acceleration voltage will broaden the designed pattern for both width and length, and narrow the spaces or even join the isolated pattern. This is resulted from the so called proximity effect. Proximity effect is unwanted exposure in resist and substrate due to scattering electrons. A narrow line between two large exposed area may receive so many scattering electrons that it actually can develop away (in positive resist) while a small isolated feature may lose some of its dose due to scattering electron that it develops incompletely.

There are some examples of what happens to test patterns when proximity effects are not corrected for. Figure 3.5 shows SEM image of designed structures with 200 nm width pattern defined by EBL. The obtained final pattern, is much wider than that of the original design. The high density patterns are joint. The original spacing of 200 nm has

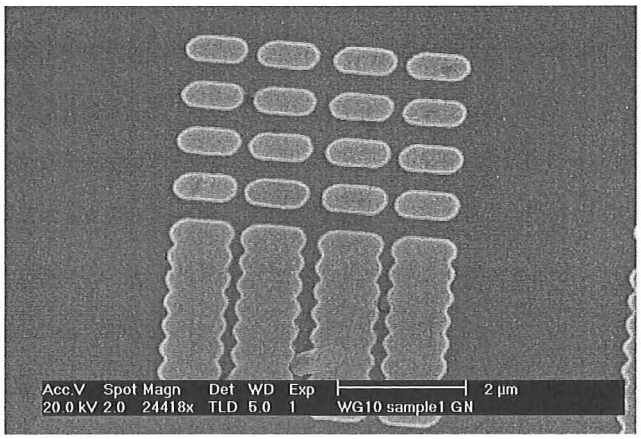

Figure 3. 5 Over exposure for both low density and high density pattern, wires are much larger than original designed pattern.

.

been totally filled up. It is clear the dose used here has been too high for producing high density patterns

The patterns shown in figure 3.6 are a bit wider than that of the original designed patterns of 200 nm. However, the wires can be resolved in both low and high density pattern. Obviously, the dose used here is reasonable for the low density pattern, however the dose seems still too high for the high density pattern.

Figure 3.7 shows that wires have been well defined and transferred in both lower density and high density patterns. The wires width seems close to 200 nm, the original designed pattern width. It is clear that the dose used here is good.

From above observation, we can see that proximity effect plays an important role. Proximity effect is always present. In low density patterns, the proximity effect will not seriously show out. While in high density patterns, proximity effect needs to be taken into account seriously. Many different schemes have been devised to minimize the proximity effect. If a pattern has a fairly uniform density and line width, then all that may be required is to adjust the overall dose until the patterns come out in the proper size. Acceleration voltage is one of the main factor cause proximity effect. High voltages, from 50 kV to 100 kV or more, minimize forward scattering, although in the same case, this can increase the back scattering [113].

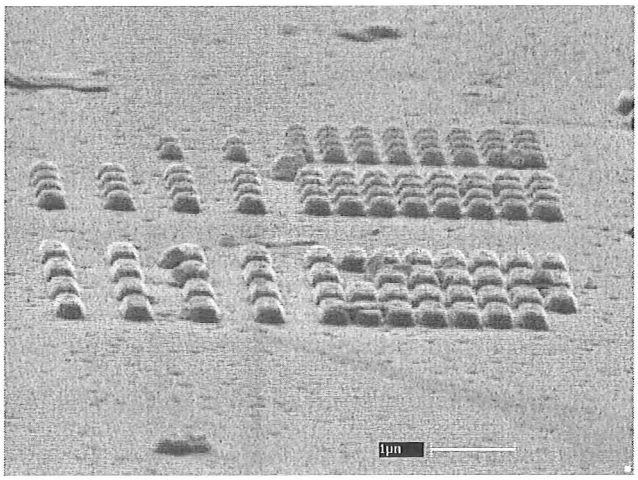

Figure 3. 6 Wires are a bit wider than the design, but can be resolved in both low density and high density pattern.

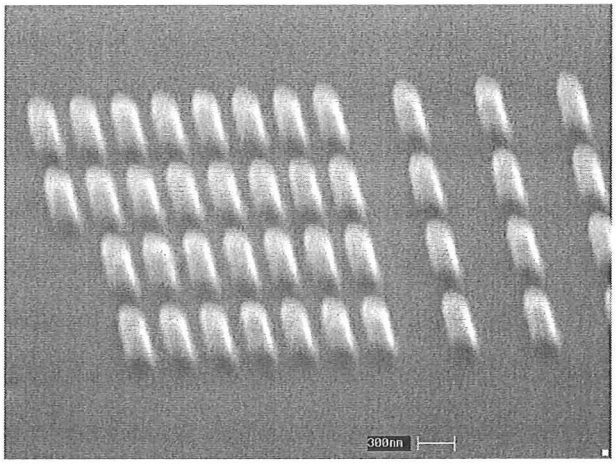

Figure 3. 7 Well defined wires in both low density and high density pattern.

Low acceleration voltage causes less proximity effect. By going to very low beam energies, where the electron range is smaller than the minimum feature size, the proximity effect can be eliminated [113]. The disadvantage is that the thickness of a single layer resist must also be less than the minimum feature size so that the electrons can expose the entire film thickness. In addition, the system design is much harder for low voltage since the electrons are more difficult to focus into a small spot and more sensitive to stray electrostatic and magnetic fields.

3.3.2 Etch optimization

The effect of varying the $\%N_2$ in the SF_6 + N_2 gas mixture on the etch rate and profile is shown in figure 3.3a. It can be seen that at low $\%N_2$ addition, the etch rate increases significantly and saturates at high $\%N_2$ addition. In addition, the dependence of the angle between the inner sidewall and the substrate surface, α, increases as N_2 content is increased from 0 to 75% in the etch gas mixture. All the patterns have been transferred uniformly into GaN.

Figure 3.8 shows scanning electron micrographs of typical GaN dots, which have been etched in 80% SF_6 + 20% N_2. A round top can be seen clearly (Residual NiCr mask has not been removed).

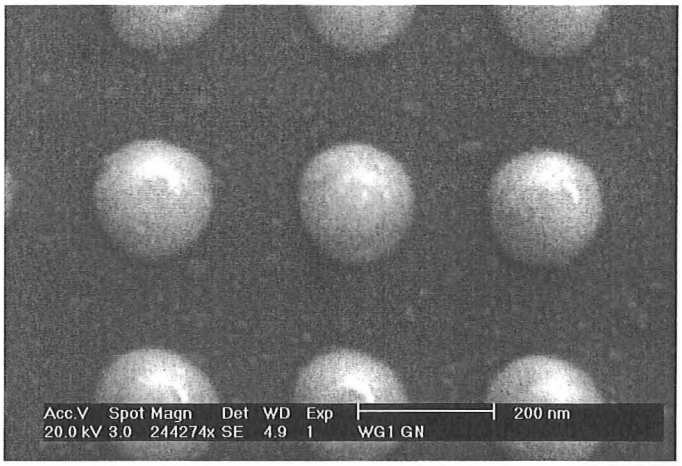

Figure 3. 8 Scanning electron micrographs of typical GaN dots, which have been etched in 80% SF_6 + 20% N_2. Detail etch conditions see text. A round top can be seen clearly.

Figure 3.9 shows scanning electron micrographs of typical GaN wires, which has been etched in 25% SF_6 + 75% N_2 (The NiCr mask has not been removed). The view point of figure 3.9a and 3.9b has a 90 ° difference. The Figure 3.9a has been imaged facing the width of wire, while the figure 3.9b has been imaged by facing the length of wire. A round corner can be observed clearly from both images.

The rounding of the top of the pattern is probably caused by faceting. In serious cases of faceting, the etching has a pronounced effect on the sidewall angle. Only 30 nm NiCr has been used as an etch mask. In this case faceting is most likely to occur due to the thinner layer at the mask edge, which is etched away during GaN etching.

The sidewall slope is more emphasized in a smaller dimension pattern than that in a bigger one (The etching profile shown in 3.9 looks like more vertical, compared the other two). The sidewall slope is possible caused by faceting and /or redeposition, which will be explained more detail in chapter 6.

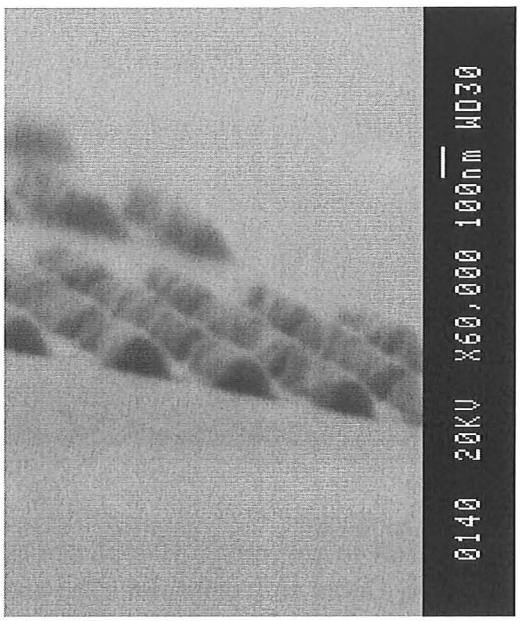

a

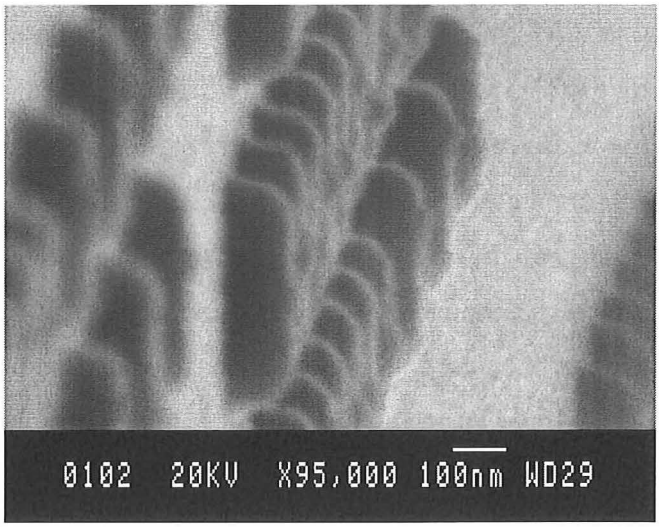

b

Figure 3. 9 SEM image of GaN wires etched in 25% SF_6 + 75% N_2 are imaged from different angles. The view point of a and b has 90 ° difference. A round corner can be observed clearly.

We have studied the surface roughness of GaN before and after etching using atomic force microscopy (AFM). Figure 3.10a shows an AFM image of 4 μm x 4 μm area for the unetched surface while figure 3.10 b) and c) show AFM images for the

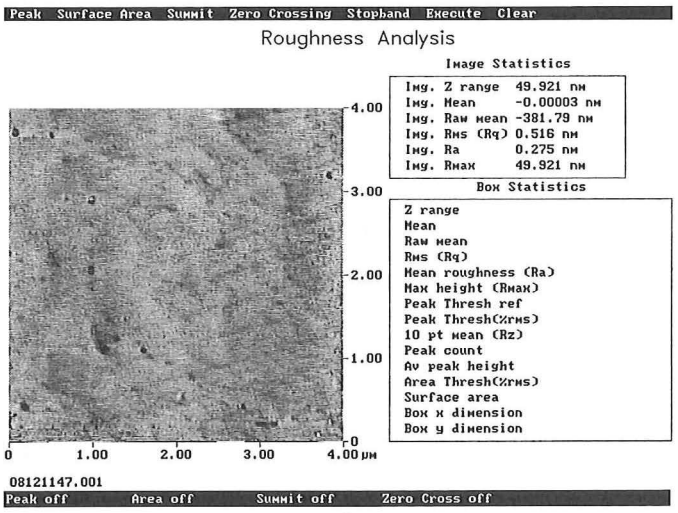

a

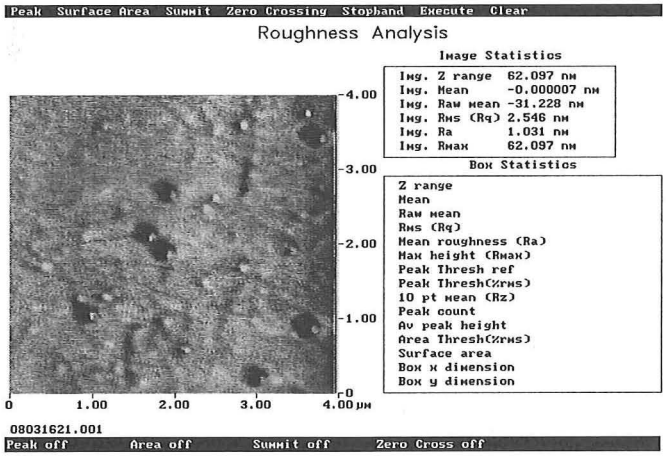

b

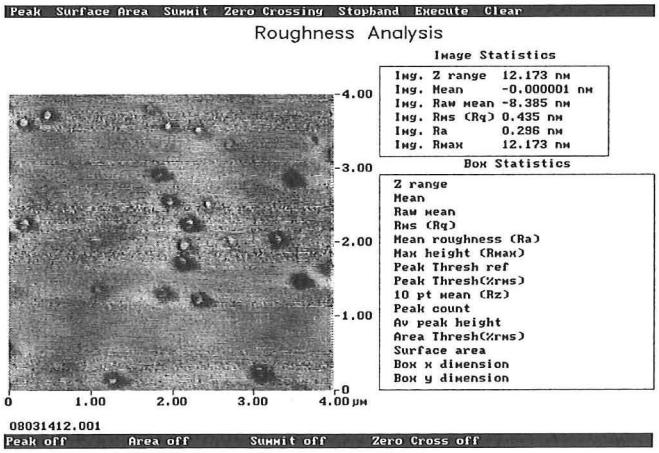

c

Figure 3. 10 a) AFM image of unetched GaN surface, b) GaN surface etched in 100% SF_6, c) GaN surface etched in 25% SF_6 + 75% N_2.

100% SF_6 etched and 25% SF_6 + 75% N_2 etched GaN surfaces respectively with the same size of area. The formation of pits are observed clearly on the RIE etched surfaces, also shown in SEM image in figure 3.4c, and has been reported previously [33].

The root mean square (rms) surface roughness as a function of N_2 content in the gas mixture is shown in table 3.1. It can be seen that surface roughness after etching is dependent on the $\%N_2$ in the gas mixture. The general trend is that as $\%N_2$ increases, the rms surface roughness is reduced. Microscopically smooth surfaces compared to the unetched surface are evident at N_2 concentrations of higher than 50%.

Table 3. 1 Root mean square surface roughness as a function of N_2 concentration in SF_6 plasma, as determined by AFM

Sample	rms roughness (nm)
Unetched	0.516
0% N_2	2.546
20%N_2	1.294
40% N_2	0.785
60% N_2	0.464
70% N_2	0.382
75% N_2	0.435

The observed increase in the etch rate, the improvement towards anisotropy in the etch profile and the smoother surfaces obtained with increasing N_2 content in the gas mixture may be caused by a number of possible mechanisms. In the reactive ion etching of GaN in SF_6 plasma, non-volatile GaF_X is produced [53], which is probably not removed efficiently. Therefore, the non-volatile GaF_X accumulates with etching time, resulting in the observed slow etching rate, over-cut profile and rough surface.

With the addition of N_2 in the SF_6 plasma, the presence of N_2 and its associated atomic species may 1) remove the GaF_X efficiently by physical bombardment, 2) react with GaF_X to form volatile NF_x and/or 3) react with nitrogen from GaN to form N_2 [125]. It is worth pointing out that the Ga-N band distance

(3.18 Å) is much larger than that of an N-N single bond distance (~1.5 Å). This has been described in section 1.2, crystal structure of chapter 1. 4) have possible charge exchange [126] of N_2^+ with fluorine containing species, result in larger fluorine ion density. One or more of these mechanisms may serve to enhance the etch rate, cause the sidewall profiles to become more vertical and smoothen the microscopic surface roughness as N_2 content in the gas mixture increases.

It is obvious that the N_2 plays an important role in etching behavior of nitride compounds. N_2 addition to fluorine plasma in etching Si_xN_y increases the etch rate. Now it has been found that adding N_2 to fluorine (SF_6) increases the etch rate in etching GaN. However, the exact nature of N_2 in the plasma needs further investigation. The N_2 role in etching behavior and creating electrical and optical damage will be discussed in chapter 4, 5, 6, 7 and 8 correspondingly.

3.4 The application of nanofabrication technique in Si/Si_xN_y super-lattice

The prospects for integrated Si electronics and optoelectronics make light emission from Si-based material a very active area of research [127]. The observation of visible PL emission from thin multi-layers consisting of 6 to 8 periods of a-Si/SiO_2 has been obtained by successive vacuum deposition of Si and ex-situ exposure to UV ozone [128]. Research on the fabrication of nano dots and wires on Si/Si_xN_y multi-layer grown by Institute for Microstructural Sciences, National Research Council Canada has been undertaken as research collaboration.

The materials used for fabrication consist of 10 layers of Si 1.9 nm and Si_xN_y 0.8 nm on Si substrate with good surface morphology. Figure 3.11 is a schematic drawing of Si/Si_xN_y structure. The Si/Si_xN_y multi-layers have been deposited on (001) Si by electron gun Si evaporation and periodic electron cyclotron resonance (ECR) plasma nitridation [128]. Exposure to the nitrogen plasma resulted in the formation of a thin Si_xN_y layer, whose thickness was self-limited and controlled by process parameters.

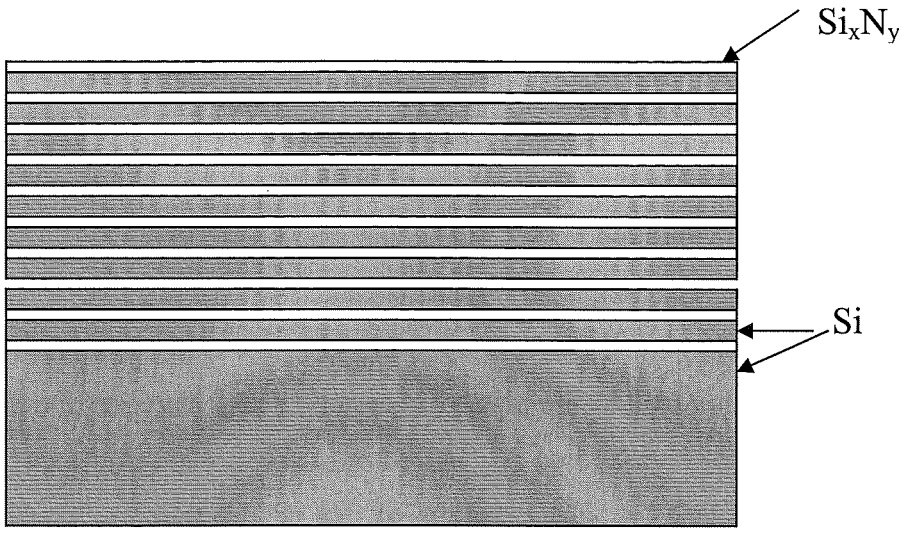

Figure 3. 11 Schematic drawing of Si/ Si_xN_y super-lattice structure.

To fabricate quantum wires and dots on Si/SiN multi-layers, we used the same procedure developed for GaN. This includes cleaning, pattern definition, development, metallization and lift off. The major difference was the etching gas composition. The gases used for growing Si/Si_xN_y is a mixture of CHF_3 and Ar.

Vertical quantum wires and dots with smooth surface and sidewall have been uniformly fabricated into Si/Si_xN_y material. Figure 3.12a is a SEM image of quantum wires on the Si/Si_xN_y multi-layers. The sidewall vertical nature is quite reasonable. Figure 3.12b is an AFM 3D image of quantum dots. Read from the images, the diameter of dots is about 70nm. The tapered sidewall is more obvious than the figure 3.12a. They are from the same sample.

The sample is etched with the following condition: a gas composition of CHF_3 : Ar = 1 : 1, a total flow rate of 42.5 sccm, an etching pressure of 32.5 μbar, a substrate temperature of 25 °C, rf power of 200 W, dc bias of 455 V and an etching time of 1 minute.

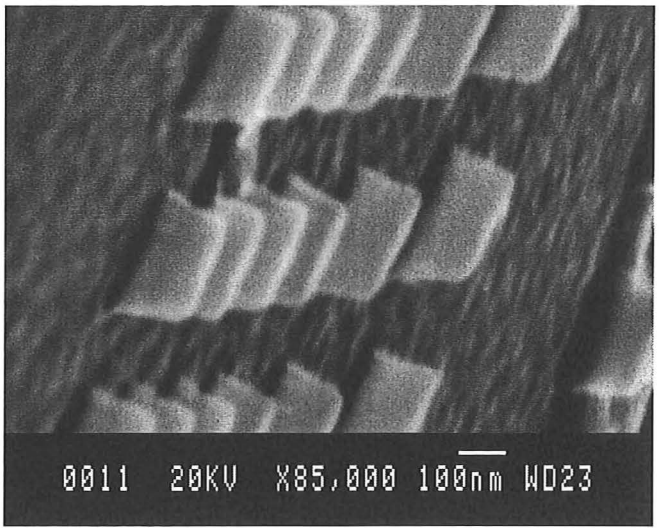

a

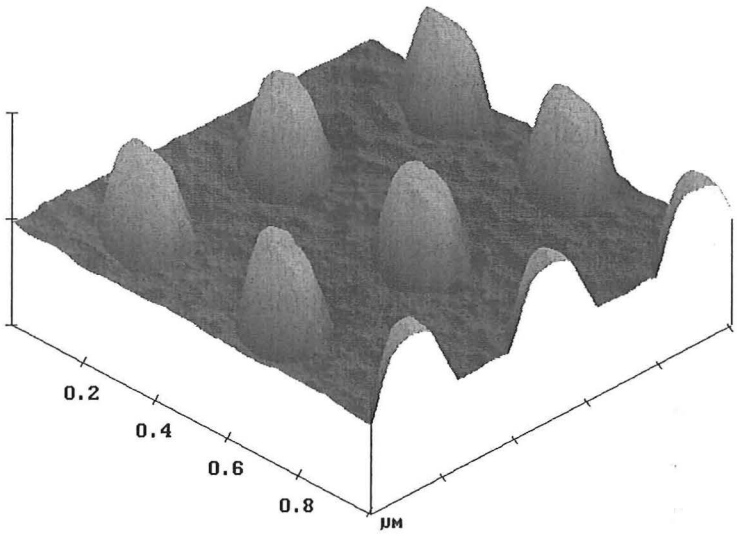

b

Figure 3. 12 a) SEM image and b) AFM 3D image of quantum wires and dots on Si/Si_xN_y multi-layers with etching conditions of gas composition CHF_3 : Ar = 1 : 1, total flow rate 42.5 sccm, etching pressure 32.5 μbar, substrate temperature 25 °C, rf power 200 W, dc bias 455 V, etching time 1 minute.

3.5 Summary

A process that allows the transfer of high-resolution nanometer-scale patterns into GaN has been developed. The e-beam dose has been optimized for the given double layers PMMA resist and the designed pattern. The doses of 2000 μC/ cm^2 to 2500

$\mu C/ cm^2$ are good for 100 nm and 200 nm dots and wires definition in the EBL system in Canterbury University.

The influence of the composition of etch gas mixture on etch rate, profile and microscopic surface roughness has been investigated. The effort has concentrated on obtaining fine patterns with steep sidewalls and smooth etched surfaces for device applications. The addition of N_2 in a $SF_6 + N_2$ gas mixture increases the etch rate, leads to more vertical sidewalls and decreases the microscopic surface roughness in the transfer of nanometre-scale GaN lines and dots. With a gas mixture of $N_2 : SF_6 = 3 : 1$, an etch rate of ~13.3 nm/min, wall to substrate surface angle of 80 ° and a root mean square surface roughness of 0.435 nm were obtained.

N_2 seems to play an important role in etching GaN, however the exact nature of N_2 role is unrevealed.

The developed procedure, but with a different etched gas composition, has been successfully applied in Si/Si_xN_y super-lattice for the fabrication of sub–100nm quantum dots.

The rounding top of the pattern is probably caused by faceting, which has a pronounced effect on the sidewall angle. In the case of thin mask, faceting is most likely to occur due to the thinner layer at the mask edge, which could be etched away during GaN etching.

Chapter 4

Reactive Ion Etching Induced Damage Effects on Electrical Properties*

4.1 Introduction

The high bond energy (robustness) of GaN and its related materials, as well as the high resolution demands in the fabrication of GaN nano-devices, make it essential to develop dry etching technologies for their processing. However, dry etching is known to induce damage, which may have serious effects on the electrical characteristics [129]. For example, during ion-enhanced dry etching, point defects and defect clusters are introduced into the substrate, which may affect the device characteristics [44]. Thus, the investigation and minimization of etch-induced damage effects in GaN is of utmost importance

Many gases have been employed for the dry etching of GaN [65, 67]. In particular, a low-pressure Cl_2/N_2 based plasma offers the possibility of fabricating almost vertical sidewalls without increasing surface roughness while maintaining sufficiently high etch rates [59]. Cl_2 reactive ion etching for the gate-recessing of GaN field-effect transistors have been demonstrated but with partial success [130], due to degradation of electrical properties. Lately, SF_6 has become an interesting alternative. Addition of N_2 to the SF_6 gas mixture has been shown to increase the etching rate, improve sidewall profile to be more vertical while maintaining the surface smooth for the fabrication of nanometer structures in GaN [20]. However, X. A. Cao et al [75] has found that compared to H_2 plasmas, N_2 plasmas cause more degradation in breakdown voltage of GaN Schottky diodes.

* This chapter is based on the published paper "Effects of reactive ion etch induced damage on electrical characteristics in GaN" J. Vac. Sci. Technol. B 18, (2000), pp 3467-3470.

In this chapter, a systematic study of reactive ion etch-induced effects on the electrical properties of GaN exposed to Ar, N_2, as well as SF_6 + N_2 plasmas will be presented. We also attempt to clarify the role of N_2 in the etch gas mixture and the importance of ion mass in inducing etch damage. The related results have been compared with etch effects on ohmic contacts produced on SiC substrates and effects of etch induced damage on GaAs diode characteristics.

4.2 Experimental detail

The material used is nominally undoped (n ~ 10^{17} cm^{-3}) 0.5 micron thick GaN with good surface morphology grown by metal-organic vapor-phase epitaxy (MOVPE) on SiC substrate. Plasma etching is carried out in an Oxford Plasmalab 80 Plus system with the following conditions for the argon plasma (bombardment): power densities of 0.41W/cm^2, 0.16 W/cm^2 and 0.03 W/cm^2, resulting in the dc biases of 477 V, 260 V and 95 V respectively. The substrate temperature of 50 °C, a total gas flow rate of 40sccm and etch pressure of 19.5 μbar were kept constant. In the case of SF_6 + N_2 plasma etching, a power density of 0.45 W/cm^2 was used, with varying percentages of N_2 added to the SF_6 plasma, giving a dc bias of around 440 V. The etching pressure has been kept constant in all experiments at 15 mTorr.

For the ohmic contact experiments, GaN surfaces are subjected to an argon ion bombardment at power densities varied from 0.03 W/cm^2 to 0.41W/cm^2. Optical lithography is used to define the patterns in the photoresist for the ohmic contact with total area of 200 μm x 200 μm. The mask pattern is shown in figure 2.4. Subsequently, thermal evaporation is used to evaporate 40 nm aluminum, capped by 40 nm gold on the etched GaN surfaces and on the control samples. Then standard lift-off technique is employed to obtain the ohmic contact pads.

For the diode experiments, ohmic contacts using Al/Au have been fabricated initially on the four corners of the unetched GaN samples. Then positive photo-resist (S1813) has been spun on the sample followed by optical lithography and standard development. The photo-resist patterned samples are then exposed to the plasma. Before evaporation of the Schottky contact, the samples have been treated with HCl:

DI water =1 : 1 for 30 seconds at room temperature. Gold, palladium, titanium and nichrome have been investigated for Schottky contact fabrication. After thermal evaporation, lift off technique is employed, and both Schottky and ohmic contacts on the same GaN surfaces have then been ready for measurement.

A Hewlett Packard (HP) 4155 semiconductor parameter analyser has been used to measure the current-voltage (I-V) characteristics. The error bars, indicated in the figures, correspond to the standard deviation from the average for the groups of contacts measured from each sample.

Atomic force microscopy (AFM Nano-Scope IIIa in Auckland University, New Zealand) has been used to monitor the microscopic surface roughness resulting from the plasma exposure. Additional GaN samples have been etched in each experiment for this purpose

4.3 Data analysis principle

The band diagram of a Schottky diode on an n-type substrate is shown in figure 1.3. The ideal barrier height of Φ_o is approached only when the diode is strongly reverse biased. The actual barrier height Φ_b is less than Φ_o due to image force barrier lowering and other factors. For instance, etch damage may induce more surface states, and therefore, change the barrier height. The built-in potential V_i is the electrostatic potential difference between free electrons in the conduction band on either side of the junction, and V_o is the potential of the semiconductor Fermi Level with respect to the conduction band

The thermionic current -voltage relationship of a Schottky barrier diode, provided that the forward bias is not too large, is given in theory by [90].

$$I = I_s \left(\exp\left(\frac{qV}{kT}\right) - 1 \right) \qquad 4.1$$

$$\text{with } I_s = AA^*T^2 \exp\left(\frac{-q\phi_b}{kT}\right) \qquad 4.2$$

I_s is the saturation current (mA), k is the Boltzmann's constant, A is the diode area (cm^2) T is the temperature (K), and A^* is Richardson's constant. Theoretical value of $A^* = 26$ A/cm^2 K^2 is for GaN and 4.4 x 10^4 A/cm^2 K^2 is for GaAs. Richardson constant varies greatly with processing conditions such as annealing [90]. Therefore, we plot an I-V curve to evaluate the data for the annealing case. Φ_b is the effective barrier height (eV).

In practice, diodes never satisfy the ideal equation 4.1 exactly and the modified equation is given by:

$$I = I_s \exp\left(\frac{qV}{nkT}\right)\left[1 - \exp\left(\frac{-qV}{kT}\right)\right] \qquad 4.3$$

Or expressed as [90]

$$I = I_s\left(\exp\left(\frac{qV}{nkT}\right) - 1\right) \qquad 4.4$$

Where n is the ideality factor. The ideality factor n incorporates all those unknown defects which makes the device conduction mechanism non-ideal. In principle, diffusion dominating the conduction leads to an ideality factor of 1, and when recombination dominating the conduction, it leads to an ideality factor of 2. It is not easy to determine the control factor in practice. In addition, a Schottky contact is unlikely to be uniform over its entire area. Barrier height patchiness leads to n>1 and responsible for other effects such as the decrease in n with temperature and with increasing reverse bias [131].

For values of V> 3kT/q, equation 4.3 can be written as a simple form

$$I=I_s \exp\left(\frac{qV}{nkT}\right) \quad 4.5$$

Equations 4.5 and 4.2 have been used for the analysis of the I-V diode data recorded here. I_s can be obtained by an extrapolation of the log (I) versus V curve to V = 0. The barrier height is calculated from the current I_s, using equation 4.2. This means the barrier height determined is valid for zero bias. Then from equation 4.5, one can calculate ideality factor n.

4.4 Results and discussion

4.4.1 RIE pre-exposure effects on ohmic contact characteristics of GaN

According to literature information [82,84,87] many metals have been evaluated for ohmic contact on GaN grown on SiC substrates.

It is difficult to make ohmic contacts on wide-gap semiconductors. A metal does not generally exist with a low enough work function to yield a low barrier. In such cases, the general technique for making an ohmic contact involves the establishment of a heavily doped surface layer such as metal-n^+-n or metal-p^+-p contact by various methods, such as shallow diffusion, alloy regrowth, in-diffusion of a dopant contained in the contact material and ion implantation. In our work, ohmic contacts using Al/Au (40 nm/40 nm) have been successfully fabricated on n-GaN without an annealing step. This is due to the possibility that Al tends to replace Ga [132] and atomically forming a mixture layer between the metal and semiconductor.

Secondly, ohmic contacts have been fabricated using Al/Au on unetched GaN surface and surfaces subjected to argon plasma exposure at different power densities. Figure 4.1 shows the current-voltage (I-V) characteristics as a function of argon-plasma power density. In the etched samples, the data show a trend of decreasing ohmic contact resistance with decreasing etch power density. The lowest specific contact resistance of 0.075 ohm-cm^2 is obtained after argon bombardment at a power

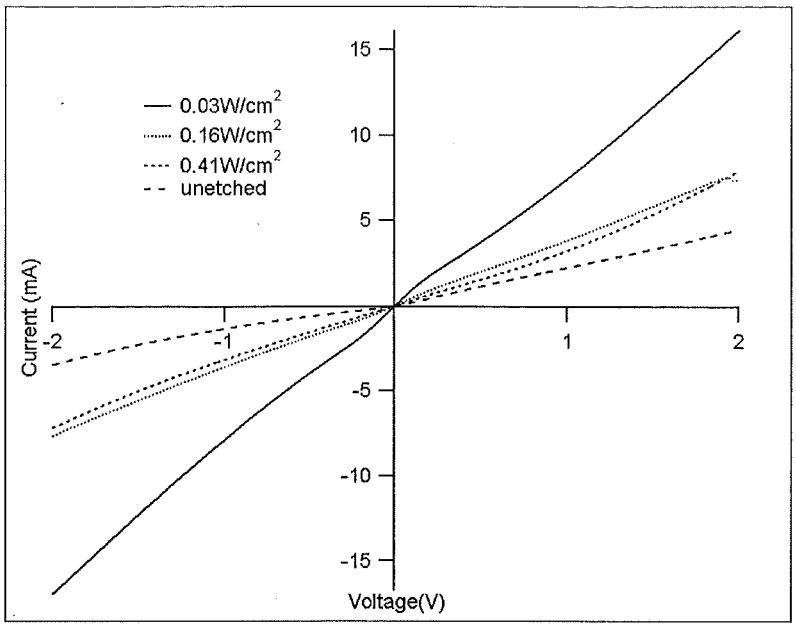

Figure 4. 1 1 I-V curve of Al/Au ohmic contact on GaN after pre-exposure to an argon plasma at different power densities. The one etched at 0.03 W/cm^2 has the lowest resistance and keep linear I-V characteristics.

density of 0.03 W/cm^2 for 2.5 minutes, a factor of 6 less than from the unetched surface.

To correlate the relationship between the surface roughness and the resistance characteristics, atomic force microscopy has been performed on similarly etched samples and the results are presented in Table 4.1.

Table 4. 1 AFM surface roughness analysis of GaN surfaces after argon bombardment with different power densities. While keeping other etching parameters the same.

Power density (W/cm^2)	rms roughness (nm)	Contact resistance (ohm-cm^2)
Unetched sample	3.6	0.491
0.41	3.7	0.229
0.16	2.4	0.191
0.03	1.9	0.075

It has been noticed that different wafers have different surface roughness. The reason for the rough surface of as grown material, could be the fact of nitrogen-deficiency, due to thermal decomposition of the nitride layers during growth. Nitrogen–deficient film exhibits a polycrystalline structure with a mixture of cubic zinc-blende and wurtzite hexagonal GaN grains retaining tetragonal bonding across the boundaries and the epitaxial orientations and polarity. Renucleation of the wurtzite phase at different [109] planes of cubic GaN results in a rough and faceted surface of the film [133]. Different growth techniques and different runs of growth could have different nitrogen deficiencies, which causes different surface roughness.

Lower energy argon ions may preferentially sputter away the spikes, while the higher energy ions may sputter away the atoms that they hit on sample surface. Thus, pre-etching with lower power density plasma produces smoother surface rather than etching at higher power density. In the $SF_6 + N_2$ case, it is possible that nitrogen incorporation reduces the nitrogen deficiency and smoothen the surface. Table 3.1 shows that the surface rms decreases with increasing nitrogen percentage. The surface composition analysis by XPS, which will be present in chapter 5, support this explanation.

The root mean square (rms) surface roughness is seen to decrease with decreasing etch power density. It appears that the smoother the surface, the lower the specific contact resistance obtained.

Previously, it has been found that argon bombardment can increase the concentration of N vacancies on the sub-surface of GaN [33, 134]. N vacancies are an intrinsic doping source and hence any increase in their concentration would increase the conduction thus decreasing the resistance of the contacts. However, the microscopic smoothness of the GaN surface after argon bombardment may suggest other possible mechanisms for the observed decrease of the contact resistances. For instance, a larger effective contact area in the metal-semiconductor junction as a result of the smoother surface may contribute to the observed effect.

The ohmic contacts on as grown material have been utilized for further experiments, instead of etched GaN, for the following two reasons. First is to identify the ohmic contact characteristics. The etching would affect the surface properties. Reproducibility of the plasma characteristics and parameters are not easy to control.

The properties of as grown material are more consistent and controllable. The second reason is that Al/Au on as grown material exhibits good characteristics of ohmic contact.

4.4.2 Effects of argon plasma pre-exposure on ohmic contacts on SiC substrate

To examine the conclusion that the low power density pre-etching in argon plasma improves ohmic contact characteristics, we have repeated the experiment on ohmic contacts on SiC substract to see if the improvements are general. The same metals and thickness have been utilized for ohmic contacts on SiC as used for GaN. The SiC substrates have been etched in an Ar plasma with the following power densities, 0.41 W/cm^2 and 0.03 W/cm^2 respectively. The other plasma parameters have been kept the same as for the GaN ohmic contacts. The I-V characteristics of etched samples are shown in figure 4.2a, the control sample is shown in figure 4.2b. Since the control sample has a very large resistance, they can not be clearly resolved in one figure.

Samples etched with 0.03 W/cm^2 have lower contact resistance, compared to the one etched with higher power density. The I-V plot on figure 4.2b shows that the control sample has bad ohmic characteristics, besides a larger resistance. The surface roughness of the samples, by observing surface topography, is shown in table 4.2. The trend is quite similar with that observed in GaN. Lower power density pre-exposure produces smoother surfaces than that of higher power density bombardment. High power density plasma produces higher ion energy, which smoothen the surfaces less effectively as explained section 4.4.1 and can induce more damage to the surface, compared to that etched by the low power density plasma. As grown material has the roughest surface with rms value of 106.17 nm, which is nearly 2 times of that of the one etched by 0.03 W/cm^2 with the rms value of 48.89 nm.

From a defects point of view, etching induces defects, which shrinks depletion region and causes tunnelling to occur, and thus the barrier height is

decreased. Therefore, the resistance gets lower after etching. This explains that etching generally reduces the contact resistance.

From a surface constitution point of view, the surface roughness and/or surface contact area are directly affecting the ohmic contact properties. The smoother the surface, the larger the effective contact area is, and the lower the resistance will be. Regarding the specified etching conditions, the best ohmic contacts are produced by etching that produces the smoothest surface.

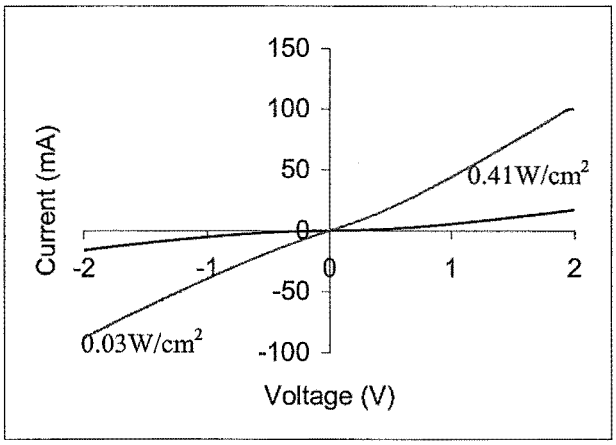

a

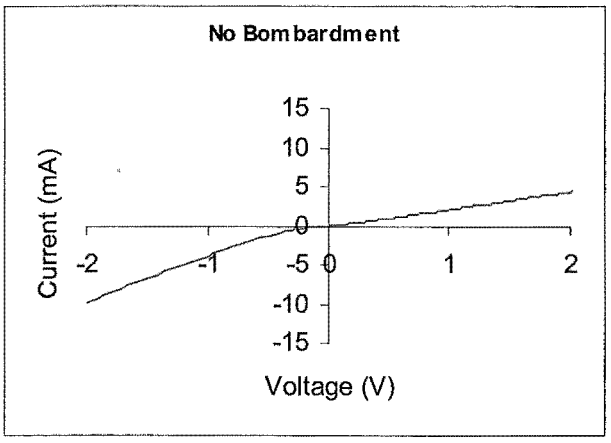

b

Figure 4. 2 a) I-V plot of the ohmic contact on SiC after RIE argon plasma etching with different power densities. The other etch parametres are kept constant temperature: 50 °C, and a total flow rate, 40 sccm, etch pressure 19.5 μbar. b) I-V plots of the control sample (unetched).

Table 4. 2 rms value of surface roughness of SiC control sample and samples etched at different rf power densities of argon plasma for 2.5 minutes. The other etch parameters are the same, temperature, 50 °C, total flow rate, 40 sccm and etch pressure 19.5 μbar.

rf power density (W/cm^2)	rms roughness (nm)
0.41	62.48
0.03	48.89
Unetched	106.17

4.4.3 Schottky contact on n-GaN and RIE pre-exposure effects on Schottky diode characteristics

4.4.3.1 Effect of metal work function

Different metals have been investigated for Schottky diode fabrication on as-grown GaN. Table 4.3 shows the ideality factor, breakdown voltage, barrier height, leakage current and different metal work function [88,135]. It seems that the barrier height of Schottky contacts does not depend completely on the metal work function. From the experimental results, it is evident that gold (Au) is the best material for the formation of Schottky diodes, amongst Ti, Pd, and NiCr, on this series of GaN material using thermal evaporation.

Table 4. 3 Ideality factor, breakdown voltage, barrier height, leakage current and work function of different metal-GaN diodes.

Metal	Ideality factor	Breakdown voltage (V) at I= -0.001A	Barrier height (eV)	Leakage current (mA) at V= - 2 V	Work function (eV) (literature data)
Au	1.05	-4.22	0.450	0.51	5.20
Pd	1.43	-0.56	0.370	11.3	5.17
Ti	1.42	-1.12	0.370	3.3	3.83
NiCr	1.45	-1.38	0.389	2.1	Ni: 5.15 Cr: 4.44

Figure 4.3a shows the I-V curve of a Au diode on GaN that exhibits excellent rectification properties with a relatively high barrier height, low reverse leakage current and good ideality factor. Therefore, our subsequent diode experiments have been performed using gold as the Schottky contact. Figure 4.3b is a schematic drawing of an ohmic and Schottky contacts structure on GaN. The Schottky contacts are defined by optical lithography, as described in section 2.2.1. The mask pattern is shown in figure 2.4.

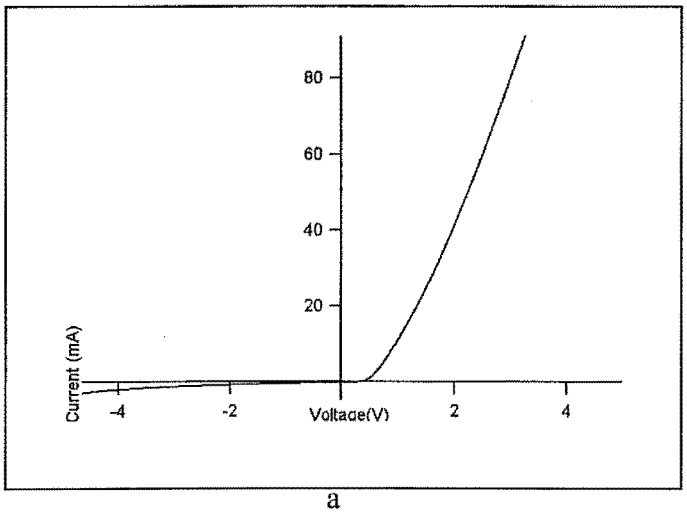

a

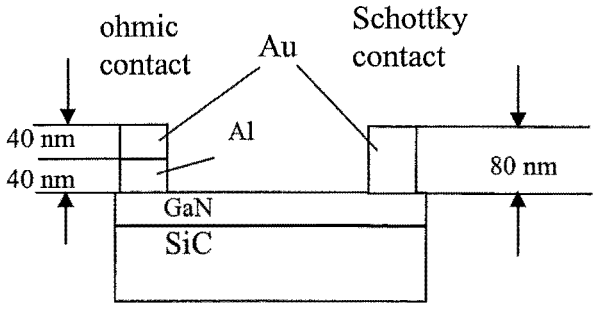

b

Figure 4. 3 a) I-V characteristics of an Au/GaN diode on as-grown GaN. It exhibits excellent rectification properties with a relatively high barrier height, low reverse leakage current and good ideality factor, and b) Schematic drawing of ohmic and Schottky contacts structure on GaN, which are ready for measurement.

Both HF and HCl substantial cleaning have been performed before actual diode metallization. The results show that the HCl treatment gives better Schottky characteristics, compare to HF treatment. The I-V plot using HCl treatment is shown in figure 4.3a. The possible explanation is that HF is a very strong acid, which might react with the top surface of GaN.

$$x\ F^- + Ga^+ = GaF_x$$

This is a possible wet etching formula for GaN in HF acid. The etch product GaF_x is possibly deposited on the surface. Any introduced defects and damage would deteriorate the diode properties. HCl basically removes the oxygen and carbon, and other contaminations on GaN surface. Therefore, the following diode experiments use HCl treatment before evaporating the metal.

4.4.3.2 Effects of varying etching gases

A study of the electrical performance of gold diodes fabricated on plasma exposed GaN has been undertaken. To compare the effects of the chemical versus physical factors, as well as the role played by the ion mass of the etchant species during the etching process on the diode behaviour, GaN surfaces have been exposed to Ar, N_2, as well as $SF_6 + N_2$ plasmas. Table 4.4 lists the ideality factor, barrier height and breakdown voltage of the diodes after argon bombardment at different power densities. The data show that the electrical properties deteriorate after argon bombardment.

This observation agrees with the ohmic contact behaviour. In the case of ohmic contact, this means that the possible existence of additional current paths and high electric fields associated with nitrogen vacancies, and defect introduction after argon bombardment may cause the low specific resistance measured. While these additional current paths and high electrical fields could result in the high ideality factor and the low breakdown voltage measured in the bombarded Schottky contacts.

Table 4. 4 Ideality factor, breakdown voltage and barrier height of Au-GaN diodes after argon plasma pre-exposure at different power densities. The other etching parameters are the same, temperature 50 °C, total flow rate 40 sccm and etching pressure 19.5 μbar.

Power density (W/cm^2)	Ideality factor	Breakdown voltage (V) at I = -0.001A	Barrier height (eV)
Control sample	1.05	-4.22	0.450
0.03	1.38	-2.93	0.431
0.16	1.32	-1.98	0.422
0.41	1.34	-2.10	0.421

The barrier height, breakdown voltage and ideality factor of a series of Au-GaN diodes whose GaN surface have been subjected to $SF_6 + N_2$ plasma are plotted in figure 4.4 a), b) and c), as a function of nitrogen percentage in SF_6 plasma. The interesting results are that diodes fabricated on GaN exposed to $SF_6 + N_2$ plasma exhibit a similar or larger barrier height, a higher breakdown voltage, and an ideality factor closer to 1, compared to the unetched sample. In particular, the diode characteristics after 40% SF_6 + 60% N_2 plasma exposure exhibit better electrical behavior compared to 100% SF_6, 100% N_2 or Ar plasma exposures.

The fastest etching rate of GaN in $SF_6 + N_2$ plasma compared to those in 100% SF_6 plasma, 100% N_2 or Ar plasmas may produce the thinnest damaged layer. In additional, because of the existence of a higher removal rate of etch products, the GaN surface may be compensated by the presence of nitrogen ions in the $SF_6 + N_2$ plasma compared to the GaN surfaces after pure Ar or SF_6 plasma exposures [53]. These factors may lead to the optimized diode characteristics observed in the 40% SF_6 + 60% N_2 case. It is worth noting that atomic force microscopy studies have shown that surfaces of GaN are smoothened microscopically after $SF_6 + N_2$ plasma exposure, which has been presented in section 3.2.

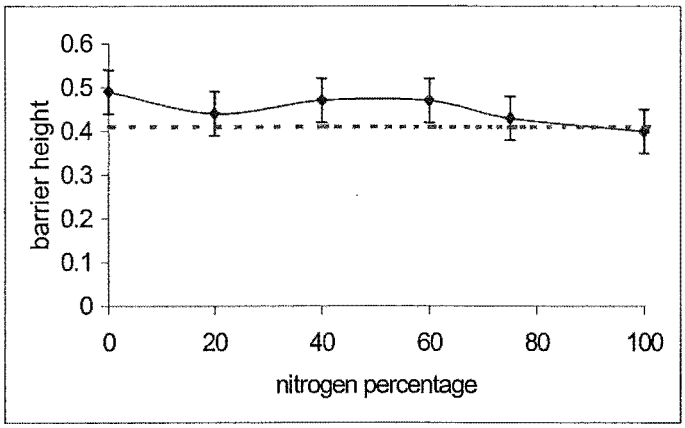

a

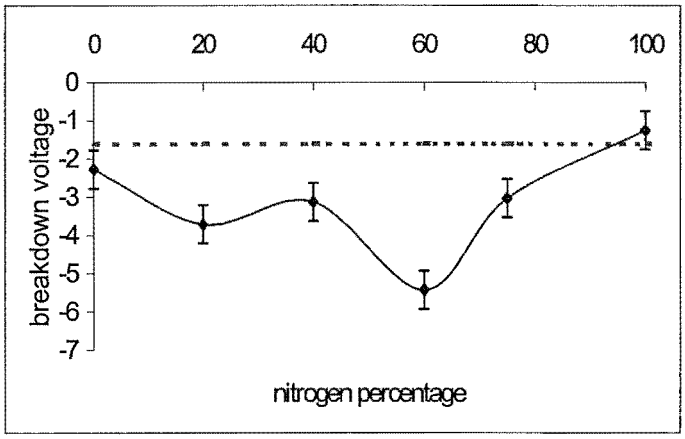

b

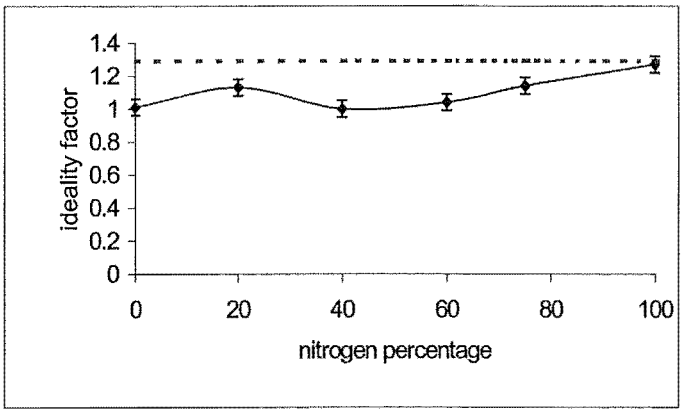

c

Figure 4. 4 a) Barrier height, b) Breakdown voltage, c) Ideality factor of Au-GaN diodes as a function of nitrogen percentage in $SF_6 + N_2$ plasma (The total flow rate has been kept constant). Dashed line is for control sample. The mixture gas improves diode properties. Etch conditions see experimental detail.

Looking more closely at the electrical data for the GaN diodes whose surfaces have been exposed to argon and nitrogen plasmas, it can be seen that compared to the control sample in the same set of experiments, argon plasma exposure degrades the electrical properties of the diodes, while N_2 plasma exposure does not. From the physical sputtering point of view, the higher ion mass of argon compared to nitrogen may create more N vacancies on the sub GaN surface after argon bombardment, see table 5.1, XPS surface composition analysis results. In addition, more defects may also be introduced deeper in the GaN substrate. From the chemical viewpoint, the existence of nitrogen ions in the plasma may serve to compensate the N vacancies created during bombardment. Such defect compensation effect has been observed by others [63] and is confirmed by our experiments [48]. Our x-ray photoelectron spectroscopy surface analysis, table 5.1, shows a higher nitrogen atomic concentration on the N_2 plasma exposed sample compared to the Ar plasma exposed sample. Both physical and chemical considerations explain the observed electrical behavior.

4.4.4 Comparison with the etch induced damage effects on GaAs

It has been postulated that GaN and related materials are more robust to etch damage because of chemical inertness properties. GaAs has been examined as a reference to compare etching damage.

The GaAs samples are lightly doped $3x10^{17}$ n-type thin film with thickness of 1μm grown on a semi-insulating GaAs substrate.

The GaAs ohmic contacts have been fabricated by thermal evaporation of Ge/Au/Ni alloy followed by 1 minute annealing in nitrogen atmosphere. An annealing temperature between 325 °C and 380 °C has been used. The GaAs ohmic contacts exhibit good ohmic contact characteristics as shown in figure 4.5. After the ohmic contacts are fabricated on unetched samples, GaN and GaAs samples are exposed to $SF_6 + N_2$ plasma together, to ensure the same etching conditions. Note that during etching, the ohmic contacts are masked to avoid exposure to the plasma, which could result in further effects on ohmic contact properties. The etching conditions are set as following; a total gas flow rate of 40 sccm, an etching pressure

of 19.5 μbar, an rf source power of 200 W and a temperature of 300 K. The etching gas composition and dc bias have been varied, sample 1 to 4 were etched with 100% SF_6, SF : N_2 = 4 : 1, SF_6 : N_2 = 3 : 2, 100% N_2 and dc bias 469 V, 424 V, 444 V, 427 V, respectively. Sample 5 has been used as grown material for control purpose. Then, the Schottky diodes are fabricated using Ti/Au for GaAs by thermal evaporation.

Table 4.5 shows the ideality factor, barrier height and breakdown voltage of GaAs samples at room temperature before and after etching. After fluorine plasma etching, the ideality factor has become closer to 1, the barrier height and the breakdown voltage has increased. The one etched with 100% SF_6 has the smallest ideality factor, the highest barrier height and the lowest breakdown voltage, while the one etched with 100% N_2 has the largest ideality factor, the smallest barrier height and the lowest breakdown voltage amongst that of all the samples. The mixture gas SF_6 + N_2 etched samples show intermediate values.

From chemical reaction aspect, a thin insulator layer formed by etch products, could cause the rectification effect [136]. Pure N_2 physical sputtering has removed the etch product better than the others as N_2 has the highest ion current density (table 5.2). While in pure SF_6 plasma, there might have formed a relatively thicker insulator layer GaF_X between the semiconductor and metal contact. The results indicate that chemical etching condition produces a better diode rectification in etching GaAs, possibly by forming an insulator layer due to the non-volatile reaction product GaF_X.

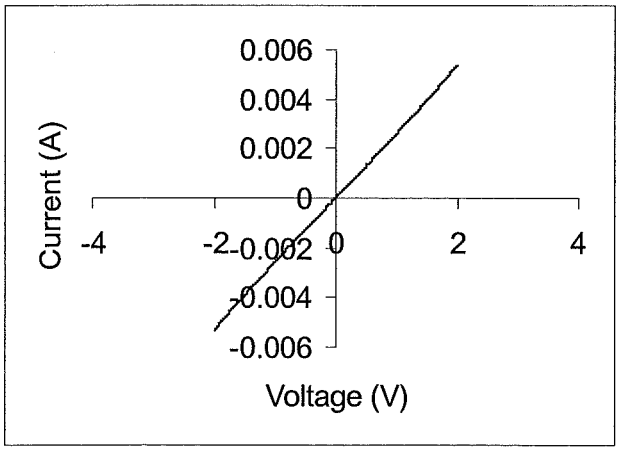

Figure 4. 5 I-V characteristics of ohmic contact on GaAs by using thermal evaporating AuGeNi alloy, and annealing in nitrogen atmosphere between 325 °C and 380 °C for 1 minute.

This part of the work is for the comparison of the robustness of GaN and GaAs to etch damage for the specified plasma conditions. So the etch damage mechanism of GaAs will not be discussed here. Because of the different substrates used in etching GaN and GaAs, it is expected that the etching mechanisms of GaAs and GaN in a fluorine plasma would be different. The results here show that, the gas mixture $SF_6 + N_2$ improves the GaAs diode properties. It is very hard to tell which material is more robust to a particular mixture gas $SF_6 + N_2$, due to different etch mechanism, which manifest the diodes properties in different way.

However, the defects have been proposed to be propagated by radiation within the material. Since GaN has a larger band gap than GaAs. It is reasonable to assume that larger energies exist for defect propagation within GaN material than that in GaAs. Thus, in the same plasma condition, GaN could have larger damage than GaAs. This may explain the fact that wide band gap material GaN does not show more robustness to etch induced damage than GaAs.

Table 4. 5 Ideality factor and barrier height of Schottky diode on GaAs after etching and before etching. The specified etching conditions see experimental detail.

Sample	Ideality factor	Barrier height (eV)	Breakdown voltage (V) at I=-0.001A
100% SF_6	1.12	0.7128	-2.18
40% N_2	1.43	0.7159	-1.65
75% N_2	1.61	0.6891	-2.17
100% N_2	2.08	0.6275	-0.99
Control	1.80	0.6614	-0.66

The mystery of the N_2 role in etching behavior has been reported. Addition of N_2 to Cl_2 etching of GaAs, producing almost vertical sidewall and improving surface morphology has been reported [137]. Addition of N_2 to SF_6 has been found to increase the etch rate in etching GaN (chapter 3 and chapter 6) and improve the diode properties of GaN and GaAs. A mixture of $SF_6 + N_2$ may improve the diode properties by self-chemical healing and the energy dissipating to reaction products

and being removed with these reaction product. The role of nitrogen in etching GaAs is also unclear. Simple sidewall passivating effect is not sufficient to explain this etch behavior, since no N was found on the sidewall by Auger electron spectroscopy [137].

4.4.5 Annealing effects on diode properties of GaN on SiC substrate

An annealing step has been used to recover the damage from physical bombardment and restore diode properties [138-139]. However, to my best knowledge, there is no publication on the effect of annealing of as grown material. To investigate the material quality and annealing effects on diode properties, the following experiment has been carried out.

Two samples of as grown material have been annealed at 500 K, 1000 K respectively, in N_2 atmosphere for 1hour. Then, ohmic contacts and Schottky contacts on annealed and control samples have been fabricated. The result is shown in figure 4.6, where I-V characteristics of control sample and samples annealed at

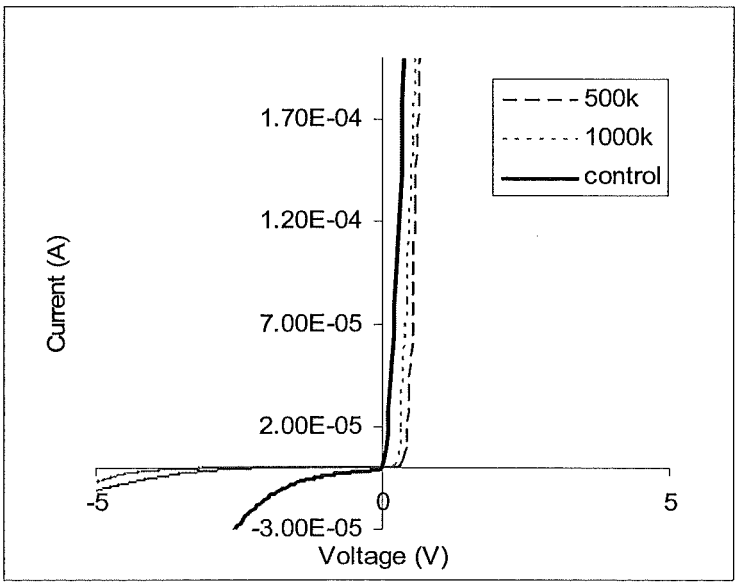

Figure 4. 6 I-V curve plot of diodes on the sample pre-annealed at 1000K, 500K in N_2 atmosphere for 1 hour and control sample. It clearly shows that annealing increases the breakdown voltage. 1000 K annealing results in the smallest leakage current and gives excellent diode characteristics by diode theoretical model fitting.

1000 K and 500 K are illustrated. After annealing, the leakage current is 1000 times smaller than that of control sample. The sample annealed at 1000 K results in the smallest leakage current and gives excellent diode characteristics by diode theoretical model fitting [140].

Nitrogen may possibly be incorporated in the GaN surface during annealing. This would lead to a surface with ideal stoichiometry and thereby reduce the surface state density. Consequently, it decreases the defects on the surface by nitrogen compensation and reduces the current paths, and further result in good Schottky diode characteristics. Another possibility is that annealing releases the thermal strain, which has been caused by the cool down procedure during growth.

The observed results indicate that the as grown material should be annealed before it is used for electronic device fabrication. Since the as grown material is often nitrogen deficient

4.5 Summary

We successfully fabricated ohmic contact on n-GaN by Al/Au without using an annealing process for the ohmic contact. Pre-exposure of the GaN surface to an Ar plasma at a power density of 0.03 W/cm^2 for two and a half minutes decreases the specific ohmic contact resistance by a factor of 4 compared to an unetched sample. The GaN surface has been found to be smoothened microscopically after the argon bombardment. A similar result has been observed on SiC substrates. Argon plasma with lower power density has produced better ohmic characteristics and smoother surface compared to plasma processing with higher power density.

The results show that gold is the best metal for GaN Schottky contacts for the given series materials. The measured diode characteristics indicate that 60% N_2 and 40% SF_6 is a suitable low damage dry etch alternative for GaN transistor gate recessing due to N incorporation and smoothening etched surface. However, this process has to be investigated upon its impact for carrier mobility.

The comparison of etch effects on GaAs and GaN diode properties show that N_2 may play an important beneficial role, but the exact nature of the nitrogen role remains unclear.

In terms of leakage current, the 1000 K annealing of GaN recovers diode properties better than that of 500 K. The annealing of as grown GaN in a nitrogen atmosphere results in better rectification, possibly due to the recovery of the surface stoichiometry close to ideal and the reduction of surface states density.

Chapter 5

Effects of RIE Etch Induced Damage on the Optical Properties of GaN*

5.1 Introduction

The potential of the wide band gap semiconductor GaN and related materials, for the realisation of optoelectronic devices has been well documented [2]. However, the successful development of such devices will require a better understanding of the materials' optical properties that can be affected by the fabrication processes. Dry etching is widely and routinely used for GaN device fabrication. However, dry etching induced defects may serve as local non-radiative recombination centres for electron-hole pairs, reducing the radiative lifetimes and luminescence efficiencies of optical devices [44]. Thus, the study of etching induced damage effects on the optical properties is important.

Photoluminescence occurs when electrons are deliberately excited up to the conduction band (stimulated absorption) by light at a fixed wavelength, causing the sample to luminescence as the electrons and holes recombine. By measuring the spectra of the luminescence, we can find out the energy difference in the transitions and how often they occur, thus determining fundamental properties such as the size of band gap and the defect state present. Many researches on optical properties of GaN and defects are very often done through photoluminescence [1-3].

GaN grown on sapphire substrate exhibits compressive strain and photoluminescence (PL) studies have correlated defect–related blue and yellow luminescence bands with etch-induced damage [50]. Donor-bound exciton peak

* This chapter is based on the published papers "A study of reactive ion etching effects on optical properties in GaN" Microelectronic Eng. 57-58, (2001), pp 585-591 and "Photoluminescence and photoconductivity study of reactive ion etched GaN on SiC substrates" IPAP CSI pp774-777

(D^0X) intensity has been found to increase after Ar and SF_6 etching, which is consistent with the contention that nitrogen vacancies [141] are related to the origin of the D^0X [33, 142]. However, according to Neugebauer et al [143]'s, theoretical calculation does not positively support the identification of the single nitrogen vacancy, but it does not exclude clusters of nitrogen vacancies. There are two native defects, the nitrogen vacancy and the interstitial gallium. Both are shallow donors at ambient pressure. Perlin et al [144] suggested that the dominant donors are nitrogen vacancies because of their lower formation energy.

In contrast, GaN grown on SiC possesses tensile strain and SiC represents an alternative substrate for GaN growth. Very recently, Chang et al [145] reported observations of reconfigurable optical properties in undoped GaN on SiC substrates by exposing the material to a high density UV light, which increased the peak intensity of the yellow luminescence at 2.2 eV. It is essential to systemically study optical properties and etch damage effects on GaN grown on SiC substrates before it be used in industry for real device fabrication.

Addition of nitrogen to the SF_6 plasma has been shown to increase the etch rate, improve the vertical nature of sidewall and the smoothness of the surface of GaN [32]. It also causes less electrical damage [47]. Lee et al [63] found that N_2 plasma treatment can recover the PL intensity, which decreased by dry-etch damage in n-type GaN. This chapter presents an investigation on optical properties of GaN grown on SiC and the dry etch induced damage effects under different plasma conditions. The photoluminescence and photoconductivity results have been correlated. To study the impact of dry etch processing on the optical properties of GaN, near band-gap luminescence of GaN sample after N_2 etching has been compared to a control sample annealed at 1000K for 1 hour in N_2 ambient and the power dependence of near band gap PL intensity has been studied.

5.2 Experimental detail

The material used here is nominally undoped n–type GaN and consists of samples from a single wafer of 0.5 μm thick film grown by hydride vapour phase epitaxy (HVPE) on a silicon carbide substrate. The carrier concentration of the GaN film is about $3 \times 10^{17}\ cm^{-3}$.

Six samples have been examined in this study. Four of them have been etched by reactive ion etching using various gases in an Oxford Plasma 80 system. The plasma parameters, etch pressure 19.5 μbar, substrate temperature 295K, total gas flow rate 40 sccm and etch duration 1.5 minutes have been kept constant. Only the etch gases have been varied. Samples 1, 2, 3 and 4 have been etched in Ar, N_2, 40% SF_6 + 60% N_2, and SF_6 plasmas at self induced DC biases of 495 V, 465 V, 417 V and 440 V, respectively. Sample 5 is the control sample while sample 6 is annealed as grown material. The annealing condition is 1000K in N_2 atmosphere for 1 hour.

Photoluminescence is excited by the 300 nm line of an argon laser, which can penetrate about 100 nm into the GaN material [146]. The laser light with incident power of 2.5 mW is focused normally on to the sample plane in a back-scattering geometry. Luminescence is collected by quartz optics and focused to the entrance of a 0.75 m SPEX model 1700 spectrometer. The signal is detected by a thermo-electrically cooled photo-multiplier tube. The samples are mounted in a closed cycle helium cryostat. Variable temperature experiments are performed between 20 K and 250 K.

4-terminal photoconductivity (PC) experiments have been done using four ohmic contacts fabricated in a linear arrangement on each sample by thermal evaporation of 40 nm of aluminium and then 40 nm of gold. Note that the contact area has been masked from the etching process. Thus, the sample conductivity is not influenced by changes to the metal-semiconductor interface.

A constant current of 400 μA is passed between the outside contacts by a Delta Electronics constant current source. White light from a Xenon lamp is filtered by a SPEX 500M monochromator, chopped at 22.7 Hz, and then focussed between the inner contacts of the sample. The voltage across the inner contacts is pre-amplified and measured by a Stanford Research Systems SR830 lock-in amplifier. The samples are housed in a continuous flow liquid helium cryostat. The temperature of the flowing gas is controlled by a purpose built controller allowing sample temperatures in the range of 5 K – 250 K to be obtained.

To correlate PL with PC experiments, the GaN samples for PC experiments have been etched simultaneously with PL samples. Etched GaN samples prepared as

part of this project have been examined using photoconductivity (PC) in conjunction with the project of Olive Dickie [147] for completeness of discussion.

X-ray Photoelectron Spectra of the Ga (2p3/2), N (1s) and F (1s) photoelectron lines are recorded for all six samples with a PHI 5400 ESCA instrument set at a constant analyser pass energy of 71.550eV, using unmonochromatised incident Mg X-ray radiation. The electrons emitted from the specimen were detected at an angle of 45^0 with respect to the specimen surface.

A standard Scientific Systems, Smart Probe System is used for Langmuir probe measurement. A platinum – iridium (instead of tungsten) tip has been used to minimize tip consumption by the fluorine plasma.

5.3 Results and discussion

5.3.1 RIE etch induced damage effects on photoluminescence spectra

The figure 5.1(a) compares the photoluminescence (PL) spectra from a control sample with samples etched using plasmas of Ar, SF_6, N_2 and $SF_6 + N_2$ for GaN grown on SiC. The strongest feature of all from the spectra is a peak at 3.445eV, which has similar temperature dependence in all samples, see figure 5.1(b). The etched samples appear to have a greater normalised intensity at elevated temperatures than the control sample. This difference is most probably due to a background from other PL bands (such as A^0 X), as only the peak intensity has been used for the data.

We attribute this feature at 3.445eV to a donor-bound excitonic peak, since a similar feature in the PL spectrum of GaN on SiC has been reported.[24] The spectra in figure 5.1(a) show that for all of the etching gases used, the D^oX intensity has been reduced, compared to the control sample. Photoluminescence intensity is very sensitive to surface recombination [119, 148], and can be related to the surface and bulk properties of the material being investigated. It has been shown previously that plasmas can cause damage to semiconductors [149]. The etch-induced defects could introduce both non-radiative centres and alternative radiative pathways into the bulk material by diffusion [150] or other means, thus changing the PL intensity. It is worth noting that D^oX intensity enhancement in GaN on sapphire substrate after etching has been observed previously [141], while a decrease in D^oX intensity is

found in the present experiments. This difference requires further investigation. In the samples etched for this experiment, the Ar and $SF_6 + N_2$ plasmas has resulted in nearly equal D^0X intensity, while the SF_6 and N_2 samples have slightly lower intensity with N_2 having the lowest.

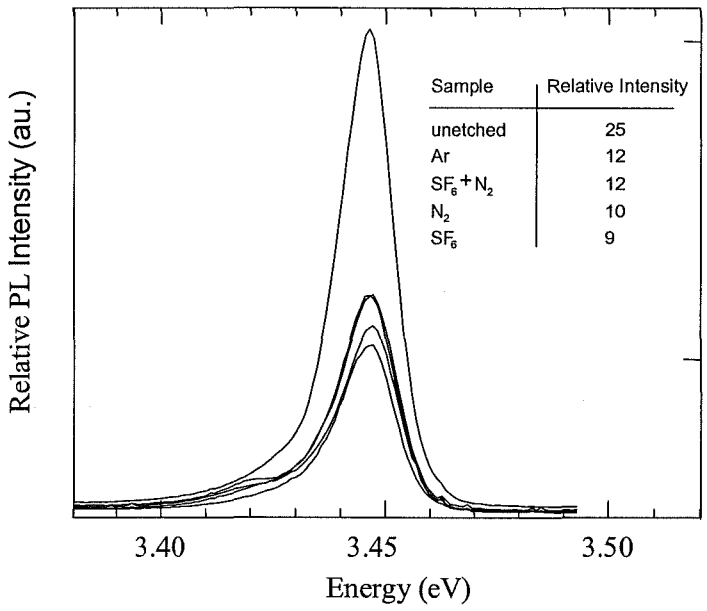

a

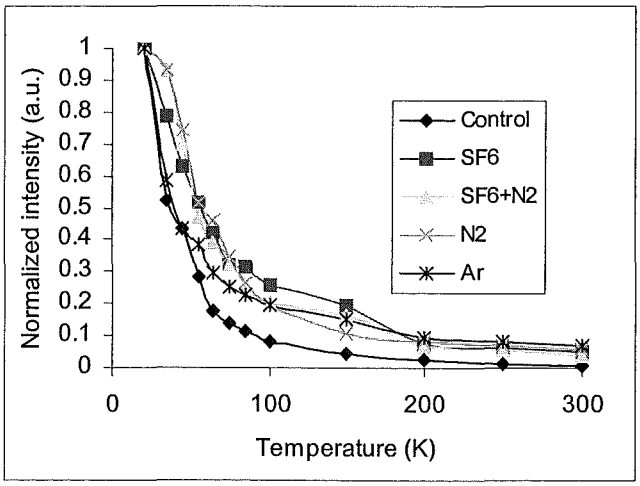

b

Figure 5. 1 a) Photoluminescence spectra at 20 K of an unetched (control) GaN sample and samples subjected to Ar, N_2, $SF_6 + N_2$ and SF_6 plasma exposures, b) Temperature dependence of the D^0X intensity for N_2, $SF_6 + N_2$ and SF_6 etched samples.

5.3.2 X-ray Photoelectron Spectroscopy (XPS) results and Langmuir probe measurement

Perlin et al [144] and Boguslawski et al [151-152] suggested that the dominant donors in GaN are N vacancies. Gil et al [142] suggested that the concentration of Ga interstitials under the equilibrium condition in Ga-rich material could be comparable to that of N vacancies, while it is difficult to determine exact chemical nature of donor.

X-ray photoelectron spectroscopy (XPS) surface analysis has been performed to determine the surface composition of all the samples. Table 5.1 shows the atomic concentration ratio of N/Ga from XPS surface composition analysis. In general, N is deficient after plasma exposure except for N_2 plasma. The surface after Ar etching has the lowest N atomic concentration. It is possible that physical sputtering removes N atoms preferentially. Samples after N–containing plasma exposures tend to have relatively higher N atomic concentration, most likely because N species from the plasma are incorporated into the material.

Table 5. 1 Atomic concentration ratio of N (1s)/Ga (2p3/2), as determined by XPS surface analysis. Etch conditions see text.

Sample	N/Ga ratio
Control sample	0.1606
Ar etched	0.0911
N_2 etched	0.1664
SF_6+N_2 etched	0.1309
SF_6 etched	0.1083

To gain insight into the degree of ion bombardment present in the various plasmas, Langmuir probe measurement has been used to determine the plasma ion current densities. Table 5.2 lists plasma ion flux resulted from Langmuir probe measurement. Result shows that an Ar plasma has the highest ion current density

compared to N_2, $SF_6 + N_2$ and SF_6 plasmas. The highest ion current density in an Ar plasma, coupled with the lowest N atomic concentration on the GaN after Ar plasma exposure detected by XPS, suggest the creation of a severe damage layer. However, PL data show a similar intensity detected from the Ar etched sample. These experimental observations suggest strongly that ion bombardment and nitrogen deficient surfaces limited to the top few monolayers are not the only factors in determining the PL intensity. Moreover, the etch-induced defect distribution within the laser penetration depth of 100nm remains unclear.

In a SF_6 plasma, chemical reaction dominates and the formation of a thick damaged layer with non-volatile product GaF_X is highly possible [53]. We have detected a F peak in XPS analysis on the GaN surface after SF_6 etching. In Ar plasma, such fluorine-containing non-volatile product is not formed. However, diffusion of defects and ion bombardment could cause damage and decrease the D^oX intensity. Langmuir probe measurement shows that SF_6 plasma has much lower ion current density than that of Ar plasma, indicating less ion bombardment in the SF_6 plasma. On the other hand, these PL results suggest lower optical damage from Ar etched sample compared to SF_6 etched sample. These experimental observations suggest that ion bombardment does not play as an important role as the chemical factors in creating etch damage in GaN.

Table 5. 2 Ion current density in various RIE plasmas with pressure 19.5 μbar and power density 0.045W/cm^2 at room temperature.

Etching gases	Ion current density (mA/cm^2)
Ar	0.1397
N_2	0.1139
SF_6+N_2	0.0503
SF_6	0.0513

In the $SF_6 + N_2$ plasma, the least optical damage has been induced in etched GaN. XPS also detected hardly any F-signal on the etched GaN surface. The possible efficient removal of the non-volatile products and the higher etch rate [145] as a

result of adding N_2 to the SF_6 plasma, the incorporation of N on the GaN surface and the low ion current density detected in the plasma are factors that help to reduce the damage caused by the $SF_6 + N_2$ plasma.

The PL intensity also can be explained by Hovel's formula [120]. A discussion on PL intensity using dangling bonds will be presented in section 8.3.3.

5.3.3 RIE etch induced damage effects on photoconductivity of GaN

Figure 5.2 shows the photoconductivity spectra of the samples under study. All samples exhibit two prominent peaks at energies of 3.457 and 3.472 eV although with very different intensities as can be seen by the relative noise. No PC signal could be obtained from the SF_6 etched sample. The bands observed in the PC spectra are significantly lower in energy than those observed by Buyanova et al [153] and Nel'son et al [154]. But the lower energy peak is close in energy to the single peak observed by DeVittorio et al [155].

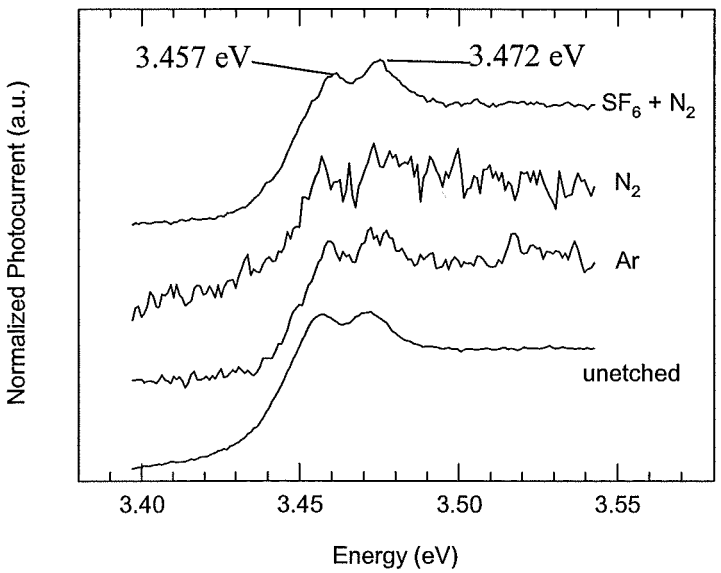

Figure 5. 2 Normalized photoconductivity (PC) spectra recorded at 5K of reactive-ion-etched GaN epilayers on SiC substrates. A sample etched with SF_6 did not exhibit a PC signal. The spectra are offset for clarity.

The two PC bands are separated by 15 meV, which is larger than that expected for the splitting of the A and B excitons. In their reflectance spectrum Buyanova et al [153] observed two free-exciton peaks at 3.472 and 3.492 eV split by 20 meV. These authors suggested that the A and B excitons were both represented in the lower energy peak while the higher energy peak was due to the C exciton. Tchounkeu et al [156] resolved 3 free excitons at energies and shifts (in meV) of E_A = 3.477 eV (0 meV), E_B = 3.487 eV (10 meV) and E_C = 3.506 eV (19 meV) in a reflectivity spectrum of GaN grown on SiC. In addition, Shan et al [161] observed free excitons at energies and shifts of E_A = 3.470 eV (0 meV), E_B = 3.474 eV (4 meV) and E_C = 3.491 eV (21 meV). Thus the splitting observed here of 15meV between photocurrent lines does not easily correspond to a splitting between free exciton bands.

However, there have been several reports of the splitting between the 1s and 2s levels of the A-exciton. Tchounkeu et al [156] report this splitting as 15 meV while Orton and Foxon [10] report values between 15 and 20meV. By using additional above-band-gap illumination from a laser, Shan et al [157] enhanced the reflectance features and were able to observe bands corresponding to the 2s states of the 3 free excitons. These bands were observed at splitting of 16 meV from the 1s state.

Therefore the interpretation of the spectra here is that the A-exciton are found within the first PC line at 3.457 eV and that the second PC line is most probably the 2s state of the A-exciton.

Our photoluminescence results are consistent with the trend observed in our photo-conductivity (PC) signal [158] except the Ar etched sample. Among the etched samples, the sample etched by SF_6 + N_2 has the strongest PC signal, the sample etched by N_2 has weak PC signal. No PC signal has been detected from the sample etched with SF_6 plasma [147]. Here we have to point out that PC signal represents A-exciton, while PL intensity is referring to D^oX. Etching in different gases might have different effects on A-exciton and D^oX.

5.3.4 Excitonic energy and epitaxial strain

The strains on GaN thin layer is largely understood due to the mismatch of lattice parameter and the difference in thermal expansion coefficients between the epilayer and the substrate. As a result, this will affect the excitonic energy [30].

Figure 5.3 shows photoluminescence spectra from two unetched GaN sample measured at 25 K. Both epilayers are grown on SiC substrates. The energy difference of the two D^oX peaks is about 6 meV. The peak energies in those two samples are lower than that previously observed for GaN emission [159], but such a shift is not unreasonable for material from different sources and with different built-in strain. Figure 5.4 [160] shows collection of excitonic energies from literatures. The energy value of 3.473 eV is at the zero strain. Data on the right side are GaN grown on sapphire, while data shown on the left are GaN on SiC. Our data is also attached and indicated, on the trend line, labeled as this work.

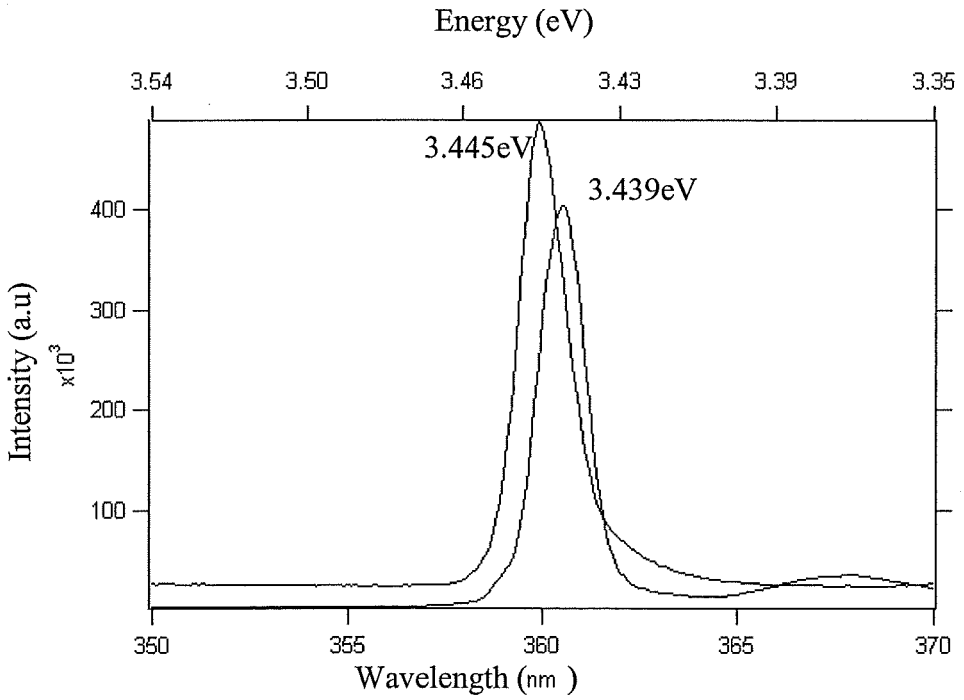

Figure 5. 3 Photoluminescence spectra from two unetched GaN sample at 25 K from two wafers. Both epilayers are grown on SiC substrates. One sample with peak energy of 3.445 eV, another with peak energy of 3.439eV. The difference is about 6 meV.

GaN samples with thicknesses of a few μm grown on sapphire substrates, compared to a thick bulk-like GaN sample with a much reduced strain [161], have shown an upshift of excitonic energy. On the other hand, for the epilayer grown on SiC substrate, a downshift of excitonic energies has been observed. These excitonic energies shift can be explained from the different thermal expansion coefficients of GaN, sapphire and SiC [162]. The GaN layer grown on sapphire then experiences a compressive strain upon cool-down from growth, which will increase the exciton energies [163]. For GaN grown on SiC, the strain is tensile, which will lead to lower exciton energies. This explanation has been evidenced by our annealing experiments. After annealing, the peak energy of GaN grown on SiC shifted to higher energy, which will be presented later in this chapter.

Edward et al [164] reported on relaxation phenomena in GaN/AlN/SiC heterostructures by modulating the strain state (tensile) of moderately thick (around 2 μm) GaN based structures grown on 6H-SiC to a range 0 to 2 Kbar of compressive stresses. They are trying to solve the strain problem and give the possibility of approaching strain free GaN.

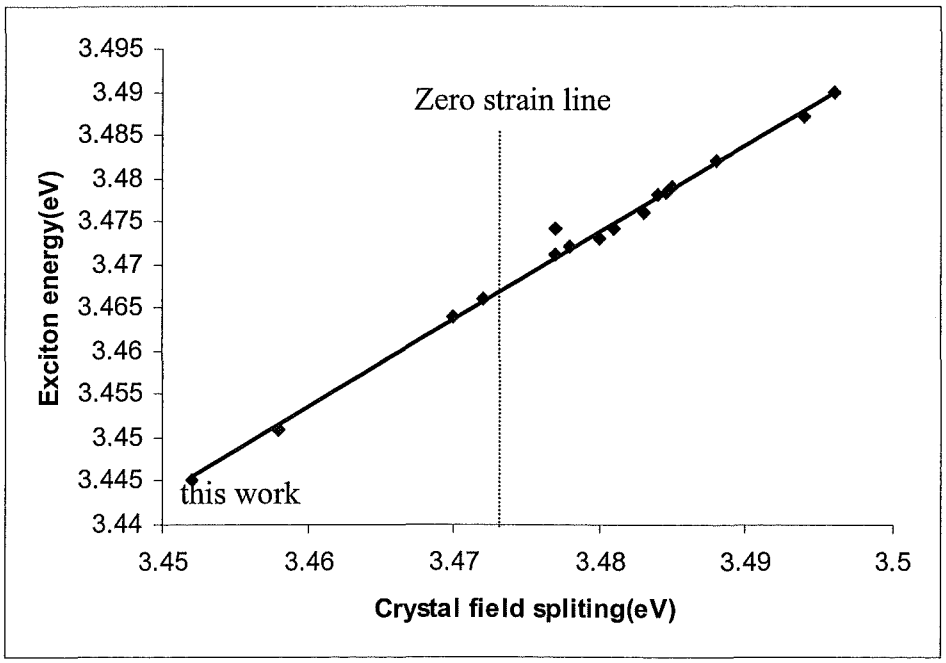

Figure 5. 4 Literature data collection of $D^{o}X$ energy. Our data is labeled as this work, on the trend line of the collected data

5.3.5 Power dependence of near band gap PL intensity

Figure 5.5 shows the PL spectra measured at 25 K of the control sample with various incident laser powers. The inset is D^oX area intensity against power. Apparently, the intensity is linearly changing with incident laser. No saturation effect has been observed.

The laser power dependence of the etched sample has been investigated. The result is similar to control sample. The D^oX intensity decreases with power density linearly and no saturation effect has been observed.

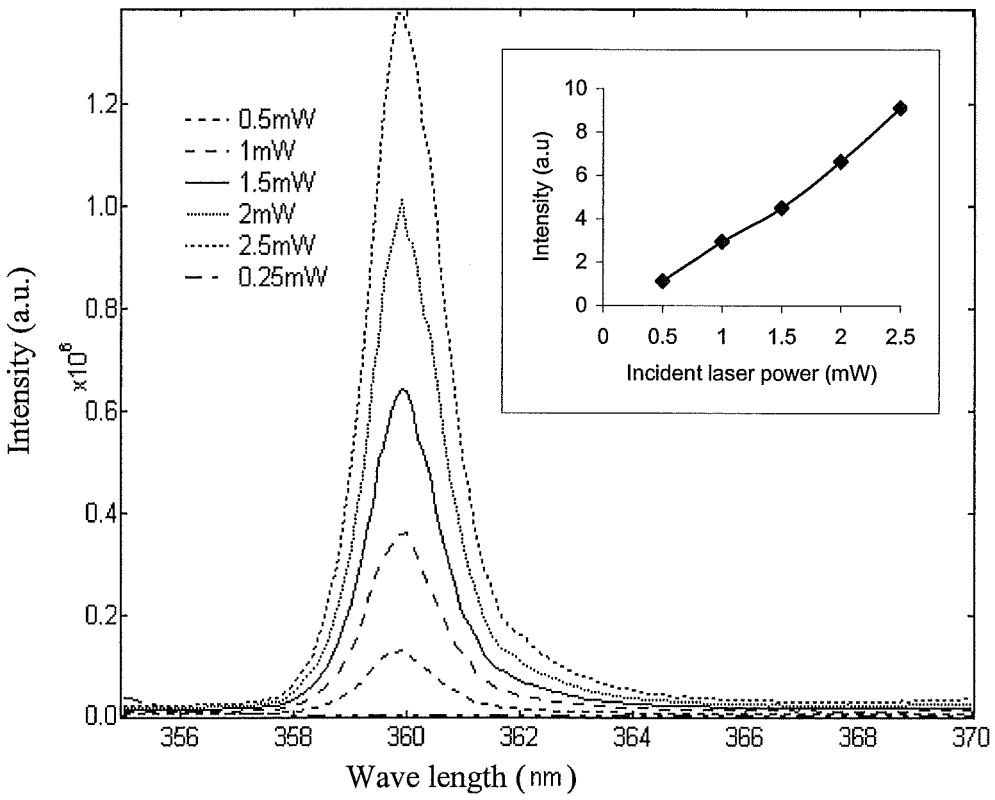

Figure 5. 5 The PL specrta show that power dependence of D^oX intensity of control sample is linear. The inset is area intensity vs. incident laser power. The sample etched by SF_6 plasma has the same trends of intensity dependence on power. No saturation effect has been observed.

5.3.6 Below–band gap PL spectra of GaN on SiC

One of the criteria used for judging the GaN material quality is the luminescence properties measured by the ratio of near band gap exciton recombination and deep level emission at room temperature.

Spectra from 340 nm to 800 nm wavelengths have been scanned to investigate the blue and yellow luminescence [165]. Figure 5.6 is a comparison of the full wavelength PL spectra at 25K. A wide blue-violet band has been observed. Surprisingly, there is no obvious yellow luminescence of this series of GaN on SiC substrate samples. Sanche et al [166] suggested that the Mg–doping may reduce, but not avoid the formation of the yellow band related defects in n-type and semi-insulating Mg-doped samples. Their explanation is that the yellow luminescence was not observed, it maybe justified by a higher efficiency of the Mg-related recombination path.

This observation is in contrast to GaN grown on sapphire reported previously [51]. There, strong yellow luminescence has been observed and the intensity increases after RIE Ar plasma etching. Teisseyre et al [30] reported that GaN epitaxy grown on GaN single crystal did not show strong yellow luminescence and luminescence near 3.2 eV (donor-acceptor pair) [30]. Their explanation is that good quality material should have no blue and yellow band emission.

In figure 5.6, there are two obvious peaks, 3.08 eV and 3.28 eV, respectively, in the blue band. In between, there is another peak, 3.17 eV. This peak can only be observed in the control sample. This indicates that etching changes the recombination centre into a non-radiative recombination centre or into another energy state recombination centre to reduce the energy states of 3.17 eV. The etching does not create new energy states as radiative recombination centres.

Meyer et al [167] suggested these peaks (3.28 eV, 3.17 eV, 3.08 eV) to be donor-acceptor pair and replicas. In our result, the 3.08 eV peak has the highest intensity while the 3.28 eV peak has about one fifth of the area of the 3.08 eV peak. This suggests that the 3.08 eV peak is the main radiative state.

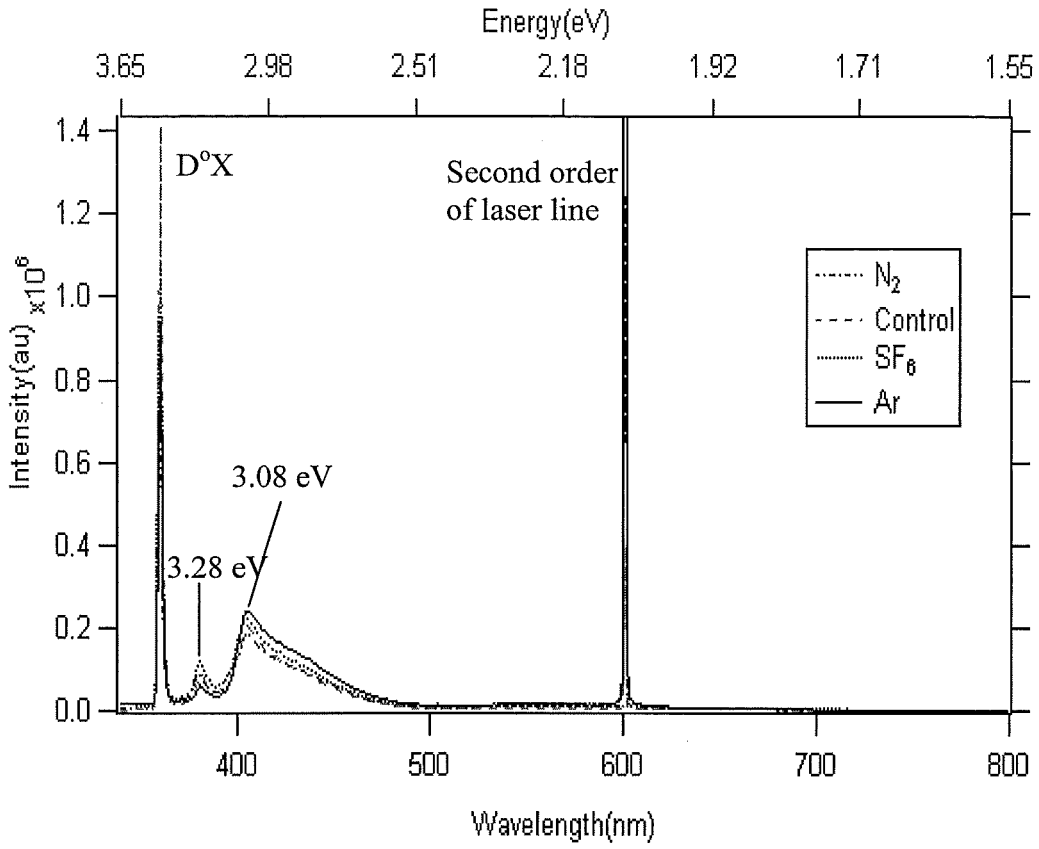

Figure 5. 6 PL spectra of control sample of GaN grown on SiC and samples etched by Ar, SF_6 and N_2 plasma respectively. Obvious blue band with two peaks at 3.28 eV and 3.08 eV. No yellow luminescence band has been observed on this series samples.

Strite et al [162] explained that the 3.27 eV range is from donor-acceptor pair recombination, involving the usual residual donors and acceptor of GaN. Their depth evaluated to 35 ± 5 meV and 220 ± 5 meV respectively [168]. However, Leroux et al [169] suggested that these peaks seem to be related to donor, or acceptor, or both. Trager-Cowan et al [170] experiments suggested that these luminescence bands are associated with structural defects. To identify and understand the defects related to recombination is valuable for optimisation of the growth procedure in device fabrication. However, it is difficult to make a decisive identification as to the chemical nature of the second slightly deeper donor.

Figure 5.6 shows that the Ar etched sample has the highest intensity peak with the energy of 3.08eV. The N_2 etched sample has the lowest intensity of this peak, similar to the control sample. The SF_6 etched sample lies in between. These

blue band peaks are not caused by etch induced defects, because the control sample has the peaks with same energies. XPS analysis results show, see table 5.1, that the N_2 etched sample has the lowest Ga atomic concentration on the surface, while the Ar etched sample has the highest Ga atomic concentration, the SF_6 etched sample is in the middle. Apparently, N deficiency follows the trend as the intensity of the 3.08 eV peak. This suggests that the 3.08 eV peak is possibly related to N vacancies.

The intensity trend of the 3.28 eV peak is different from the nitrogen vacancy trend. The Ar etched sample has the lowest PL intensity and the SF_6 etched sample has the highest PL intensity, while the control sample and the N_2 etched sample has similar intensity, in between.

Figure 5.7 a, b, and c are the temperature dependences of the spectra of the control sample and the samples etched by N_2 and SF_6+ N_2 plasma respectively. The insets show the intensity ratios of the peaks 3.28 eV, 3.17 eV and 3.08 eV to their D^oX. The empty blankets are due to these peaks' intensity too low to resolve.

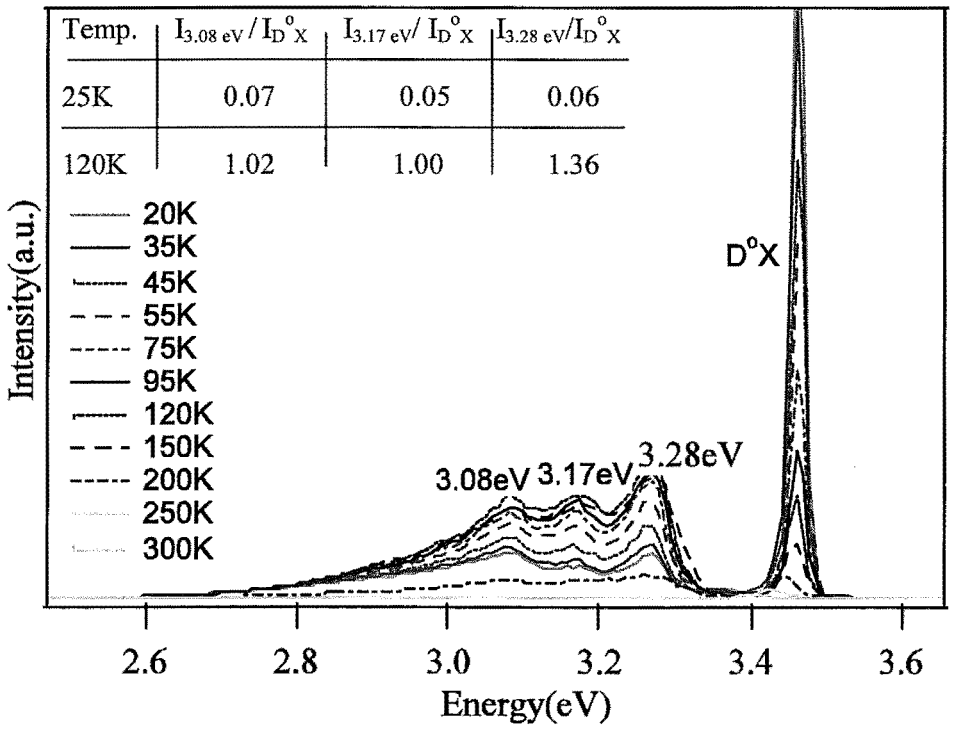

a

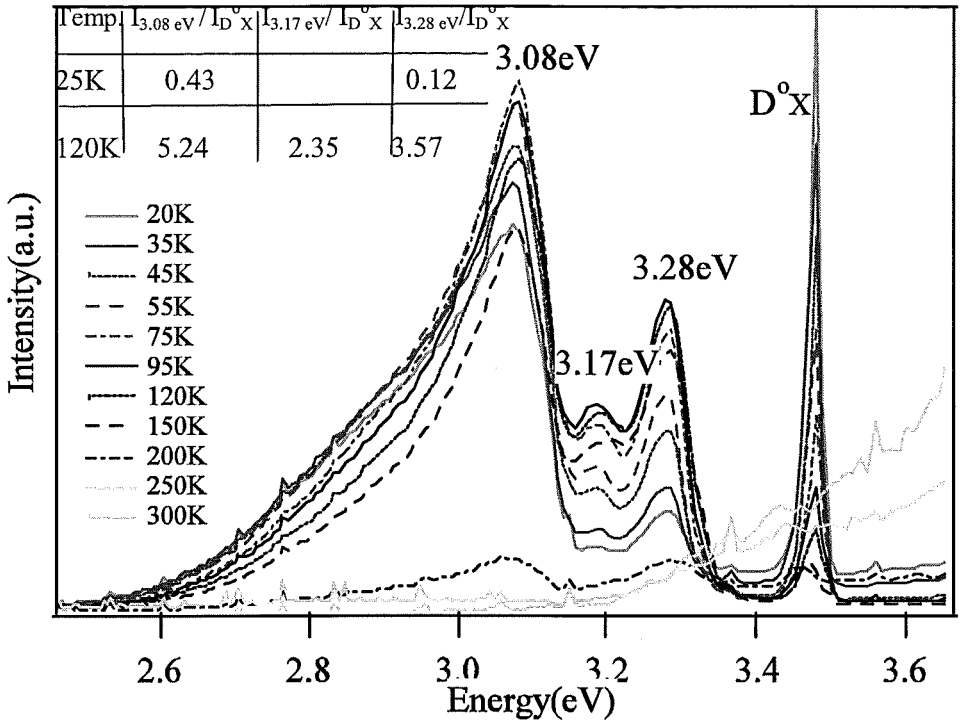

b

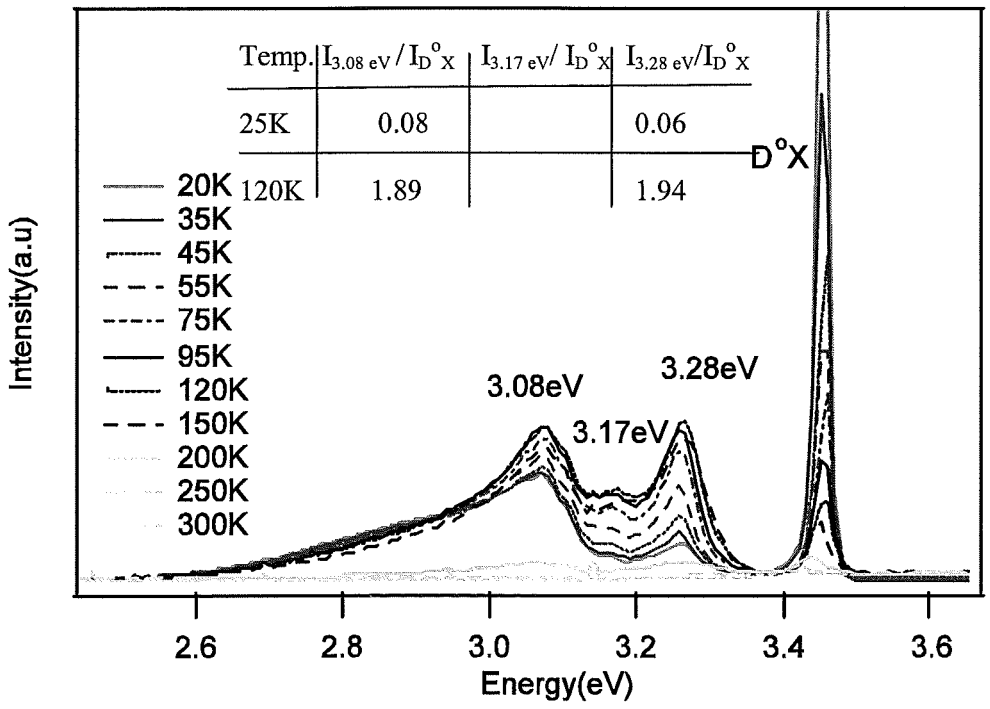

c

Figure 5. 7 Temperature dependence of PL spectra of a) control sample, b) N_2 etched and c) $SF_6 + N_2$ etched sample. The blue band increases with temperature until 120 K, and starts to decrease, suddenly drop to back ground level at about 200 K. The insets show the intensity ratios of the peaks 3.28 eV, 3.17 eV and 3.08 eV to D^oX. The empty blankets are due to these peaks' intensity too low to resolve.

At 25 K, after N_2 etching, the intensity ratio of peak 3.08 eV to its D^oX is 0.43, which is about 6 times more of control sample's 0.07; the intensity ratio of peak 3.28 eV to its D^oX is 0.12, which is double of control sample's 0.06. While the $SF_6 + N_2$ etching increases the intensity ratio of peak 3.08 eV to its D^oX very limited amount of 0.01 and does not change the peak 3.28 eV to its D^oX ratio. This further indicates that the $SF_6 + N_2$ plasma induces less optical damage than N_2 plasma. This result is consistent with near band gap PL observation described in sections 5.3.1 and photoconductivity result, which will be presented in section 5.3.3.

All the samples have similar behaviour of blue band temperature dependence. The intensity of the blue band keeps increasing with temperature first and reaches the highest intensity at around 120 K, shown in the insets of figure 5.7. Then decreases with temperature slowly, about 200 K, the blue band intensity suddenly decreases to back ground level. This is a very interesting phenomenon, which could be used for temperature control light emitting devices. This observation is similar to that of Meyer et al's, [167] where they explained the blue band emission evolving with increasing temperature, as a result of the thermal ionisation of the donor and the increase in the carrier concentration in the conduction band.

To gain insight into the nature of these peaks, the intensity vs. temperature plots of control sample and samples etched by N_2 and $SF_6 + N_2$ are shown as figure 5.8 . P1, P2, P3, and P4 stand for peak of 3.08 eV, 3.17 eV, 3.28 eV and D^oX respectively.

For the control sample, the peak intensity of 3.17 eV is comparable to that of peaks 3.28 eV and 3.08 eV, as shown in figure 5.7a and 5.8a. After N_2 etching, the peak intensity of D^oX and 3.17 eV decrease dramatically, see figures 5.1, 5.7 b and 5.8b. This observation indicates a possible transfer of intensity from D^oX and peak 3.17 eV to peaks 3.28 eV and 3.08 eV after etching. This could be explained as etch induced defects form efficient radiative recombination centres or paths, which has the energy states of 3.28 eV and 3.08 eV. This implies that peaks 3.08 eV and 3.28 eV are related to N concentration in GaN. This analysis confirms the previous result that peak of 3.08 eV is related to N vacancy. In addition, the P1 increases intensity faster than the P2 and P3 and reaches the highest intensity earlier than the others. This suggests that P1 has different chemical nature of the other 2 peaks.

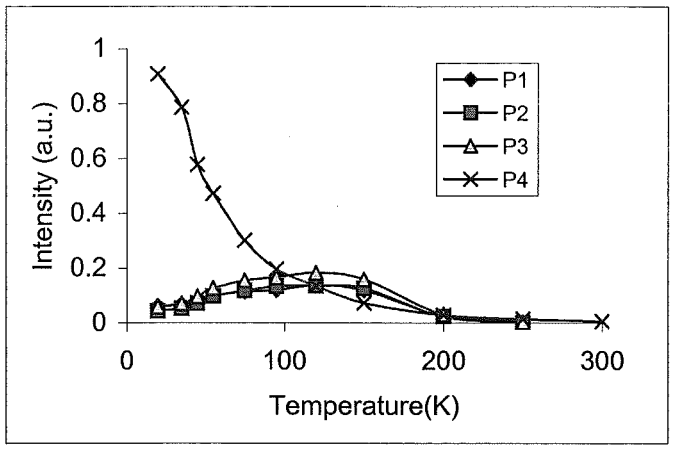

a

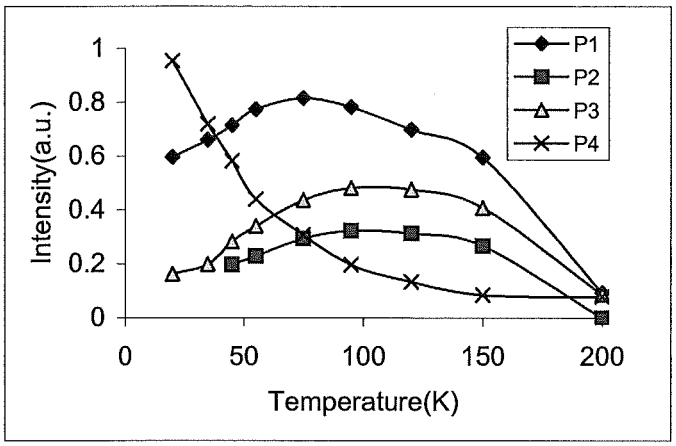

b

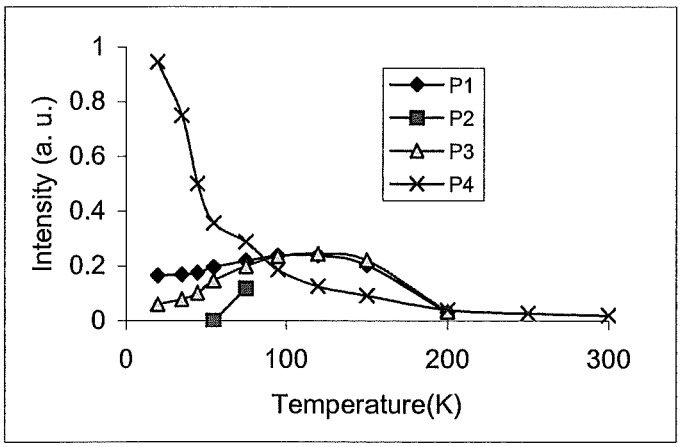

c

Figure 5. 8 The intensity vs temperature plot of the four peaks, 3.08 eV (P1), 3.17 eV (P2), P3 for 3.28 eV (P3) and D^oX (P4) of a) control, b) N_2 etched sample and c) $SF_6 + N_2$ etched sample.

After $SF_6 + N_2$ etching, the P1 and P3 remain comparable in intensity and its temperature dependence behaviour. While D^oX and the P2 have dramatically decreased, see figure 5.1, 5.7 c and 5.8c. The difference effects on these peaks by different etching gases are obvious. These also show that these three peaks P1, P2 and P3 are separate defects related.

5.3.7 Annealing effects on spectra

To investigate further the processing effect on GaN, the luminescence of the D^0X peak is compared between the N_2 etched sample and a control sample annealed at 1000 K for 1 hour in N_2 ambient. The spectra obtained for the sample before and after the annealing, are shown in figure 5.9. The dominant peak of 3.445 eV can be associated with the D^0X emission. It is apparent that the D^0X intensity has decreased, both after N_2 etching (figure 5.1a) and annealing in N_2 environment (figure 5.9).

Gaussian deconvolution of the control sample of PL reveals the neutral acceptor-bound exciton emission (A^oX) [155] at 3.439 eV. The intensity of both D^0X and A^oX are reduced by approximately 50% for the annealed sample. This allows the free A-exciton to be revealed at 3.453 eV. However, Orton et al reported that annealing in N_2 atmosphere activates the acceptors [10]. The authors attribute the acceptor to Ga vacancies. While Bruno et al [167] reported that substituting for Ga sites and being donors are possible elements from fouth group of the periodic table: C, Si, Ge, etc. Carbon is believed to act as an acceptor, and some experiments indeed provide evidence for p-type conduction due to Carbon [171].

Note that the reduction in D^0X intensity as a result of annealing is a different mechanism compared to that of etching. In the etched samples, D^0X decreased by a similar factor but in no case there was an indication of the free exciton to appear. Thus for this series of samples, etching appears to inhibit near band-gap luminescence in general while annealing in nitrogen reduces emission intensity of both the emission intensity of the acceptor and donor-bound defect states.

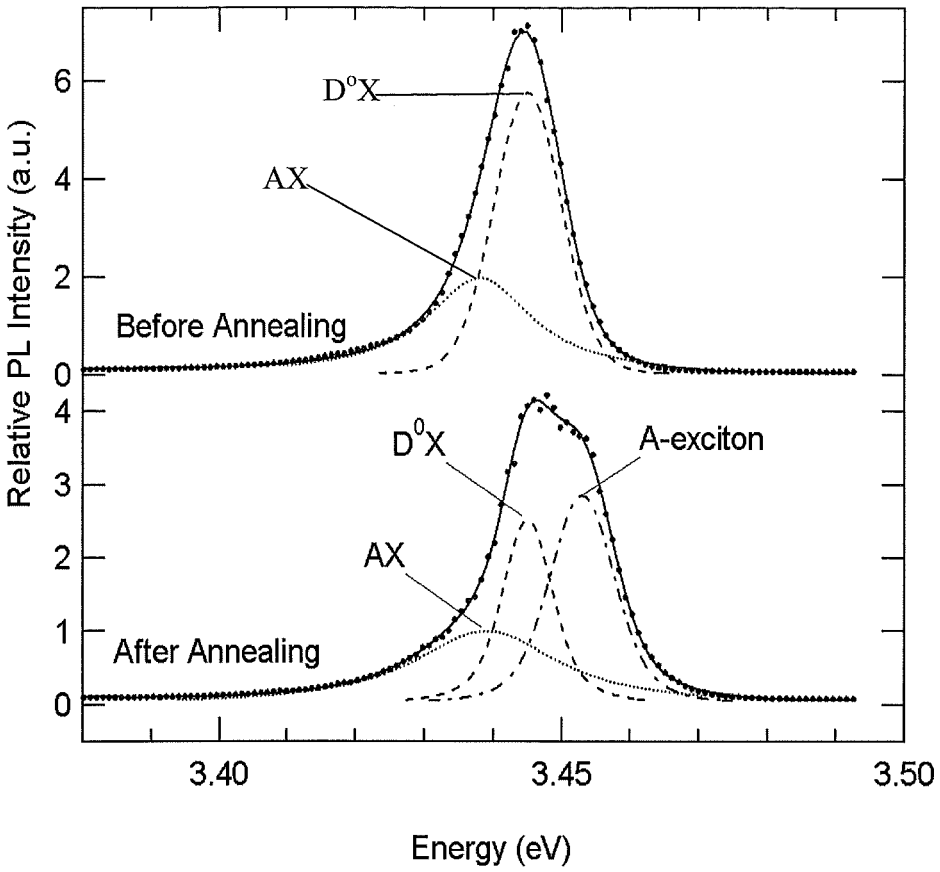

Figure 5. 9 Photoluminescence spectra at 20K of control sample before and after annealing in N_2 atmosphere. After annealing, the intensity of both D^0X and A^0X are reduced by approximately 50% for the annealed sample. This allows the free A-exciton to be revealed at 3.453 eV.

5.4 Summary

In conclusion, we have used photoluminescence and photoconductivity to study epilayers of GaN on SiC substrates that have been etched with RIE plasma of Ar, N_2, SF_6 and mixed SF_6+N_2 gases. The photoluminescence spectra are dominated by the neutral-donor-bound D^0X emission, while the photoconductivity bands are determined to be intrinsic free-exciton features.

Reactive ion etching reduces the photoluminescence (PL) intensity of GaN films grown on SiC substrates. Ar and SF_6 +N_2 plasmas are found to cause the least optical damage compared with SF_6 and N_2 plasmas. The role of ion bombardment does not play an important role in creating optical etch-induced damage in GaN. There is evidence of nitrogen incorporation on the GaN surfaces exposed to N-containing plasmas. Comparison of the PL analysis of the etched and annealed GaN sample indicates that annealing in N_2 reduces the emission intensity of the acceptor and donor-bound defect states while etching inhibits the near band-gap luminescence in general.

No saturation effect has been observed with various incident laser power experiments in both control and etched sample.

The blue band emission has been investigated. The peaks 3.28 eV, 3.17 eV, 3. 17 eV, are more like separate defects related. The peak 3.08 eV is possibly related to N vacancy.

Chapter 6

Etch Mechanism in the ICP Etching of GaN in Fluorine and Chlorine Plasmas*

6.1. Introduction

The applications [2, 172, 173] of GaN and related material and the reasons [54, 174,175] for using dry etching have been reported in chapter 1. Reactive Ion etching (RIE) of GaN has been widely investigated [176]. A range of gases, such as SF_6 + N_2, $SiCl_4$, CCl_2F_2, and BCl_3 have been used [177]. In all RIE plasmas, high ion bombardment is required to break the III-N bond and to promote desorption of etch products from the surface. As a consequence, etch rates are relatively low, with the fastest etch rate obtained in chorine-based plasmas. Furthermore, ion bombardment may create defects that degrade electrical and optical properties of the material [32, 44, 47, 129, 177]. High-density plasmas (HDP) are generally considered as a major improvement for GaN device fabrication [6, 70]. HDP processing yields a high reactive species content with independent control of the ion energy. Among HDP, the inductively coupled plasma (ICP) approach has been most commonly used for the etching of GaN. High etch rate and anisotropic profiles have been reported with ICP [58] compared to RIE. However, Zhang et al [177] found ICP Cl_2 + Ar discharges to degrade the performance of GaN Schottky diodes notwithstanding the ion energy control.

Chapters 3 and 4 show that a SF_6 + N_2 RIE plasma did not degrade the diode properties, while the etch rate is slow in RIE. Therefore, it would be interesting and essential to study the ICP etching of GaN in SF_6 + N_2 and its effects on GaN

* The fluorine plasma information in this chapter has been presented in published paper "Dry etch-induced damage in an inductively coupled plasma" J. Vac. Sci. Technol. B Nov./Dec. 2001.
Chlorine plasma information has been included into a draft of "ICP chlorine plasma etching of GaN and etch induced damage characterization" submitting to J. Appl. Phys.

properties, for this purpose, it is necessary to understand the etch mechanism first. In this chapter, we report an investigation of ICP processing of GaN with $SF_6 + N_2$ gas mixtures, and a comparison with the etch behaviour in chlorine plasma. The ICP etch mechanism has been studied and etch condition has been optimised for fast etch rate, vertical profile and smoother surface.

6.2 Experimental details

Nominally undoped 3 μm thick GaN and 0.3 μm thick doped ($1\text{-}5x10^{17}cm^{-3}$) GaN, both on 0.4 μm AlN buffer on sapphire, are used for the etch mechanism study. All films have been grown by metal-organic vapor-phase epitaxy (MOVPE).

The ICP plasma reactor used is a load-locked Alcatel etch system (METLAB) operating at 13.56 MHz. The etch gas is introduced from the top of the reactor. Dry etching has been carried out at the following basic conditions. For the fluorine plasma, the etching gas composition $SF_6 : N_2 = 1 : 1$, total flow rate 50 sccm, etching pressure 5 μbar, substrate temperature 25 ^{0}C, ICP source power 1500W, DC bias 200 V. In the separate series of experiments, the DC bias, source power, gas composition, temperature, and pressure have been varied to determine the etch performance (rate and profile) under these conditions. In the case of the chlorine plasma: gas composition 75% Ar + 25% Cl_2, total flow rate 100 sccm, etching pressure 10 μbar, DC bias 300 V, ICP source power 500 W, temperature 25 °C. In separate series of experiments, gas composition and DC bias have been varied.

Energetic ion bombardment control is provided by an independent rf-bias (13.56 MHz) of the substrate. The substrate temperature is controlled by a substrate holder, cooled by liquid nitrogen and equipped with a heating system and helium (He) back flow. Note that two ICP etch systems have been employed, for fluorine and chlorine plasma respectively. In ICP fluorine plasma system, substrate temperature can vary from –150 °C to 30 °C, while in the ICP chlorine plasma system, substrate temperature can vary from 0 °C to 220 °C.

Langmuir probe and optical emission spectroscopy of plasma have been used to quantify the ion flux and atomic fluorine radical concentration respectively, the latter by actinometry (with Ar) [107, 178].

The etch depth has been measured using stylus equipment (alpha-step). The etch profile has been inspected by scanning electron microscopy.

6.3 Results and discussion

6.3.1 Influence of dc bias on etch rates and ion yield

The ion yield, defined as the nominal number of GaN species removed per ion, is computed from the etch rate and the ion current (appendix C). The ion yield provides an objective measurement for the ion-induced etch behavior. It is useful to compare the reactive etch gas with a pure sputter gas, as it tells the chemical enhancement involved. Ion yield is extremely useful in comparing different reactive gases, the different ion densities in various plasmas are normalized in terms of ion yield.

Figure 6.1 a, b show the GaN ion yield and etch rate vs. DC bias in $SF_6 + N_2$ (1 : 1), and figure 6.2 a, b show GaN ion yield and etch rate vs. DC bias in the Ar

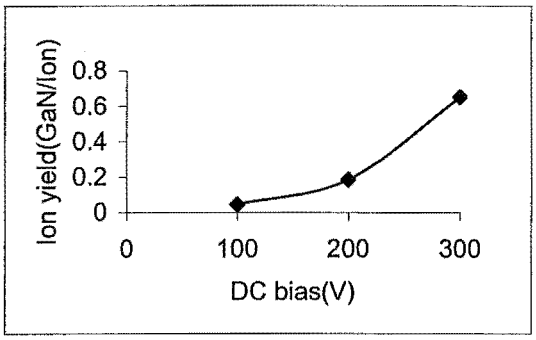

a

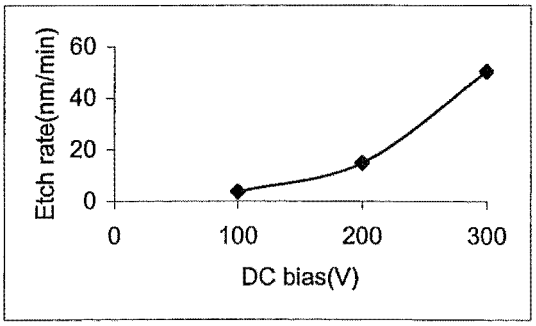

b

Figure 6. 1 a) Ion yield and, b) Etch rate vs. DC bias in $SF_6 + N_2 = 1 : 1$ plasma. It can be seen that the etching of GaN starts at 100 V in the $SF_6 + N_2$ plasma. The ion yield increases exponentially with ion energy, with the ion yield at 300 V being 3 times higher than that at 200 V. Etch conditions see text.

plasma, respectively. It can be seen that the etching of GaN starts at 100 V in the SF_6 + N_2 plasma while in the Ar plasma, etching starts at 150 V. Since only physical sputtering occurs in an Ar plasma, this observation suggests that the SF_6 + N_2 plasma has a slight chemical enhancement compared with pure physical sputtering in the Ar plasma. Furthermore, in the SF_6 + N_2 plasma, the ion yield increases exponentially with ion energy, with the ion yield at 300 V being 3 times higher than that at 200 V. This strongly suggests the etching mechanism in SF_6 + N_2 contains an ion-induced chemical one as the ion energy is increased.

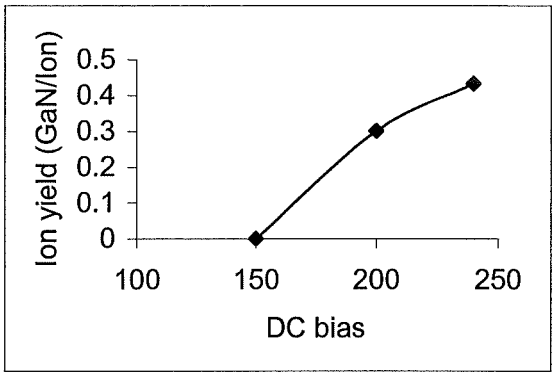

a

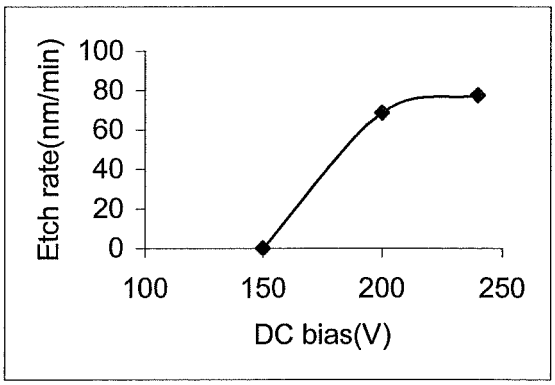

b

Figure 6. 2 a) Ion yield and, b) Etch rate vs. DC bias in Ar plasma. It can be seen that the etching of GaN starts at 150 V in the Ar plasma. Since only physical sputtering occurs in an Ar plasma, this observation suggests that the SF_6 + N_2 plasma has a slight chemical enhancement compared with pure physical sputtering in the Ar plasma.

6.3.2 Influence of nitrogen percentage on etch rate and ion yield

Within the mixture gas $SF_6 + N_2$ process, an interactive (enhancement) effect was noticed between the two reactants, see figure 6.3a. The (1:1) mixture shows a substantially higher yield than the individual components. In an analogy to Si_3N_4 etching using $CF_4 + O_2 + N_2$, an intermediate state where the nitride surface is attacked first by N radicals under formation of the molecular N_2 could play a role [179]. The nitrogen atom from plasma reacts with nitrogen atom from GaN surface and form N_2. The formed N_2 molecule may diffuse to bulk gas, shown in 6.3b, leaving Ga atoms with dangling bond on the surface to react with fluorine.

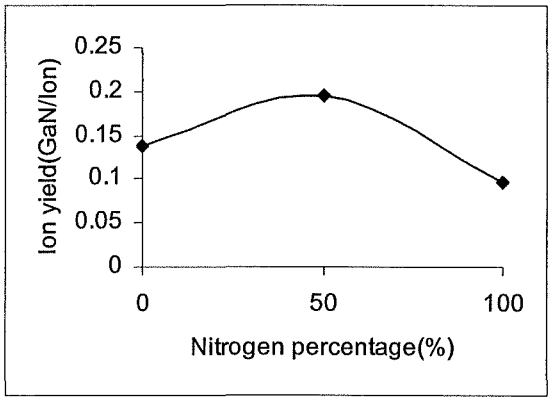

a

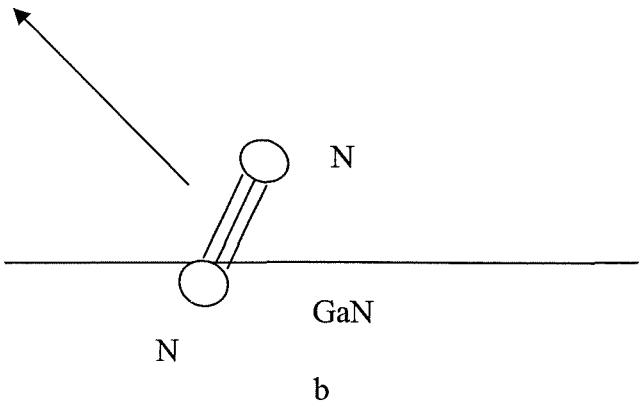

b

Figure 6. 3 a) Ion yield vs. nitrogen percentage in $SF_6 + N_2$ plasma. The mixture gas produces the highest ion yield compared to the pure N_2 and pure SF_6. b) Analogy to Si_3N_4 etching in $CF_4 + O_2 + N_2$ plasma. An intermediate state where the nitride surface is attacked first by N radicals under formation of the molecular N_2 could play a role [179]. The nitrogen atom from plasma reacts with nitrogen atom from GaN surface and form N_2. The formed N_2 molecule may diffuse to bulk gas.

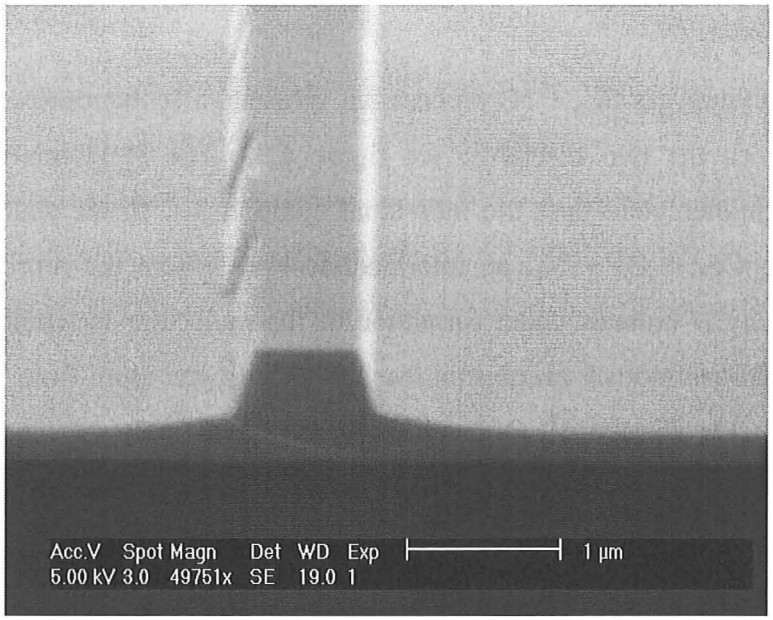

a

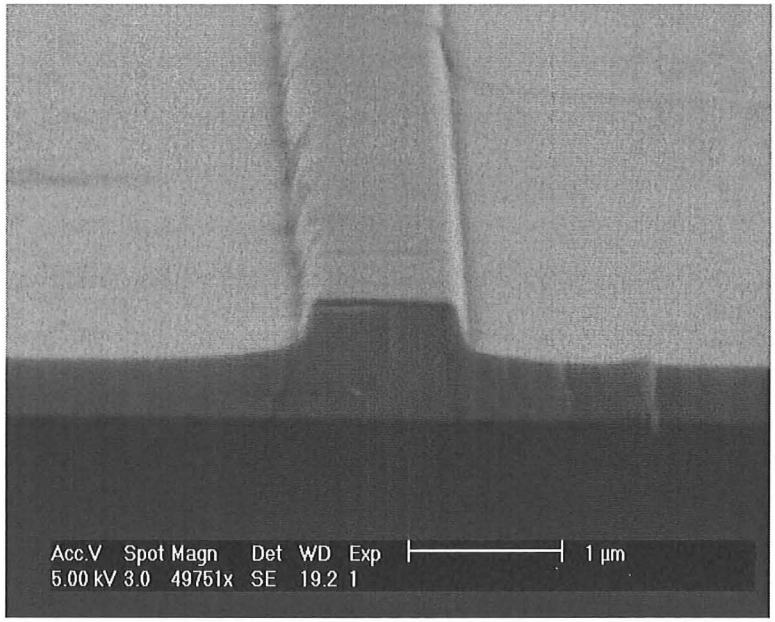

b

Figure 6. 4 a) SEM image of etch profile etched by mixture gas $SF_6 + N_2$, $\alpha = 73.32$ °, etching time, 20 minutes, b) By pure SF_6, $\alpha = 73.56$ °, etching time 20minutes. Other parameters are kept constant see text. It is obvious the mixture gas produces deeper etch depth than pure SF_6 gas, while the etch profiles are identical.

Figures 6.4 a, b are GaN etch profiles with different etch depth using pure SF_6 and mixture gas $SF_6 + N_2$ with all other etching conditions the same, total gas flow 25 sccm, substrate temperature 25 °C, DC bias 200 V and etching time 20 minutes. It is obvious that the sample etched by the mixture gas has the deeper etch depth than that etched by pure SF_6. In addition, we noticed that the profiles are identical here. α is the angle between the inner sidewall and the substrate of etched profile. This result is in contrast to the result we obtained in RIE fluorine plasma presented in chapter 3, where the gas mixture of $SF_6 + N_2$ (1:1) produces a more vertical profile than pure SF_6 plasma. This will be explained in section 6.3.6.

6.3.3 Influence of ICP source power on etch rate and ion yield

Figures 6.5 a, b show the GaN etch rate, and ion yield and ion density vs. ICP source power. The etch rate increases with ICP source power and reaches the maximum at 1500 W and then saturates. The ion yield reaches the maximum value at a low ICP source power and decreases as the ICP source power increases after 1000 W.

The higher ion efficiency at a power level below 1000 W, suggests an etching regime that is limited by the supply of ions to desorb the reaction products at the surface. At a power level beyond 1000 W, the ion yield starts to decrease with increasing the ICP source power. The high ion current density implies a high molecular ionization at high power, while the chemical supply is measured to be constant (shown in figure 6.5c). Consequently, the ions are less efficient in removing the etch products, compared to the low ICP source power regime. The high ICP source power regime, therefore, is a chemical supply limited etch regime.

The balance regime of physical and chemical components around 1000 W, the etch mechanism changes from physical limited one to chemical limited one, is highly efficient etch regime.

It is worth noting that fluorine radical concentration keeps more or less constant with ICP source power as shown in figure 6.5c.

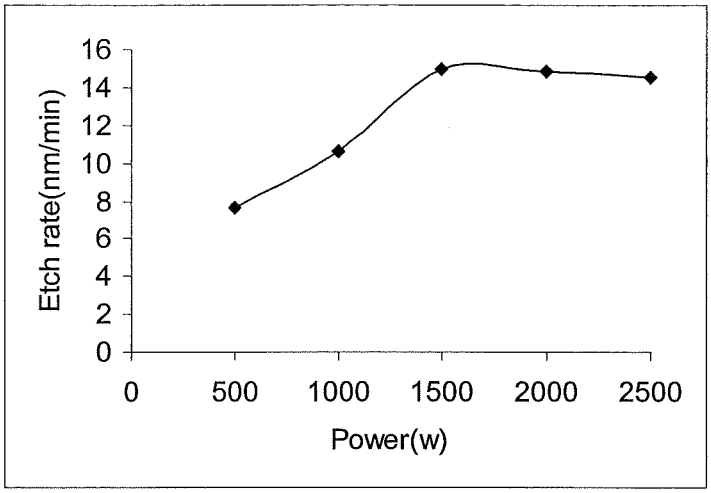

a

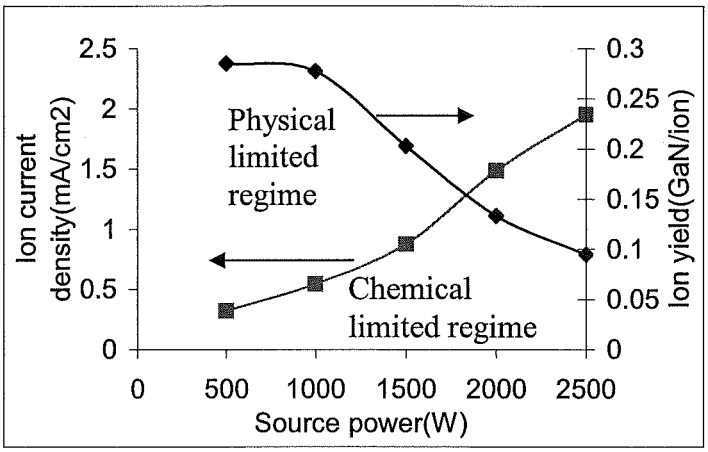

b

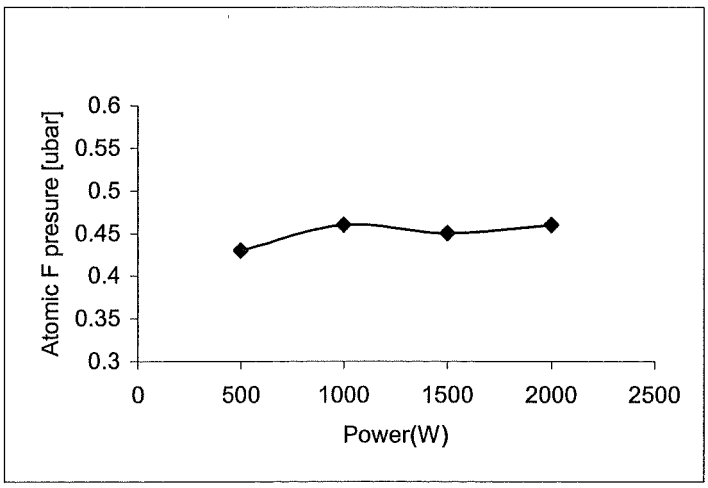

c

Figure 6. 5 a) Etch rate, b) Ion yield and ion current density, c) Atomic F pressure vs. ICP source power. The etch efficient regime is from 1000 W to 1500 W, where physical component and chemical component are balanced. Etch conditions see text.

6.3.4 Temperature dependence and activation energy

The dependence of substrate temperature in the etch behavior gives a better view on the underlying thermodynamics. The relationship between etch rate and activation energy can be expressed as follows,

$$\text{Etch rate} = A \exp(-E_a / k T) \qquad 6.1$$

Where A is the temperature dependence constant, E_a is the activation energy (eV), k is the Boltzmann constant and T is the temperature of substrate (K).

Figure 6.6 shows the Arrhenius plot for the GaN etch rate in the basic $SF_6 + N_2$ process. An activation energy of 0.053 eV is deduced, which is comparable to 34 meV activation energy of GaN at dopant level of 6×10^{16} (cm^{-3}) determined by Wickenden et al [180]. This is a rather low activation energy compared to 0.55 eV of intrinsic silicon activation energy [181]. Since GaN does not etch spontaneously, the weak temperature dependence in the etch rate is an integral aspects of the ion-induced etch product formation. The exact nature of this step is unclear yet. At temperatures below – 50 °C, the etch rate is constant and completely dominated by physical sputtering.

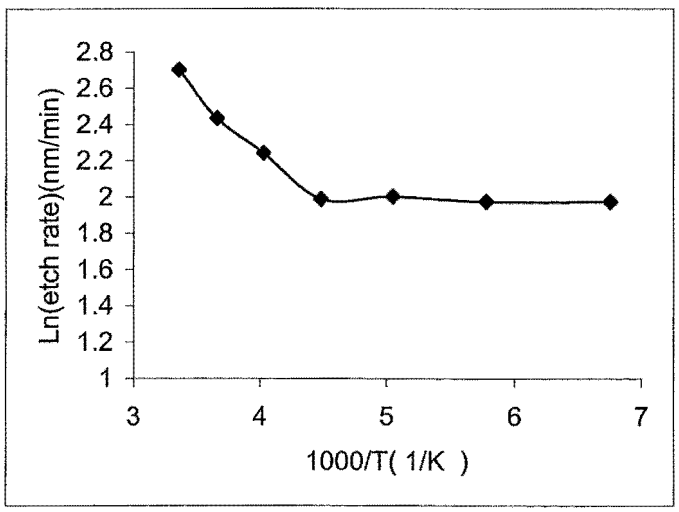

Figure 6. 6 shows the Arrhenius plot for GaN etch rate in the basic $SF_6 + N_2$ process. An activation energy of 0.053 eV is deduced. This is comparable to 34 meV of GaN with dopant level of 6×10^{16} (cm^{-3}) determined by Wickenden et al.

Figures 6.7 a, b show the etch profiles obtained at different temperatures. The sample imaged in figure 6.7a has been etched for 20 minutes at room temperature, and figure 6.7b etched for 45 minutes at –50 °C. The rest of the plasma parameters are kept constant, total gas flow rate 25 sccm, mixture SF_6 : N_2 = 1 : 1, DC bias 200V, pressure 3 μbar. It can be seen that the profiles are identical for lower temperature and room temperature. The anisotropic profile confirms the ion-induced etching mechanism [182].

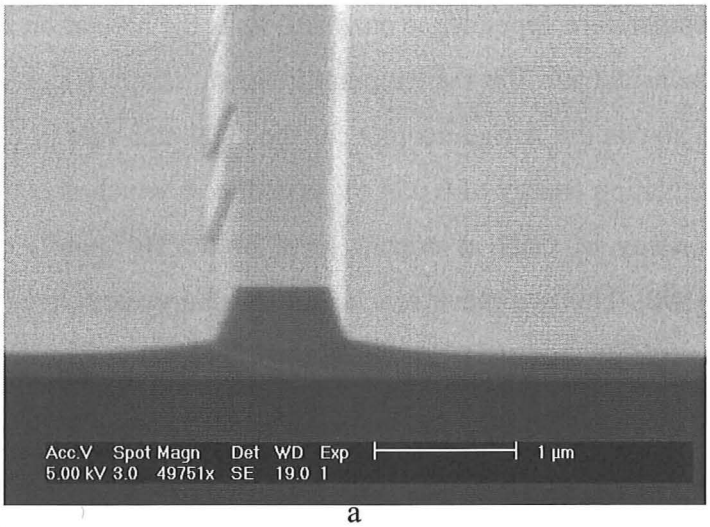

a

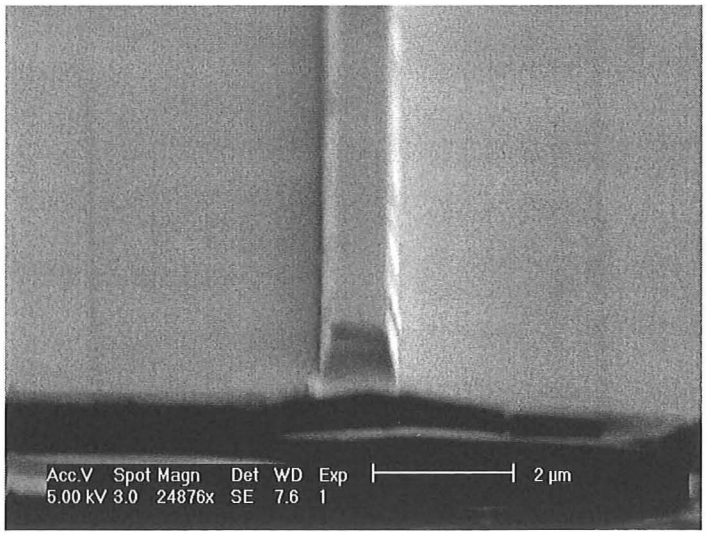

b

Figure 6. 7 a) The etch profile produced at room temperature and b) The profile produced at – 50 degree. There is a significant change in etch rate at temperatures above – 50 °C, and identical profile for different temperature due ion-induced etching dominates the plasma. The etch conditions see text.

6.3.5 Influence of pressure on etch rate and ion yield

Figure 6.8 a shows the ion yield and etch rate and figure 6.8 b shows the atomic F radical concentration and the ion current density vs. etching pressure (by changing the total flow rate). Substrate temperature of 25 °C, gas mixture $SF_6 : N_2 = 1 : 1$, ICP source power 1500 W and DC bias 300 V were kept constant.

In regime 1, the etch rate and ion yield increase with pressure, ion current density decreases sharply, F radical concentration increases with pressure. This observation suggests that in this regime ion sputtering is efficiently removing the etch products, and etch behaviour is dominated by physical etching. This implies radical flux is the limiting factor. The etch rate increases with increasing the chemical supply and reaches the highest etch rate of 67 nm/min at 2.9 μbar (Detailed etching conditions are total flow rate 25 sccm, $SF_6 : N_2 = 1 : 1$, etching pressure of 2.9 μbar, substrate temperature of 25 °C, ICP source power of 1500 W, dc bias of 300 V).

In regime 2, the etch rate and ion current density decrease with pressure. Ion yield and fluorine radical concentration keep increasing with pressure. Obviously the etch rate gets limited by the amount of ions. This suggests that in this regime, etch products start to accumulate on the surface and ions are more and more efficiently used. The regime changes from radical-limited to ion-limited. Ion yield reaches the maximum at 5 μbar.

In regime 3, the etch rate, ion yield and ion current density, all decrease with pressure, while the F radical concentration keeps increasing. Over-supplying chemical radicals and further decreasing ion current density slows down the etch rate. Etch products accumulate on the surface and poison the surface. More portions of ions sputter the etch products instead of etching the GaN. Apparently, this is physical limited regime.

In regime 4, etch rate, ion yield and ion current density are no long varying with pressure. F radical concentration is increasing with pressure. In regime 3 and regime 4, the very possible explanation is that the surface has been covered with an excess of etch products. Thus, the desorption by ion impact becomes the etch rate limiting step. The constant ion current density produces a constant etch rate and ion yield. Obviously, this is a physical limited regime.

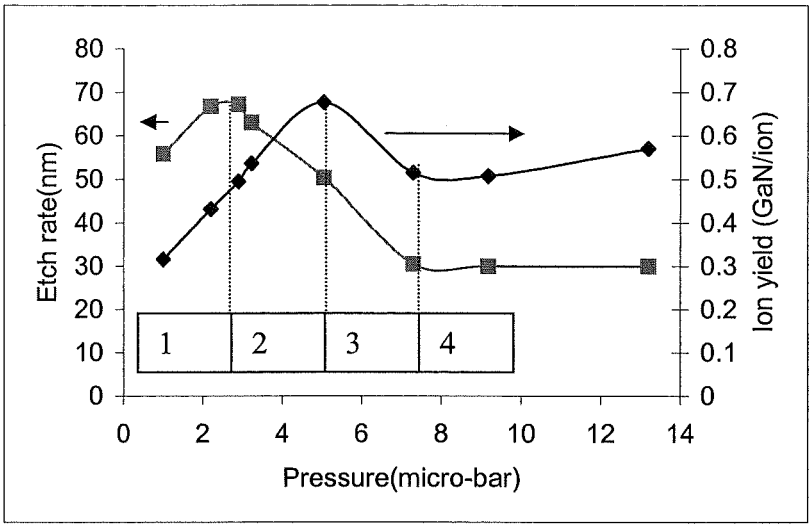

a

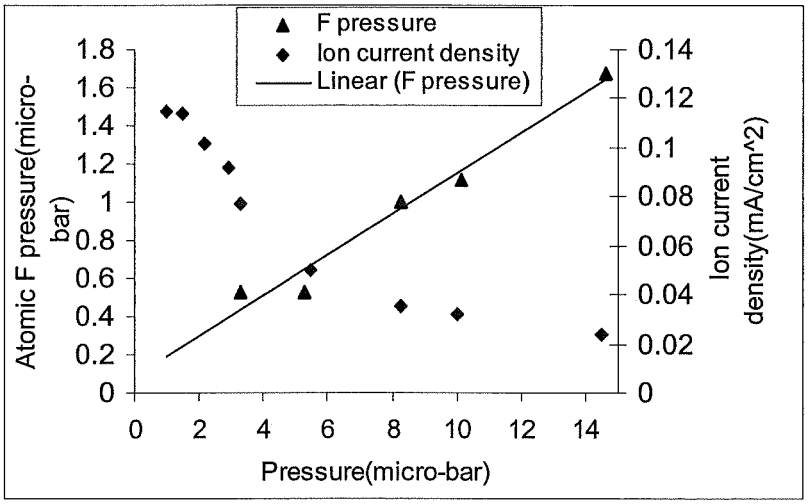

b

Figure 6. 8 a) shows the ion yield and etch rate, and b) F radical concentration and ion current density vs. etching pressure (by changing the total flow rate). From regime 1 to 2, the etch process turns from chemical limited, to a physical limited. Regime 3 and 4 are physical limited. Etch conditions, substrate temperature of 25 °C, gas mixture SF_6 : N_2 = 1:1, ICP source power 1500 W and DC bias 300 V have been kept constant.

The above results and discussion show that the highest etch rate is achieved when the surface coverage with etch products is kept at a minimum, and at the same time there should be a sufficient supply of reactive species to the surface.

6.3.6 Comparison of fluorine plasma etch mechanism in RIE and ICP

In chapter 3, RIE etching results show that the etch rate increases and etch profile gets more vertical with increasing $\%N_2$ in the fluorine mixture gas. See figure 3.3a. The etch profiles produced by ICP of pure SF_6 plasma and $SF_6 + N_2$ plasma are of a more vertical nature and are almost identical, as shown in figures 6.4 a ,b.

The possible reason is that lower ion current density in RIE limits the desorption step, while ICP has no desorption problem due to the relative higher density of ions, sputtering away the material more efficiently. The principle of redeposition causes tapered sidewall will be presented in figure 6.9.

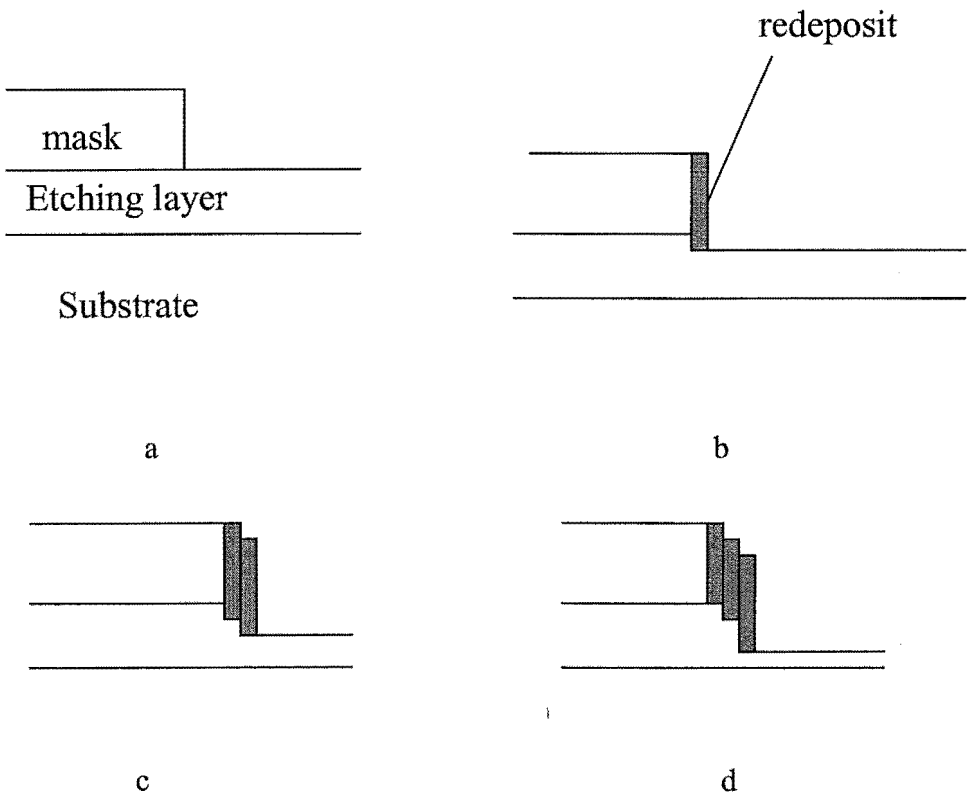

Figure 6. 9 Limitation of dry physical etching, redeposition of materials sputtered from the bottom of trench, forms facet or round corner at mask edge. a, b, c and d are the sequence of process.

Ion etching or physical etching does not lead to undercutting of mask, but the walls of an etched cut are not necessarily vertical. A variety of factors can contribute to this loss of fidelity in pattern transfer. Loss of dimension is either caused by non-volatile sputtering products (redeposition) or by special ion-surface interactions. Figure 6.9 [95] shows one of the physical sputtering limitations: redeposition of non-volatile products on a step edge. The redeposition involves sputtered non-volatile species from the etched surface settling on the sidewalls of the mask and trench. The phenomenon manifests itself mainly on sloped sidewalls. Figure 6.10 is a SEM image, showing the redeposition products after removal of an etched GaN wire (etched in $Ar + Cl_2$).

Physical etching or sputtering is non-selective etching because large ion energies compared to the differences in surface bond energies and chemical reactivities, are involved in ejecting substrate material. In general, this method is slow, compared to other dry etching methods, with etch rates limited to several hundreds of angstroms per minute, compared to thousands of angstroms per minute and higher for chemical and ion assisted etching.

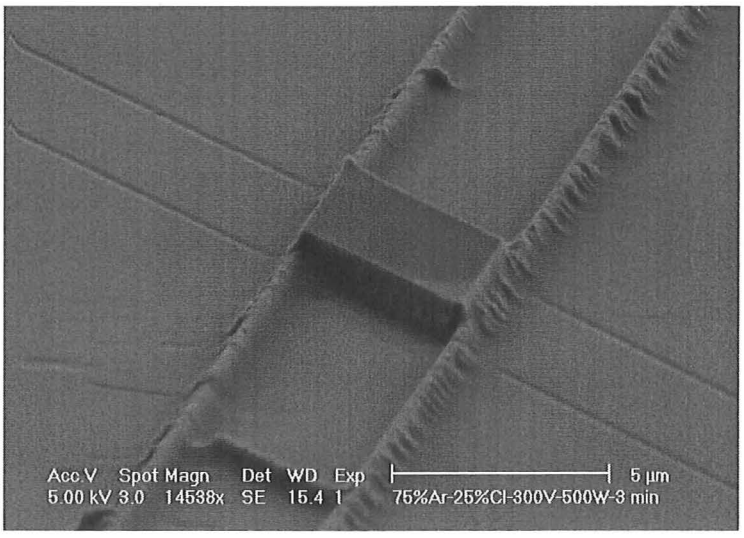

Figure 6. 10 SEM image of redeposition after removal of an etched GaN wire (etched in $Ar + Cl_2$). Redeposition forms sloped sidewall.

The RIE etching of GaN in fluorine plasma shows slow etch rate 13.3nm/min, sloped sidewalls and rounder corners, compared to ICP etching with a fast etch rate of 67 nm/min, better vertical nature of sidewall in fluorine plasma. Look again at the differences between RIE and ICP in chapter 2. ICP (actually all high density plasma) can dissociate molecules more efficiently. ICP has more reactive species and a higher ion density. The common ions in SF_6 plasma are SF_5^+, SF_3^+, SF^+, S^+ and F^+. General rule is that the higher the source power, the smaller the molecular fragments [183]. For example, Malyshev et al reported that chlorine plasma has mainly Cl^+ ion in ICP and mainly Cl_2^+ ion in RIE [184]. Therefore, more F radicals are expected in SF_6 ICP than in SF_6 RIE plasma. Obviously, F radical is much more chemically reactive towards GaN than molecular SF_6 under the same conditions.

All of these aspects suggest both of RIE and ICP fluorine plasma in etching GaN are ion – induced etching, while ICP has a larger chemical enhancement. This analysis agrees with the observation in 6.3.1.

6.3.7 ICP chlorine plasma etching GaN

To compare chlorine etching with fluorine etching, ICP etching of GaN has been carried out in a Ar + Cl_2 plasma. Figures 6.11 a, b show etch rate and ion current density vs. Cl_2 percentage, keeping other plasma parameters constant. Ion current density decreases initially very sharply with increasing Cl_2 content, and then slowly decreases to saturation. We obtained the fastest etch rate at gas composition of 75% Ar + 25% Cl_2. This observation can be explained by a chemical and physical balance point of view. In low Cl_2 percentage regime, figure 6.11b shows high ion current density. Physical sputtering is sufficient to remove etch products. This suggests a chemical limited mechanism in the lower Cl_2 percentage regime. After the balance point of 25% Cl_2, the chemical portion starts to dominate, while the ion current density still decreases. It indicates a physical limited regime. Another small bump in etch rate at around 75% Cl_2 percentage is unclear.

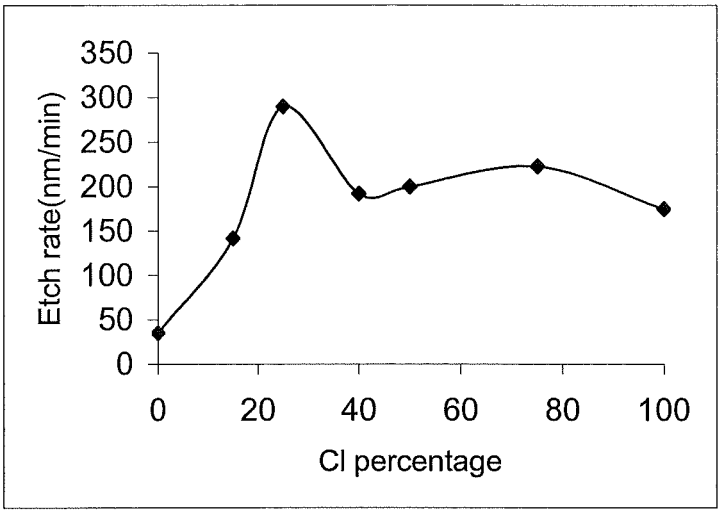

a

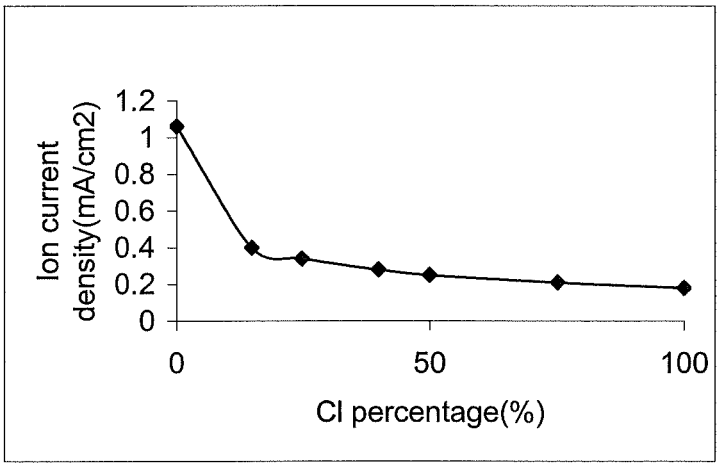

b

Figure 6. 11 a) Etch rate and b) Ion current density vs. Cl_2 percentage. At 75% Ar + 25% Cl_2 reaches the fastest etch rate, due to balance chemical and physical components.

Figures 6.12 a, b show etch rate and ion current density vs. DC bias in 75% Ar + 25% Cl_2 gas composition. The etch rate increases fast with DC bias in the low DC bias range, and more slowly in the high DC bias regime. This observation is in contrast to that observed in fluorine plasma. Ion current density is increasing slowly with DC bias with DC bias above 100 V. The conclusion can be made that chlorine plasma etching of GaN is ion-induced.

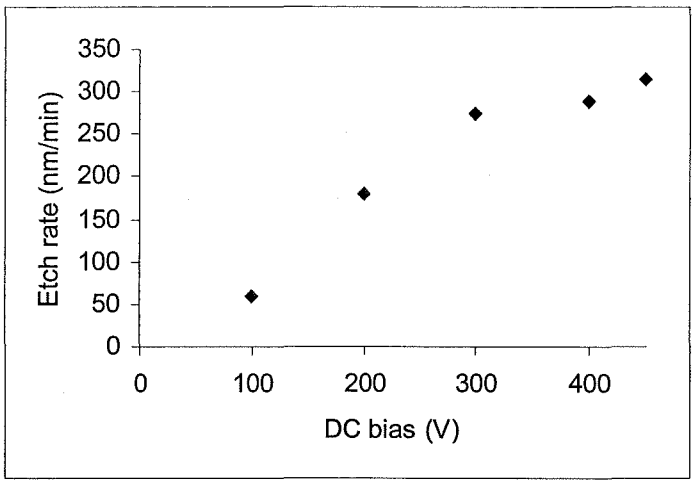

a

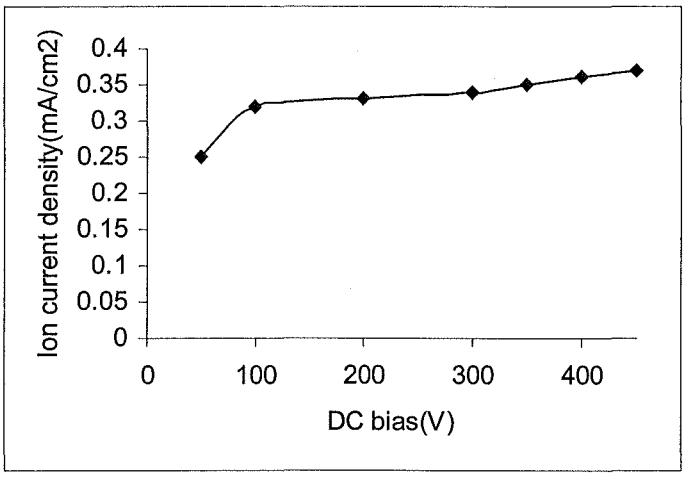

b

Figure 6. 12 a) Etch rate, b) Ion current density vs. DC bias in Cl_2 + Ar plasma etching GaN. The etch rate increases with DC bias fast at low DC bias, and slowly in the high DC bias regime. Ion current density keeps increasing with DC bias. Etch conditions see text.

The fastest etch rate is 314 nm/min, which was obtained in chlorine plasma with the following etch conditions: substrate temperature of 25 °C, the total flow rate of 100 sccm, etching pressure 10 μbar, dc bias of 450 V. The etch rate is about a factor of 5 more of that in fluorine plasma. Figure 6.13 shows the SEM image of the etch profile obtained with the particular etch conditions. The anisotropic profile confirms the ion induced etching mechanism

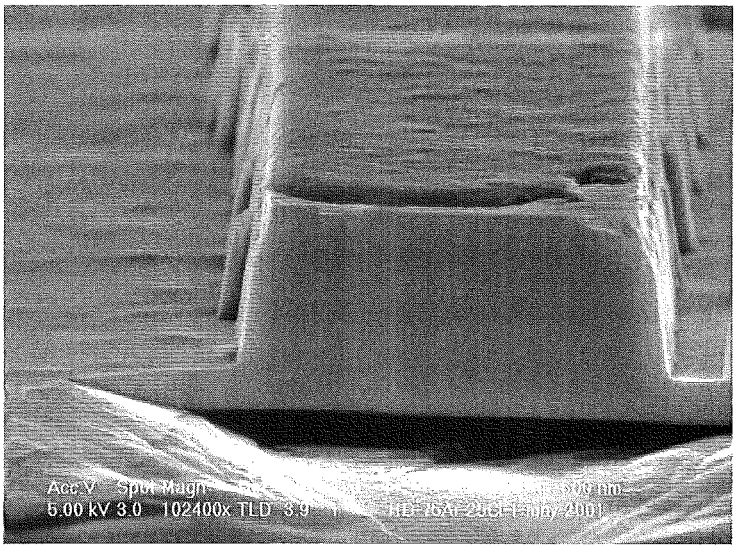

Figure 6. 13 SEM image of etch profile obtained at the fastest etch rate of specified etching condition. An almost vertical profile can be seen. The etch conditions see text.

Investigation of the impact of BCl_3 on the etching GaN has been carried out. A small amount of BCl_3 added to Cl_2 can increase the etch rate significantly in etching magnetic material [185] and GaAs [186]. 10 sccm of BCl_3 has been added to a 90 sccm flow of Cl_2 to compare with 100% of Cl_2 plasma etching GaN while all other parameters are kept the same. The etch rate has increased by about 10% in the BCl_3/Cl_2 mixture gas. Pearton and Shul et al [187] attributes this increase to a higher ion mass species to promote the desorption of etch products more efficiently, so that the etch rate increases. In an identical electrical field, the bigger ion mass has larger ion energy, which could enhance the physical sputtering.

An alternative explanation is that BCl_2^+ is very reactive and powerful in etching. For example, BCl_3 / Cl_2 is essential to etch Al. Without BCl_3 (BCl_2^+), Cl_2 is unable to etch Al.

However, in etching magnetic materials, BCl_3 has a different impact. There is nothing to do with high ion mass [185].

6.3.8 Comparison of the etch mechanism of the fluorine plasma with chlorine plasma in etching GaN

To gain insight into the general rules, the etching mechanisms of fluorine plasma and chlorine plasma have been compared.

The most useful plasma etching is neither pure physical nor entirely chemical. By employing the synergy of physical and chemical components, the shortcomings of both sputter-based low etch rate, and purely chemical isotropic dry etching, can be surmounted.

In physical–chemical techniques, ions may enhance etching by the following. Ion bombardment [188] induces a reaction by making the surface more reactive for the neutral plasma species, for example, by creating surface damage. Ions may clean the surface of film-forming reaction products, allowing etching with reactive neutrals to proceed on the cleaned area. Finally, ion may supply the energy to drive surface reactions. Defining which step primarily causes enhanced etching is often hard to determine.

In the particular cases in this study both fluorine plasma and chlorine plasma etching of GaN, contain physical and chemical components. The chlorine plasma achieves a much faster etch rate (a factor of 5), compared to the fluorine plasma.

The possibilities for chlorine plasma having faster etch rate compared to fluorine plasma, are that etch product GaClx in chlorine plasma is more volatile than fluorine plasma etch product GaFx [189]. This implies that chemical enhancement in fluorine based plasma is less than in a chlorine based plasma.

6.4 Summary

ICP etching of GaN in a $SF_6 + N_2$ plasma is found to be dominated by an ion-induced mechanism. The most efficient etch regime is observed for ICP source power at range of 1000 W to 1500 W, where the etch mechanism is ion-limited. The fastest etch rate of 67 nm/min has been achieved at etching conditions of a total flow rate of 25 sccm, $SF_6 : N_2 = 1 : 1$, etching pressure of 2.9 μbar, substrate temperature of 25 °C, ICP source power of 1500 W, dc bias of 300 V.

Comparison of RIE and ICP fluorine etching of GaN, shows both RIE and ICP fluorine etching of GaN are ion–induced, with ICP displaying much more chemical enhancement.

In the 75% Ar + 25% Cl_2 ICP plasma, the etching mechanism is ion induced. The best gas composition to gain a fast etch rate in the Ar + Cl_2 mixture is 75% Ar + 25% Cl_2. The fastest etch rate in the Ar + Cl_2 plasma is 314 nm/min, with etching conditions of a total flow rate of 100 sccm, etching pressure of 10 μbar, substrate temperature of 25 °C, ICP source power of 500 W and DC bias of 450 V.

Chlorine plasma has a five fold faster etch rate, compared to fluorine plasma, probably because of more volatile etch product $GaCl_3$ compared to GaF_x.

Chapter 7

ICP Etch Induced Damage Effect on Diode Properties of GaN•

7.1 Introduction

Dry etch techniques have been employed for GaN device fabrication due to its chemical inertness of material and minimization of device size. We have systemically studied conventional RIE fluorine plasma etching GaN [32, 190] and its effect on electrical [47] and optical properties [48]. The RIE fluorine plasma has relatively slow etch rate, 13.3 nm/min, and round corners at the edge of mask. RIE etching reduces PL intensity dramatically, while the gas mixture of $SF_6 + N_2$ etching improves the electrical diode properties. High density plasma, especially inductively coupled plasma (ICP) has been recommended for etching GaN due to high reactive species content and high ion current density at controllable ion energy. Huge efforts have been devoted to develop ICP etching of GaN. We have studied the etch mechanism of ICP processing of GaN and optimized the etch conditions for fast etch rates, 67 nm/min in fluorine plasma and 314 nm/min in chlorine plasma, high selectivity, Cr : GaN = 1 : 5 in chlorine plasma, NiCr : GaN = 1 : 5, and an almost vertical profile [191].

Industrial application demands fast etch rate, vertical profile and smooth surface etc. However, structural optimization is not sufficient in device fabrication. The given etch conditions may deteriorate device optical [44] and electrical

---

• The fluorine information in this chapter has been presented in published paper "Dry etch-induced damage in an inductively coupled plasma" J. Vac. Sci. Technol. B Nov./Dec. 2001.
Chlorine information has been included into a draft of "ICP chlorine plasma etching of GaN and etch induced damage characterization" submitting to J. Appl. Phys.

properties [129], for instance, chemical reaction, ion bombardment, ion implantation and redeposition may form a damage layer. Chemical reaction is possibly polluting the surface. Chemical reaction products and redeposition will give rise to a large depletion layer. Ion bombardment may induce new surface states and defects may diffuse into the bulk. Specially ion implantation raises bulk effects by means of channeling and radiation enhanced diffusion. A large depletion region is generally related to electrical properties, while surface states and bulk properties are more related to optical properties. The techniques used to monitor etch damage have been discussed in detail in chapter one.

Thus, the research on ICP processing induced damage is highly essential. In this chapter, the fluorine plasma and chlorine plasma effect on diode and photoluminescence properties will be presented. To unravel the underlying mechanism, XPS and AFM have been employed to analyze surface atomic concentrations and surface roughness respectively

7.2 Experimental details

The material used here is nominally un-doped 0.5 micron thick GaN on highly doped SiC for the electrical and optical characterization work. All the materials used here have been grown by metal-organic vapor-phase epitaxy (MOVPE).

The ICP plasma reactor used in this study is a load-locked Alcatel etch system (MET Lab), which has been described in sections 2.1.3 and 6.2.

Plasma etching is carried out with the following basic conditions.

Fluorine plasma: gas composition of SF_6 : N_2 = 1 : 1, total flow rate of 100 sccm, etching pressure of 10 μbar, substrate temperature of 25 °C, ICP source power of 1500 W. Then the dc bias has been varied.

Chlorine plasma: gas composition of 75% Ar + 25% Cl_2, total flow rate of 100 sccm, etching pressure of 10 μbar, substrate temperature of 25 °C, ICP source power of 500 W. Then dc bias has been varied. At dc bias 300 V, gas composition has been varied.

The surface roughness has been measured by atomic force microscopy (AFM; Autoprobe M5 from Park instruments has been described in section 2.3.2).

An average area of 80 μm x 80 μm has been selected for sampling. Analysis of the chemical composition of the dry etched surface is achieved with X-ray photoelectron spectroscopy (XPS has been described in section 5.2) using unmonochromated Mg Kα radiation for detecting Ga (3s) F(1s) and N(1s) information. The detail about XPS set up has been described in section 2.6. The special sample preparation procedures carried out in order to avoid sample deterioration by the ambient have been described elsewhere [121].

7.3 Electrical diode characterization and discussions

7.3.1 Diodes characterization of ICP fluorine plasma exposed GaN

Diodes fabricated on dry etched GaN surface are a good monitor for the plasma-induced surface damage as manifested by the Schottky barrier height and the ideality factor extracted from the I-V behavior. Figure 7.1 shows the variation of barrier height (a) and ideality factor (b) with dc bias of the fluorine ICP plasma, the dashed lines correspond to diode results from the unetched material. Compared to the diode characteristics from unetched surface, the barrier height decreases and the ideality factor increases with increasing dc bias until 100 V. With further increasing dc bias, the barrier height increases and correspondingly the ideality factor gets closer to 1, both optimums at the maximum bias of 300 V for the measured range.

A possible explanation is given by the ion yield behavior vs. dc bias in figure 6.1. Up to a dc bias of 100 V, no etching takes place, only chemical reactions exist at the surface. A thick reaction layer is possibly formed on the semiconductor surface without appropriate removal of the etch products. Note that GaF_X species are relatively involatile. At dc bias beyond 100 V, the etch products are increasingly being removed, leaving a cleaner surface with less defects. This has been evidenced by XPS measurement and will be presented in section 7.4.1.

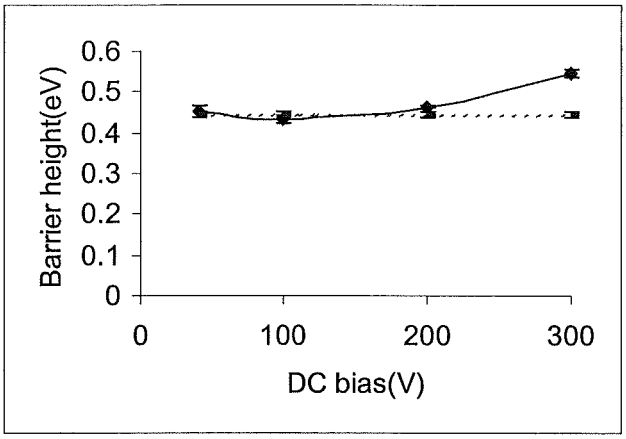

a

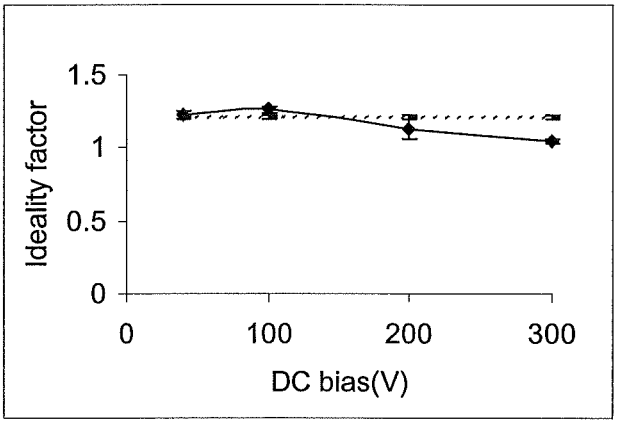

b

Figure 7. 1 a) Barrier height, b) Ideality factor and vs. dc bias in SF_6 : N_2 = 1 : 1, ICP plasma, total gas flow 100 sccm, substrate temperature 25 °C, ICP source power 1500W, etching pressure 10 μbar and etching time 1 minute. Higher DC bias etching improves diode properties. Dashed lines refer to unetched sample.

As a consequence, the damage goes to a minimum at 300 V. Apparently, the ion impact at higher dc bias does not create additional defects in the GaN bulk. This damage behavior vs. ion energy sharply contrasts with the general finding in numerous RIE and ion beam studies, where etch-induced damage increases with ion energy.

7.3.2 ICP chlorine plasma effects on diode properties

To verify chlorine plasma etch-induced damage effect on GaN electrical properties, electrical characterization of chlorine plasma pre-exposed GaN has been carried out. Figures 7.2 a, b show barrier height and ideality factor vs. dc bias in 75% Ar + 25% chlorine plasma. All the etched GaN samples have a larger ideality factor and a lower barrier height, compared to the control sample. This observation is in contrast to that of a gas mixture of SF_6 + N_2, where etching at higher dc bias improves the diode properties to ideal.

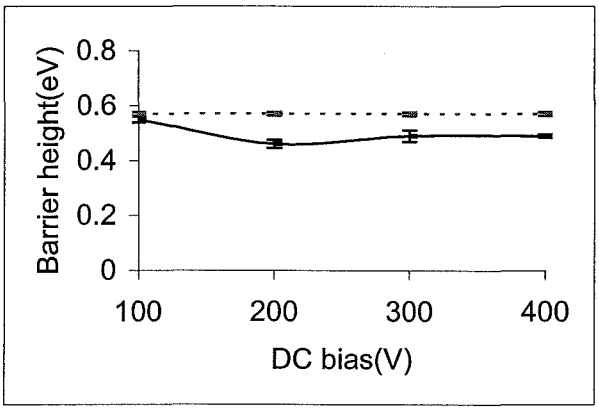

a

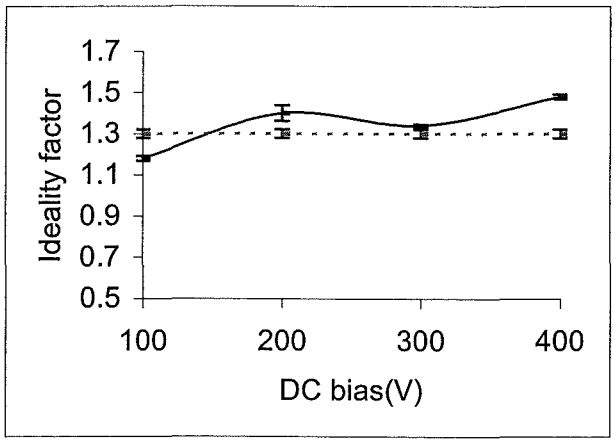

b

Figure 7. 2 a) Barrier height and, b) Ideality factor vs. dc bias in 25% Cl_2 + 75% Ar ICP plasma, substrate temperature 25 °C, etching time 1 minute, 500 W ICP source power and 100 sccm total flow rate and 10 μbar etching pressure. Higher DC bias etching deteriorates diode properties. Dashed lines refer to unetched sample.

This can be explained as following, chemical pollution on the surface is possibly the reason for the observed damage. The ideality factor increases with increasing dc bias first and saturates afterwards. Barrier height decreases with increasing dc bias and saturates afterwards. This result is also different from that observed in fluorine plasma. However, the chlorine plasma result is consistent with Zhang et al [177], who has reported that ICP Cl_2 + Ar plasma reduced diodes reverse breakdown voltage and Schottky barrier height and that all the plasma conditions were found to produce a nitrogen – deficient surface.

Figure 7.3 shows the diode electrical properties, a) barrier height, and b) ideality factor vs. %Cl_2 in Ar + Cl_2 plasma. The other plasma parameters have been kept constant. Pure Cl_2 plasma yields the highest ideality factor and the lowest barrier height, compared to plasma from pure Ar and Ar / Cl_2 mixture gas.

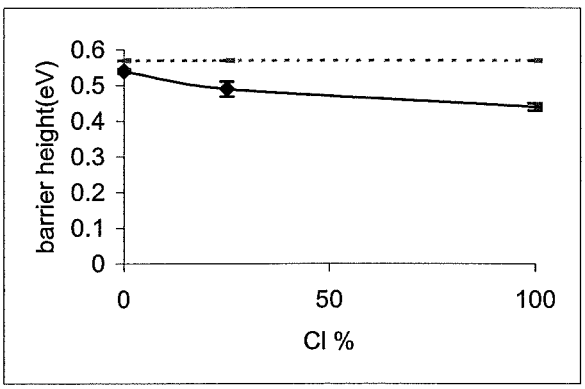

a

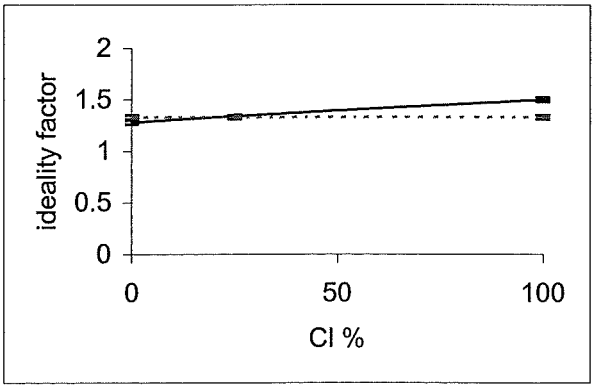

b

Figure 7. 3 a) Barrier height, b) Ideality factor vs. Cl_2 percentage in Ar + Cl_2 plasma. Etch conditions see text. Chlorine based plasma etching deteriorates diode properties. Pure chlorine plasma deteriorates the diode properties the most. Dashed lines refer to unetched sample.

From physical plasma point of the view, higher ion mass could possess a higher energy in the identical electrical and/or magnetic field. Higher energy could induce more physical damage. Malyshv et al has reported [184] that the main positive ion in ICP chlorine plasma is Cl^+, instead of Cl_2^+ in RIE chlorine plasma. It is known that Ar^+ is the main positive ion in Ar plasma. The ion masses of Ar^+ and Cl^+ are very close. Figure 7.3 shows that the chlorine plasma induces a stronger deterioration of the diode properties than an Ar plasma and a mixture of Ar + Cl_2 plasma. This indicates that ion mass does not play the main role in creating electrical damage during ion bombardment.

In previous chapter, figure 6.7b shows that Ar plasma has much larger ion current density than pure chlorine plasma under the same plasma conditions, so physical aspect, like ion bombardment in an Ar plasma is much more intense than in a chlorine plasma. Nevertheless, the effects of etch induced damage on diode properties from chlorine plasma are much larger than that from an Ar plasma, as shown in figure 7.3. This suggests that intense of the bombardment does not play an important role in creating electrical damage. However the ion energy does, see figure 7.2, the degradation of diode properties gets larger with increasing DC bias.

From chemical point of view, Ar is an inert gas, its etch mechanism is pure physical sputtering. While chlorine based plasma has a strong chemical enhancement. Cl - containing etch products, see table 7.2, are present on the GaN surface. This explains that the chlorine based plasma deteriorates the electrical properties.

All these aspects of consideration and analysis indicate that chemical aspects of in ICP chlorine etching as well as ion energy, determine the electrical damage.

7.4 Surface analysis result and discussion

7.4.1 XPS surface composition analysis

The role of the surface condition in the diode behavior vs. dc bias is supported by X-ray photoelectron spectroscopy (XPS) on dry etched surface. Table 7.1 shows the atomic concentration ratios for F (1s) / Ga (3s) and N (1s) / Ga (3s).

Table 7. 1 X-ray photoelectron spectroscopy analysis results of GaN surface pre-exposure to SF_6 : N_2 = 1 : 1, with total flow rate 100 sccm, substrate temperature 25 °C, ICP source power 1500 W and etching pressure 10 μbar by Mg radiation.

samples	F1s/Ga3s	N1s/Ga3s
control		0.12
100 etched	0.88	0.11
300 etched	0.58	0.15

It is clear that the F/Ga ratio drops by 40% in switching from 100 V to 300 V bias, which is indicative for the significant removal of etch products at the higher bias condition. An additional trend observed from XPS is that the $SF_6 + N_2$ plasma induces an increase in nitrogen enrichment with dc bias. A 25% increase of the N/Ga ratio is observed at 300V compared to the control sample. It appears that N is incorporated into the GaN surface without creating apparent electrical damage. It is worth noting that a recovery of the GaN surface condition is observed using a N_2 plasma post-treatment [63].

The GaN surface composition after chlorine plasma etching has also been investigated by XPS. Very strong chlorine peaks have been detected on the samples etched by chlorine plasma as shown in figure 7.4.

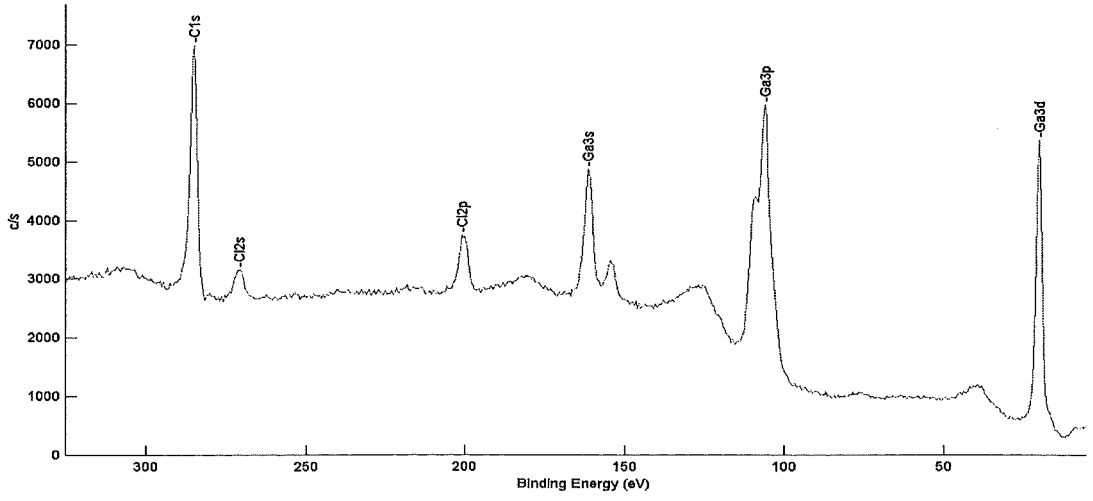

Figure 7. 4 XPS spectrum of GaN surface etched by 75% Ar + 25% Cl_2. The strong Cl peaks have been detected on the surfaces after chlorine based plasma etching.

The Cl radicals could be implanted into GaN surface during etching since higher reactivity of Cl towards GaN (compared to F) and the volatile reaction product $GaCl_3$ keeping the surface exposure to plasma.

The table 7.2, listing the Cl2p/Ga3s ratios, shows the Ga deficiency after chlorine plasma etching because Cl is preferential to react with Ga, form volatile etch product $GaCl_3$ and thus results N enrichment on the GaN after chlorine plasma etching. This is different from N incorporation into GaN after $SF_6 + N_2$ plasma etching mentioned previous. The outcome of N enrichment is the same after chlorine and $SF_6 + N_2$ etching. One would expect the similar effects from N enrichment on diode properties

All these results indicate that chlorine species incorporated into the surface is the main factor causes electrical diode damage.

Table 7. 2 X-ray photoelectron spectroscopy analysis of GaN surface composition of the sample without and with pre-exposure to chlorine plasmas.

samples	Cl2p/ Ga3s	N1s/Ga3s
control		0.14
Ar		0.13
75%Ar+25%Cl_2	0.54	0.21
Cl_2	0.48	0.20

7.4.2 Surface morphology analysis

AFM measurements of fluorine plasma etched samples are listed in table 7.3. The root mean square roughness (rms) of the sample that are etched at 300 V is smaller than that etched at 100 V. The relative value of peak to valley (r p-v) of the sample etched at 300 V is smaller than that of etched at 100 V. Thus, etching at 300 V creates smoother surfaces as manifested by smaller rms and lower r p-v value. This reflects as a higher barrier height and smaller ideality factor in electrical diodes properties compared to those etched at 100 V and 200 V.

It is also noticed that the control sample displays a bigger ideality factor and a lower barrier height than that of the surface etched at 300 V. This could be explained by the r p-v value, in table 1, of the control sample, which is much larger than that of the surface etched at 300 V. The rough surface of as grown material has been explained in chapter 4, due to deficiency of nitrogen on surface. The spikes may cause Schottky diodes break down because of high electrical field at certain applied voltage.

Table 7. 3 Atomic force microscopy analysis of GaN surface without and with pre-exposure to fluorine plasma at dc bias100 V and 300 V.

sample	rms(Å)	r p- v (Å)
control	158	2400
100	298	1720
300	164	1080

Figures 7.5 a, b are the SEM images of GaN surface with grating lines after fluorine plasma etching and plain surface after chlorine plasma etching respectively.

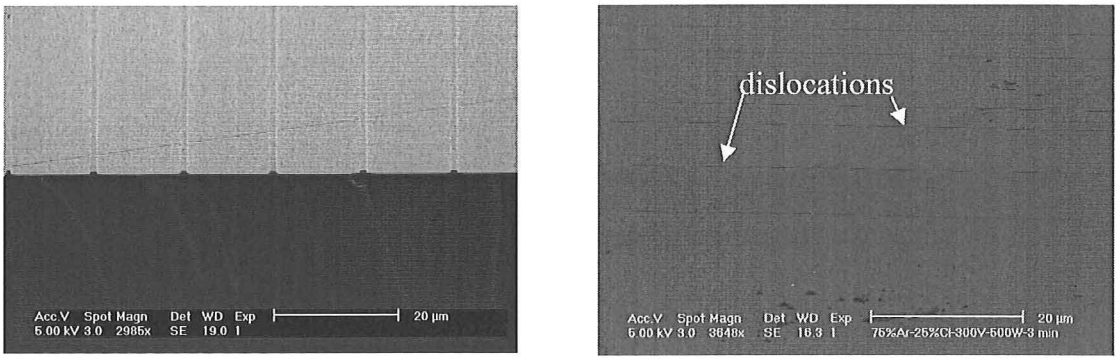

a b

Figure 7. 5 SEM images of GaN surfaces with pre-exposure to a) $SF_6 + N_2$ plasma, b) $Ar + Cl_2$ plasma. Hardly find trenches on the surface after fluorine plasma etching, while there are many trenches on the surface after chlorine plasma etching.

The surprising difference between chlorine plasma and F plasma treatment is that there are many line dislocations shown on the surface after chlorine plasma etching. This indicates that chlorine is much more reactive than fluorine in etching GaN. Most of the dislocations are obviously more reactive, and thus are easily etched. As a consequence, electrical properties could be deteriorated by creating trenches after etching, if the dislocations intersect the electrical devices.

7.5 Comparison of the studied plasmas regarding the etch induced damage on diode properties

In general, dry etching introduces damage, which deteriorates electrical properties of an ideal material. Because dry etching 1) builds up a reaction layer (chemical damage) on the surface, 2) induces defects and elemental deficiency by ion bombardment, 3) implants ions, 4) drive in the defects by radiation and diffusion, and 5) roughens the surface by redeposition. However, the exact nature of these created defects are still unknown, the defects in the material give rise to electrical active states in the band gap and change the electrical properties. For example, etched surface produces a larger leakage current, which results in a better ohmic contact. However, the diode properties will be deteriorated by the same effect.

In our study of high ion energy $SF_6 + N_2$ plasma etching, improvement of electrical diode properties has been observed. The main reason is that the as grown GaN we used is a non-ideal material. For examples, N deficiency surface composition and bad surface roughness deteriorate the electrical properties. Thus, any treatment (including dry etching) improves electrical properties if it modifies the material to a better surface stoichiometry and surface roughness.

In the case of the $SF_6 + N_2$ plasma with high ion energy, F radicals preferably react with Ga atoms, and N atoms from plasma are incorporated into the surface. These alter the etched surface composition, which improve the surface stoichiometry. At the mean time, high energy ions remove the spikes on the surface, resulting in a smoother surface. Also they remove the reaction layer more efficiently [192],

resulting in a cleaner surface. Thus explains the observed improvements in electrical properties with high ion energy etching in $SF_6 + N_2$ plasma.

In chapter 4, the RIE fluorine plasma pre-exposure effects on electrical diode properties have been presented. In the RIE case, purely physical sputtering (argon plasma) seems to degrade electrical diode properties as well as 100% SF_6. While a mixture of chemical and physical components, for instance, the gas mixture of $SF_6 + N_2$, would improve the diode properties.

In a ICP fluorine based plasma, the gas mixture of $SF_6 + N_2$ plasma effects on diode properties has been investigated. The interesting result is that the mixture gas improves the diode properties towards ideal in the higher ion energy regime (dc bias). This is due to chemical healing by N incorporation and energy dissipation to reaction product. At lower ion energy such as 100 V of dc bias, diode property characterization shows the onset of chemical etching, resulting in degradation of the electrical properties. This indicates that chemical component determine the diode properties in fluorine based plasma.

In the case of chlorine based plasma etching of GaN, the gas mixture of 75% Ar + 25% Cl_2 shows that diode properties get more deteriorated when ion energy increases first and saturates afterwards. This indicates that higher ion energy may cause more electrical damage. Additionally it is observed that the chemical component has a large influence in deteriorating the diode properties as is in the fluorine based plasma

The main difference between ICP chlorine based plasma and fluorine based plasma in etching of GaN is that reaction products $GaCl_3$ is more volatile that GaF_x. It is reasonable to assume that a ICP chlorine-based plasma results in an thinner reaction layer on the etched surface, compared to the surface after fluorine based plasma etching due to redeposition of GaF_x. Thus, the ion energies in chlorine plasma will be possibly directly transferred to the substrate, while in fluorine based plasma, the ion energies may dissipate to the reaction products.

The above comparison and discussions show that a mixture of $SF_6 + N_2$ could be a possible candidate for production of electronic devices, such as transistors fabrication. It should be mentioned that we have not investigated the etch effect on the mobility. Mobility is an important parameter of electrical properties.

7.6 Limitation of diode characterization technique

To monitor etch induced damage on top surface, diode characterization has been employed to probe electrical properties. To correlate electrical and optical measurement to etch induced damage, surface composition analysis by XPS is essential, as we have discussed in chapter 2. The information from electrical and surface analysis has had a great deal to optimize etch condition and address etch induced damage of GaN.

However, these techniques have limitations. It is essential to discuss the limitation for better understanding and analyzing the etch induced damage or defects.

Diode characterization can fully reflect the defects, because current pass through the whole thickness of GaN, in the case of highly doped SiC substrate and nominally undoped GaN film. Etch induced defects may shrinks the depletion region and cause tunneling to occur. This reflects as low contact resistance and barrier height in diode properties. This method is not able to tell the difference between the presence of a shallow layer of defects limited to top 1 nm and a deep layer of defects propagated to 100 nm in depth. Therefore, the information from diode characterization has surface and bulk effect, without indicating the thickness of damage layer.

XPS only detects top few nm information. So, the information form XPS only represent the surface effect, not bulk. When one correlates the surface composition result by XPS to PL and/or diode results, it is worthwhile to be careful of these limitations.

7.7 Summary

High ion energy in SF_6+N_2 ICP processing improves the electrical diode properties as almost ideal diode characteristics are obtained at a dc bias of 300V. The diode improvement is a result of the combination of smoothening the surface, the removal of surface contamination and the incorporation of N in the GaN surface. In contrast,

$Ar + Cl_2$ plasma treatment deteriorates diodes electrical properties due to chemical pollution and high ion energy dissipation on the surface.

Chemical aspect determines the electrical damage in ICP fluorine plasma etching. Chemical pollution and ion energy play an important role in creating electrical damage in ICP chlorine plasma etching.

A $SF_6 + N_2$ ICP plasma could be an option for fabrication of devices of electrical sensitive properties, such as gate recessed transistors. Additional, these plasmas produce reasonable etch rate, smooth surface and good profile. However, it should be subject to mobility investigation.

Diode characterization reflects the information from whole thickness of GaN film. The limitation of diode characterization is ignoring the distribution of defect depth and XPS only detects top nm surface.

Chapter 8

ICP Etch Induced Damage Effect on Optical Properties of GaN*

8.1 Introduction

The effects of ICP processing of GaN using $SF_6 + N_2$ and $Cl_2 + Ar$ gases on electrical diode properties have been investigated in chapter 7 and found that $SF_6 + N_2$ is suitable for electrical device fabrication with reasonable etch rate and vertical profile. To find suitable etching condition for optical device fabrication, the effects of fluorine and chlorine plasmas on photoluminescence have been undertaken. In this chapter, PL spectra of GaN grown on SiC before and after $SF_6 + N_2$ and $Ar + Cl_2$ etching will be compared and discussed regarding near band gap PL intensity and peak positions. In addition, XPS has been employed to analyze surface atomic concentrations.

8.2 Experimental details

The material used here is the same as described in chapter 7 and the ICP plasma reactor used in this study is a load-locked Alcatel etch system (MET Lab), which has been described in sections 2.1.3 and 6.2.

The basic etching conditions have been described in section 7.2. For optical characterization, in fluorine plasma, dc bias and gas composition have been varied.

* This chapter is based on the draft of "ICP chlorine plasma etching of GaN and etch induced damage characterization" submitting to J. Appl. Phys.

In chlorine plasma, dc bias has been varied. Then at dc bias 300 V, gas composition has been varied.

Analysis of the chemical composition of the dry etched surface is achieved with XPS (described in section 5.2) using unmonochromated Al and Mg Kα radiation for detecting Cl and N information respectively. This is necessary because the Ga auger line overlaps the N peak in case of Al radiation, while the Cl peak is overlapped when Mg radiation is used. Both of radiation sources detect Ga peaks for normalization. The Ga (3s) signal has been corrected for overlap with a parasitic Si line. Special sample preparation procedures carried out in order to avoid sample deterioration by the ambient have been described elsewhere [121].

Photoluminescence experimental details are the same as that described in section 5.2. Variable temperature experiments have been performed between 20 K and 250 K.

8.3 Optical characterization and discussions

8.3.1 ICP fluorine plasma effects on photoluminescence of GaN

The photoluminescence spectra after ICP process with different dc bias and different gas composition of fluorine plasma have been investigated. Figure 8.1 is the near band gap PL spectra of as grown GaN and GaN samples subjected to following etching conditions, gas composition of SF_6 : N_2 = 1 : 1, total flow rate of 100 sccm, substrate temperature of 25 °C, etching pressure of 10 μbar, ICP source power of 1500 W, with dc bias of 100 V, 200 V and 300 V. The strongest feature of the control sample is at energy around 3.445 eV. This energy is on the extended D^oX line (see figure 5.4). The temperature dependence of these features has similar behavior. The Peak intensities decrease with temperature increasing and disappear at room temperature. From the discussion of excitonic energy in chapter 5, we attribute this peak as D^oX.

Figure 8.1 shows D^oX PL intensities of all the etched samples have about 20% of that of the control sample. Obviously etching reduces D^oX PL intensity.

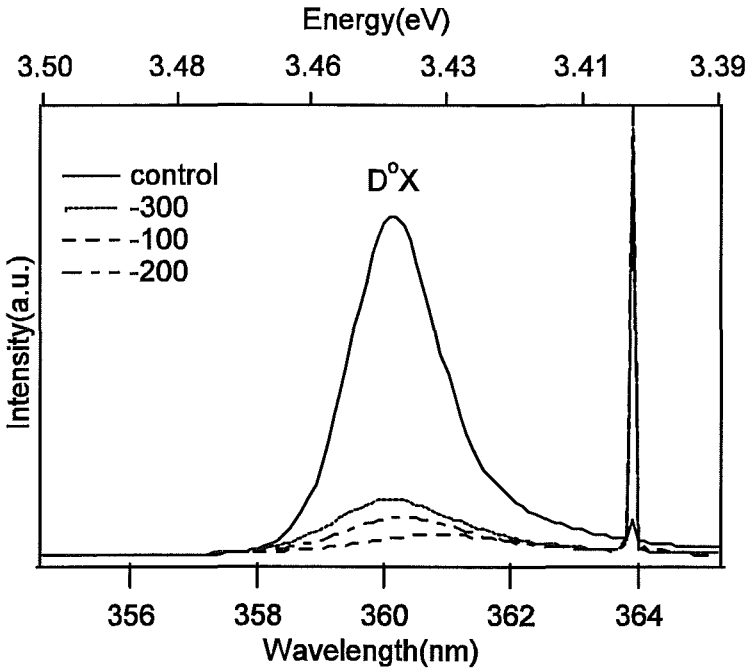

Figure 8. 1 Photoluminescence spectra of GaN grown on SiC etched by SF_6 + N_2 plasma with different dc bias. Etching reduces the near band gap PL intensity in general. Higher ion energy etching does not create more optical damage. Etch conditions see text.

This observation is similar with that of RIE etching process. Among the etched samples, 300 V dc bias etched sample has the highest PL intensity and 100 V dc bias etched sample has the lowest PL intensity. The changes of PL intensity will be discussed in later section 8.3.3. The peak of 100V bias spectra seems shifted to a low energy. However, the reason remains unknown.

Figure 8.2 shows the spectra of as grown material and the GaN samples subjected to plasma exposure with the etching conditions of SF_6, SF_6 + N_2 and N_2, substrate temperature of 25 °C, total gas flow rate of 100 sccm, dc bias of 40 V, ICP source power of 1500 W. After etching, the PL intensity has been reduced compared with that of as grown sample. This is consistent with previous results.

Among the etched samples, the mixture gas etched sample has the highest PL intensity, while the pure N_2 and pure SF_6 has much lower PL intensity. This indicates that a gas mixture of SF_6 + N_2 produces the least optical damage, possibly due to the least ion current density in the gas mixture and the least intense ion bombardment,

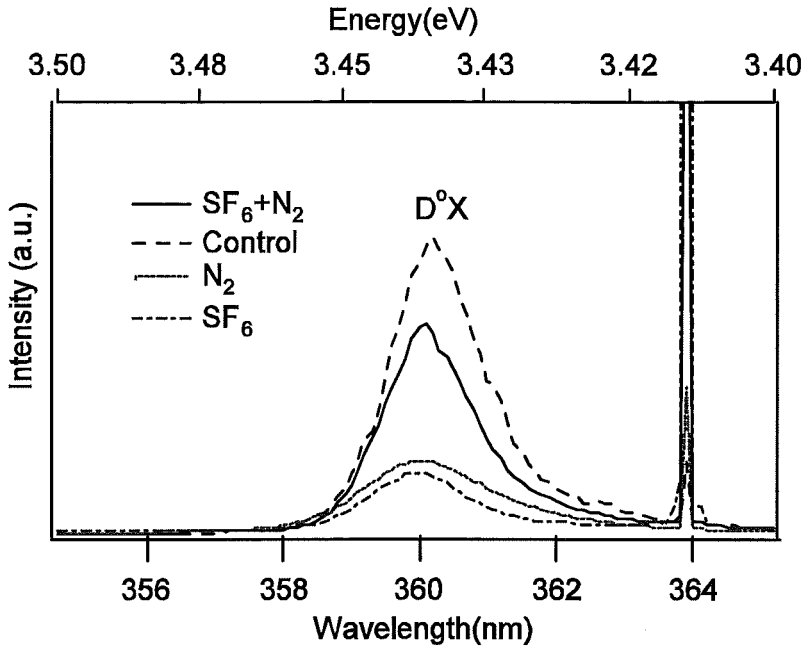

Figure 8. 2Photoluminescence spectra of GaN grown on SiC etched by $SF_6 + N_2$ ICP plasma with different gas composition, Etching reduces the near band gap PL intensity. Mixture gas produces the least optical damage. Etch conditions see text.

compared to pure SF_6 and pure N_2 plasma, as shown in table 8.1. This observation has the same trend as that obtained in RIE, see chapter 5.

Table 8. 1 Ion current density vs. gas composition by Langmuir probe measurement in ICP fluorine based plasma. The other plasma parameters are ICP source power of 500 W, etching pressure of 5 μbar and total gas flow rate of 50 sccm.

Gas composition	Ion current density (mA/ cm^3)
SF_6	0.336
$SF_6 + N_2$	0.322
N_2	0.427

8.3.2 ICP chlorine plasma effects on photoluminescence of GaN

Figure 8.3 shows PL spectra of as grown GaN and GaN samples exposed to chlorine plasma, i.e. 75% Ar + 25% Cl_2 and 100% Cl_2 respectively. The peak at 360 nm is attributed to D^oX as explained 8.3.1. After chlorine plasma etching, the D^oX peak

position shifts to higher energy by about 10 meV, this is different from that we observed after fluorine ICP and RIE plasmas etching, where no obvious shift has been observed.

Figure 8.4 shows the spectra of as grown GaN and GaN after argon plasma etching. The D^oX peak does not shift, which is consistent with the RIE argon plasma result. Figure 8.5 displays the long wavelength PL spectra of the same samples shown in figure 8.3. It is observed that all the peaks and the blue band shift to higher energy by about 10 meV.

The shifting of the D^oX peak of GaN grown on SiC to higher energy after annealing has been reported previously [48]. However, to the best of my knowledge, the shifting of the peak to higher energy after plasma etching has not been reported before. Many papers highlight the relationship between internal strain and peak energy [161-162]. The excitonic energies measured are affected by residual strain in epilayers due to the mismatch of lattice parameters and the different thermal

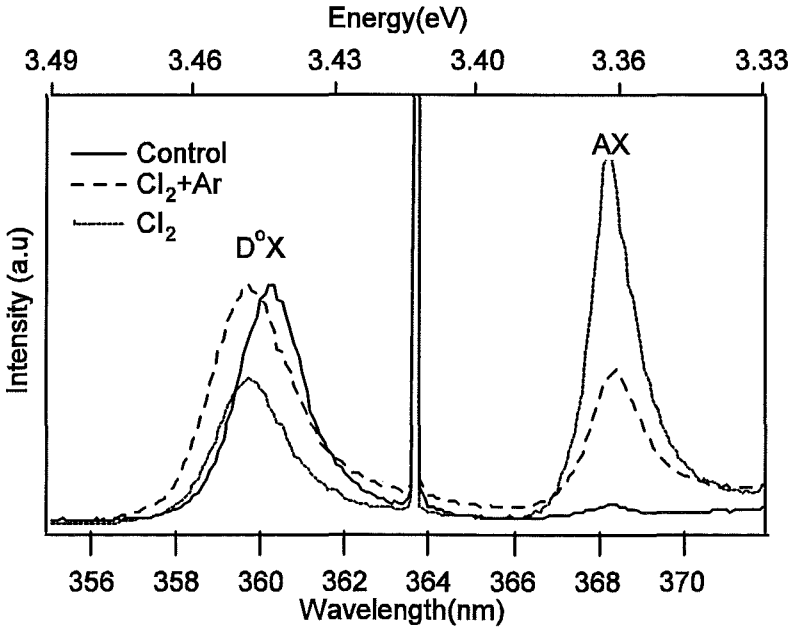

Figure 8. 3 The near band gap PL spectra of control sample, the ones etched by ICP $Ar+Cl_2$ and pure Cl_2 plasmas respectively. The one etched by pure ICP Cl_2 reduced the D^oX intensity. Chlorine based plasma etching causes the peaks shift to higher energy.

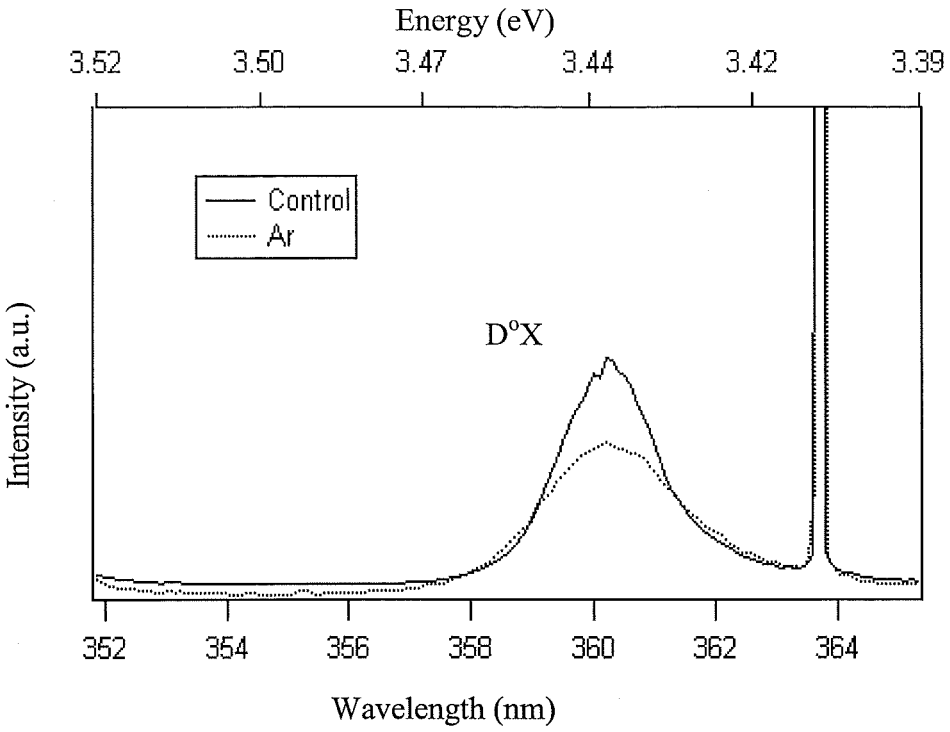

Figure 8. 4 PL spectra of as grown material GaN grown on SiC and the one etched by ICP Ar plasma. After Ar etching, D°X intensity is reduced, but the peak position keeps the same. The etch conditions see text.

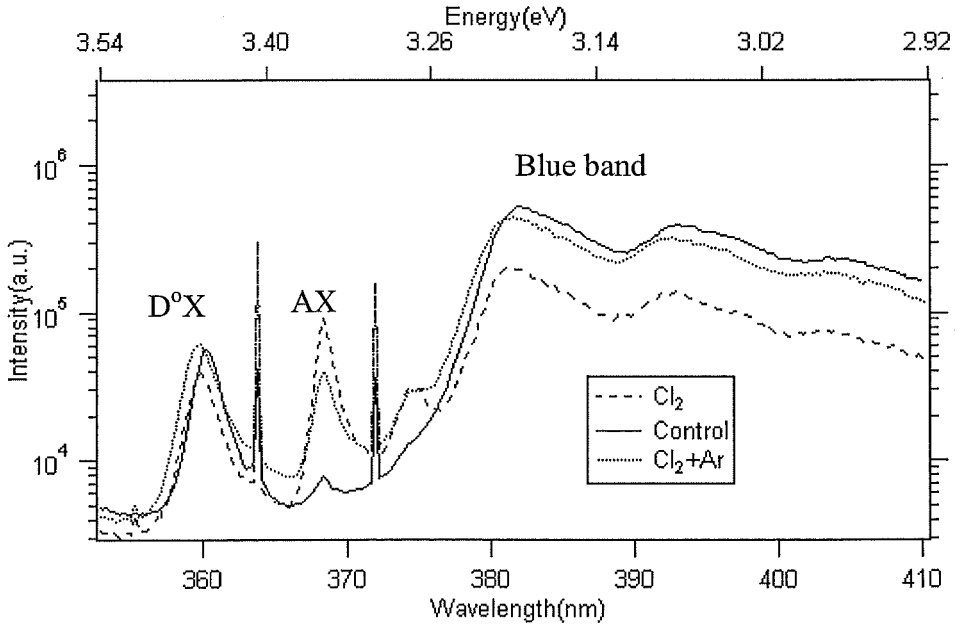

Figure 8. 5 The spectra of GaN of control sample and the ones etched by pure Cl_2 and 25%Cl_2 + 75%Ar. Huge blue band at range 3.28eV also shifts to higher energy after etching in chlorine based plasma. The intensity trends are the same as that of D°X.

expansion coefficients between GaN and sapphire and SiC substrate. As we explained in chapter 5, GaN grown on sapphire experiences a compressive strain upon cool-down from growth, which will increase the exciton energies [193]. GaN grown on SiC experiences tensile strain, which reduces the excitonic energy. Then, any treatments, which could release or partly release the strain, should shift the excitonic energies closer to zero strain energy manifested in a shift of the peaks to higher energy level in the case of GaN grown on SiC.

As discussed in section 7.4.2, in the case of chlorine plasma etching, there is a strong preferential etch of dislocations. This may further release the strain of the GaN epilayer, resulting in the observed peak shifts. Since film stress, thermal induced mechanical relaxation processes, and diffusion in films are influenced by dislocations [194]. For fluorine based plasmas and Ar plasma, no preferential etch of dislocations has been observed, correspondingly no peak shift is observed. Figure 8.6 is the schematic drawing of line dislocations present in lattices. It illustrates that if the dislocation is preferential etched, strain is further relaxed.

It should be pointed out that no yellow luminescence has been observed in this series of GaN grown on SiC before and after ICP fluorine and chlorine plasma etching. In addition, figures 5.6 and 5.7 show no yellow luminescence in that series of GaN grown on SiC before and after RIE Ar and SF_6 + N_2 etching. This is in contrast to that observed in GaN on sapphire [50,51], where strong yellow luminescence in control sample and yellow luminescence evolvement after RIE Ar plasma etching have been observed. These results may suggest that yellow luminescence relates to substrate.

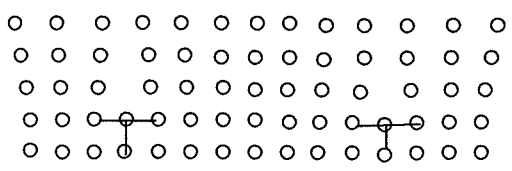

Figure 8. 6 Schematic drawing of line dislocations presented in lattice. The dislocations are labeled with T.

8.3.3 PL intensity discussions

Dry etching initially creates a damage layer with the depth of a few nm. A small percentage of ions could be scattered into a channeling [150,195] direction. Once these ions scattered that direction, they can penetrate deeply into the substrate material up to 100 nm or more [196]. However, it can be only a small amount of these ions, less than 0.1% of initial ion flux, the result is measurable [150,196]. Radiation above the band gap has a synergetic effect. The electron and hole recombination in semiconductor transfers momentum and energy to defects in the material, resulting in enhanced motion of the defects [196]. This mechanism has been fully accepted [150,195,196].

Cao et al reported [75] an electrical damage layer with a thickness of 50-60 nm at the top surface in GaN after ICP N_2 and H_2 plasmas etching using self dc bias of 221 volts.

Hu et al reported [196] a deep damage layer, the depth of the damage layer larger than 100 nm from the top surface as a result from low energy ion bombardment about 300 volts in III-V semiconductors due to channeling and illumination enhanced diffusion. Their conclusion is that the conventional geometry used for low-energy ion processing of GaN may in fact be the most deleterious one [150].

From above literature review, it is convinced that a thin disordered layer, a few monolayers deep, is created at the surface of the material being etched. The effects caused by channeling and radiation enhanced diffusion, could be measured deeper to 10 magnitude of that initial layer. This explains the observed PL intensity changing with etch condition and different gas.

According to Hovel [120], the PL intensity can be written as follows (chapter 2),

$$\Phi_{PL} = \frac{\Phi(1-R)\cos(\theta)}{\pi n(n+1)^2} \frac{L}{\tau_{rad} S_r} \qquad 2.11$$

where ϕ is the incident photon flux density, R the reflectivity, θ the emission angle, n the index of refraction, L the minority carrier diffusion length, τ_{rad} the radivative lifetime, and S_r the surface recombination velocity, which is related to surface states density. In this case, the etching would primarily change the surface state density.

The surface states are referring to dangling bonds on the top surface. The surface of as grown GaN is nitrogen deficient. Therefore, there are some extra dangling bonds, besides from non-perfect crystal structure. In the case of fluorine-based plasma, some possible chemical reactions are assumed as following. 1) Fluorine atoms preferentially react with Ga atoms and reduce the dangling bonds, 2) The N atom from plasma may react with the N atom on the surface of GaN as explained in chapter 3.

$$N + N = N_2 \uparrow$$

which creates more dangling bonds. 3) N incorporation from N-containing plasma reduces the dangling bond.

Figures 8.1 and 8.2 show ICP fluorine plasma etching reduces PL intensity in general. A possible explanation is that dry etch induces defects (probably dangling bonds), and thus reduces the PL intensity [197]. Ions are the most possible to be implanted into GaN during fluorine plasma etching due to high ion energy and small diameter ions, such as N^+, F^+ etc. The implanted ions mainly stay in the interstitials, thus increases dangling bond and reduces the PL intensity. The depth of ion implantation also will be a few nm towards a few hundred nm, depends on ion energy. Ion current density increases slowly with DC bias when other plasma parameters are kept constant, as shown in figure 6.12b. Higher energy may implant ions deeper, however PL is not able to tell the difference in depth of defects distribution. Therefore, it should be reasonable to assume that there will be a similar amount of ions implanted into GaN the top 100 nm depth in different DC bias. In ICP, small ions such as N^+, F^+ dominate the $SF_6 + N_2$ plasma in such lower flow rate as 100 sccm [183]. Therefore, ion implantation and defects propagation are main factors, which reduce PL intensity dramatically in fluorine based plasmas.

Among etched samples, 300 V dc bias etching has the highest PL intensity compared to samples etched at 100 V and 200 V. The sample etched at 100 V has the lowest PL intensity. A possible explanation can be given as following. In lower dc bias, N incorporation sounds less possible due to the lower ion energy, while at higher bias, ions have a larger energy and will more readily incorporated into GaN. With constant gas flow and composition and a constant ICP source power, it is reasonable to assume that the N, F radical concentrations and ion current density should be constant. This suggests that the chemical reactions in these plasmas should be the similar. This analysis is consistent with XPS result, table 7.1. The sample etched at 300 V DC bias shows N/Ga = 0.15. This value is a 25% increase of the control sample (0.12) and about 30% larger than the N/Ga value of the sample etched at 100 V (0.11). This trend may suggest that a surface after etching at 300 V DC bias has less dangling bonds than a surface etched at 100 V, covered by N incorporation. Consequently, the PL intensity is higher at 300 V DC bias.

However, the XPS results are from top few nm and PL spectra are related to about 100 nm depth of GaN. It is reasonable to assume that the chemical reaction and incorporation are on the top nm surface and have rare bulk effect. Thus, these chemical reaction and incorporation are minor effects in changing PL intensity, compared to ion implantation and defects propagation. However, they do distinguish the PL intensity between the etched samples. This explains the figure 8.1.

Figure 8.2 shows that the mixture of $SF_6 + N_2$ etched sample has the highest PL intensity, compared to the samples etched in SF_6 and N_2. A possible explanation is given by the ion current density differences, listed in table 8.1 and defects implantation. Small ions such as F^+ and N^+ dominate the $SF_6 + N_2$ plasma and N^+ dominates N_2 plasma at such a low gas flow (100 sccm) [183, 198]. These small ions could be implanted into GaN and even propagate deep into the bulk. The ion current density of the mixture of $SF_6 + N_2$ is about half of N_2 plasma. This indicates that less defects would be implanted into GaN after $SF_6 + N_2$ etching. This implies less dangling bonds after $SF_6 + N_2$ etching. Thus the PL intensity of the sample etched by $SF_6 + N_2$ plasma is stronger that of pure N_2 plasma etched. One may argue that the N incorporation in N_2 plasma could be more than that in $SF_6 + N_2$ plasma.

Pure SF_6 plasma has similar amount of ion current density compared to $SF_6 + N_2$ plasma. The chemical reaction Ga + F $\rightarrow$ GaF_x would be similar. The main difference is that $SF_6 + N_2$ plasma offers N to incorporate into GaN surface, while there is no N can be offered form pure SF_6. The XPS surface composition analysis shows that N/Ga ratio after RIE $SF_6 + N_2$ is higher than that of RIE SF_6 plasma. It is reasonable to assume that in ICP, it would have similar N/Ga ratio trend. It implies that less dangling bonds in GaN after $SF_6 + N_2$ etching. Consequently, the sample etched in pure SF_6 has lower PL intensity than the sample etched in the $SF_6 + N_2$.

In the case of a chlorine plasma, the diameters of ions, such as Cl^+, Ar^+, are much larger than that of N^+, F^+ ions in fluorine plasma. Thus, ion implantation will be very less in chlorine plasmas compared to that in fluorine plasmas. Thus, ion implantation is a minor factor in chlorine plasma. However, chemical reaction, such as the Cl atom reacting with the Ga atom, reduces the dangling bonds. The Ga deficiency after chlorine based plasma etching has been evidenced by XPS analysis (table 7.2). This reduces the amount of dangling bonds on the etched surface. In addition, dislocations are being etched in chlorine plasma and reduce the number of dangling bonds. (Like grain boundaries in semiconductors, dislocations have uncompensated dangling bonds.) These three mechanisms may possibly play a counter active role. As a result, the PL intensity is not as much decreased as in the case of the fluorine based plasma etched samples.

In a pure chlorine plasma, the chemical reaction is not as strong as in a 75%Ar + 25% Cl_2 plasma due to a 50% lower ion current density in a pure chlorine plasma (see figure 6.11b). So compared to Ar + Cl_2 plasma, less chemical reaction of Ga + Cl $\rightarrow$ $GaCl_3$ is going on and less dislocations will be etched in pure Cl_2 plasma. This means sample etched in pure chlorine plasma has more dangling bonds, compared to the sample etched in Ar + Cl_2. This explains the PL intensity of sample etched by 75%Ar + 25% Cl_2 has higher intensity than that etched in pure Cl_2, as shown in figure 8.3.

From channeling aspect consideration, F and N have much smaller ion masses compared that of Cl ion, so the diffusion length [195] is much larger for F and N, compared to Cl.. This also principally explains the SF_6+N_2 plasma decreases PL intensity drastically, while Cl_2+Ar does not.

8.4 XPS surface analysis of GaN grown on SiC

XPS has been employed to help analysis of the chemical issues of the bound excitons. Figures 8.3 and 8.5 show that new peak at energy of 3.374 eV pops out after chlorine plasma etching. This peak is marked as AX. While as grown material and samples etched in fluorine plasma, show very low or no AX peak, as shown in figures 8.1 and 8.2.

Table 7.2 shows a factor of two more in the N/Ga ratio on the GaN surface after a chlorine based plasma, compared to the surface of the control sample (0.14). This indicates a dramatical decrease of the Ga content on the etched surface. The material used here is n-type GaN, which is nitrogen deficient. During chlorine plasma etching, the Ga atom reacts with the Cl atom, and forms the $GaCl_3$. This is a very efficient reaction, because $GaCl_3$ is volatile reaction product. XPS result indicates the formation of Ga vacancy is highly possible after chlorine based plasma etching. The combination of XPS result and PL observation may suggest that the Ga vacancy relate to AX. This analysis agrees with that of Orten et al's. Orton et al attributes gallium vacancies to acceptor [10].

Top surface N/Ga ratios after pure chlorine and 75% Ar + 25% Cl_2 etching are similar. While the AX intensity of the sample etched in pure chlorine is higher than that of the one etched in 75% Cl_2 + 25% Ar plasma. It might be due to intensity transfer as such a phenomenon has been observed from the blue to the yellow luminescence previously [50]. But it needs further investigation for clarifying.

8.5 Comparison ICP with the RIE etch effect on optical properties

Etching can affect optical PL spectra, by 1) changing the surface states to change PL intensity, 2) creating new defects state (atomic vacancy or activate the vacancy) to create new peak, and 3) releasing strain to shift the peaks.

In chapter 5, RIE fluorine plasma effects on optical properties have been presented. There, etching dramatically reduces near band gap PL intensities to about half. The mixture of SF_6 + N_2 produced surfaces that have relatively higher PL intensity in the near band gap emission, compared to pure SF_6, N_2, and Ar plasmas.

Ion bombardment does not seem to play only role in creating optical damage. No new peak shows out at near band gap after fluorine based RIE plasma etching.

The similar result has been obtained in ICP fluorine based plasma. Etching reduces the near band gap PL intensity. The DC bias dependence effects on PL spectra show high ion energy does not reduce the near band gap PL intensity more than that of low energies, suggesting that physical aspect does not dominate etch induced damage effect on optical properties. This is consistent with RIE conclusion.

The main difference in fluorine based and chlorine based ICP processing effects on optical properties is that ICP chlorine plasma etching does not reduce the total near band gap PL intensity, but shifts the peak energy to a higher value.

8.6 Limitation of PL characterization techniques

To monitor etch induced damage on optical characteristics of GaN film grown on SiC, PL has been used to probe optical properties. XPS has been used to analysis surface composition.

PL probes about top 100 nm of GaN by using 300 nm wavelength laser in this study. Thus, PL is detecting the whole thickness of 100 nm region of etch induced damage layer, which affects PL spectra. However, one will not be able to tell the difference of defects distribution in depth by PL spectra within 100 nm. PL indicates surface and bulk effects, because surface recombination velocity directly affects PL intensity.

XPS only detects top nm information. So, the information form XPS only represent the surface effect, not bulk. When one correlates the surface composition result by XPS to PL, one needs to be careful of these limitations.

8.7 Summary

Ion bombardment does not seem to play an important role in creating optical damage. This result is consistent with RIE observation.

The new peak AX popping up, is possibly caused by formation of Ga vacancies. Shifting of peaks to higher energy values is due to strain relaxation. The strain is possibly released by preferential etching of the line dislocations.

Yellow luminescence of GaN may relate to substrate.

The concept of dangling bond explains the near band gap PL intensity after different plasma treatments.

75% Ar + 25% Cl_2 is suitable for fabrication of optical device such as laser diode and light emitting diode.

The limitation of PL characterization is ignoring the distribution of defects in depth. PL characterization reflects combination of surface and bulk in 100 nm depth, while XPS only detects top nm surface.

Chapter 9

Quantum Wire (QW_r) Device Fabrication and Depletion Region*

9.1 Introduction

The past tens of years have seen an explosion in both the amount and depth of work on electronic system with reduced dimension [199]. There are some novel effects such as quantum size effects, which offers new opportunities. As device dimensions shrink to nanometer-scale, on the fabrication technology, the key issues remain to keep things small, precise and anisotropic. This is critical when one works on sub – 100 nm gates, contacts, isolation trenches and shallow junctions.

As mentioned, dry etching is used routinely in etching small dimension features and dry etch induced damage degrade material properties and device quality. However, the damage caused by etching on the top surface and on sidewall is different due to different etch mechanism. It is necessary to distinguish the difference between surface damage[200] and sidewall damage [201]. If one considers ions as balls hitting the surface, then one would expect a difference between the surface, which is constantly bombarded and the sidewall, which, once it is formed, is only bombarded by ricocheting or scattering atoms [60] illustrated in figure 9.1 [202]. This suggests that the damage on top surface once has been established, should be independent of etch depth due to self limiting effect. In contrast, the electrical depletion at the sidewalls during plasma processing is cumulative.

* This chapter is based on "Dry etch –induced damage in an inductively coupled plasma" J. Vac. Sci. Technol. B Nov/ Dec. 2001

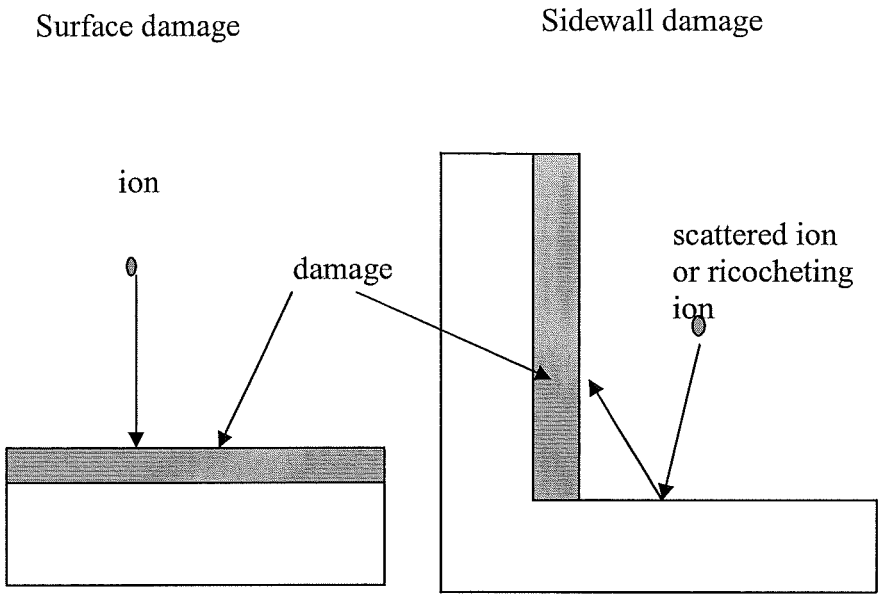

Figure 9. 1 The difference of etch induced damage on sidewall and top surface. Note the effect of scattering ion or ricocheting ion on sidewall damage.

We have investigated the damage effects on top surfaces by evaluating diode properties in chapter 4 and chapter 7, and photoluminescence spectroscopy in chapter 5 and chapter 7. Studying sidewall damage is another important issue in assessing the impact of plasma processing on the electrical and optical performance of the material. Gu et al [203] reported significantly low nonradiative sidewall recombination and an optically inactive layer due to process induced defects. Although, different material system has different degree of sensitivities. As reported, for open wires and dots (nanometer structures defined by etched surfaces), PL efficiency diminishes significantly in GaAs/AlGaAs material system at lateral dimensions of the order of 1000 nm, and in InGaAs/InP wires [204] for wire widths below 100 nm. These effects have been attributed to nanoradiative sidewall recombination and an optically inactive layer. It is important to determine the limits of the minimal pattern size at which a device is useful. In this chapter, the quantitative study on sidewall damage regarding electrical depletion depth will be presented.

The quantum wire device has been designed to measure the conductance as a function of wire width. By measuring the cut off conduction in the nano-size

channels, the sidewall damage of etched structures could be quantitative. For the first time, experimental results on sidewall depletion in GaN quantum wires are presented.

The purpose of this chapter is to report a device fabrication process, some measurements on n - type wires at room temperature and to interpret these measurements in terms of etch damage. Because of lack of material supply, this part of experiments could not be completed. Some problems in fabrication process have been encountered and its corresponding solutions will be presented.

9.2 Principle

The requirement of this experiment is narrow wires of different widths formed in n - type GaN epitaxial layer, which is grown on an insulated substrate. By cutting down to the wire width, zero conduction is expected when the width of wire is just equal to twice of depletion width. In practice, the cut off width is wider than the surface depletion region. The difference can be described as the depth of etch induced damage of the sidewalls. This is a very useful technique, and used to understand the nature of sidewall damage.

The detailed principle of this technique is following. The epitaxial layer will be allowed to be processed up to the substrate. A series of samples of different wire widths (100 nm to 1000 nm) were generally defined by high resolution electron beam lithography. After metallization, the mesa level pattern has been transferred through to the substrate by mean of Inductively Coupled Plasma (ICP) etching. The conductance of wires such as these studied by Thoms et al [205] shows that, if the conductance G was plotted as a function of wire width w, then G would extrapolate to zero at a width w_c (some data of this type are shown in figure 9.4b. The w_c was found to be significantly greater than that expected on the basis of a straightforward 1D depletion model, namely 2δ, where δ is the depletion depth in the doped epilayer. The δ can be expressed as following [206],

$$\delta = \left(\frac{2\varepsilon_r V_o}{N_D e} \right)^{1/2} \qquad 9.1$$

ε_r is the permittivity, V_0 the surface pinning potential, N_D the ionized donor density and e the electronic charge. This conclusion has been confirmed by Thoms et al [203] by studying conventional chemically etched wires for which they found a cut off width close to 2δ. This indicates that, as expected, the damage is much less in wet etching fabrication technique.

In the case of GaN, the depletion region consists of surface depletion width and etch induced damage layer. According to equation 9.1, one can calculate theoretical surface depletion region, δ = 13 nm, by giving ε_r =10, V_0 = 0.8 eV, N_d = 1 x 10^{17}

However, some assumptions have been made for this calculation. The Fermi level energy is pinned due to the presence of surface states before etching. The donors are 100% ionised, thus the depletion depth calculated in the theoretical case can only take N_d into account. It is assumed that etch-induced defects only change the width of the depletion region. The conduction band is pinned an energy of 0.8 eV [207]. The differences in dielectric constant between different materials are ignored.

According to Long et al [206], the etch damage enhanced depletion layer thickness is equal to $w_c/2$, is given by

$$\frac{W_C^2}{4} = \delta^2 \left(1+2\left(\frac{\lambda}{\delta}\right)^2 \right) \qquad 9.2$$

where λ is the trap region. This result is correct in the limit of the depletion layer being very much thicker than the trap region. They concluded that, if the etching conditions are broadly the same, one would expect the cut-off width measured in a transport experiment to scale directly with δ.

9.3 Device design and fabrication process

9.3.1 Device design

At first, the device patterns have been designed. The schematic drawing is shown in figure 9.2 for EBPG5. In the pattern design, it would be wise to make sufficient overlap in the joint parts of the pattern to open circuit. The device pattern consists of three layers. Layer one is the contact pads (100 μm x 100 μm), their extends and markers (20 μm x 20 μm), layer two is the connection lines, and layer three is quantum wire itself. The connection lines between the quantum wire and extend of the contact pads are necessary to avoid extra noise of current from sudden change of conduction channel size.

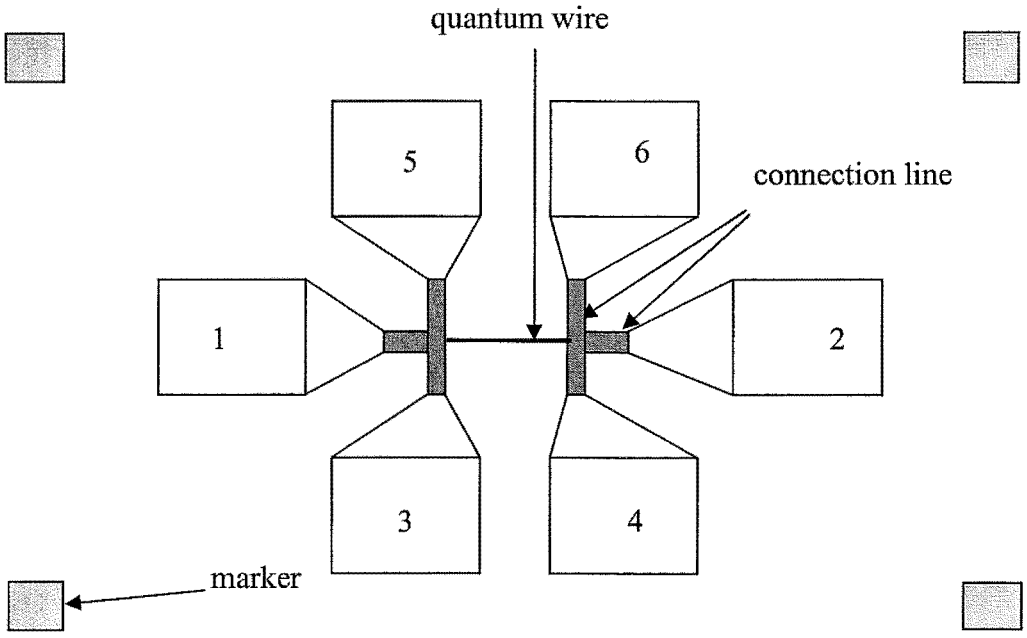

Figure 9. 2 Design of quantum wire device.

9.3.2 Fabrication process

The material we used here is 0.3 μm n - type GaN grown on sapphire. The dopant concentration is 1 x 10^{17} (cm^{-3}). The GaN films have been grown by metal-organic vapor-phase epitaxy (MOVPE). The quantum wire device fabrication process on insulated substrate is illustrated in figure 9.3. The detailed recipe sees appendix A.

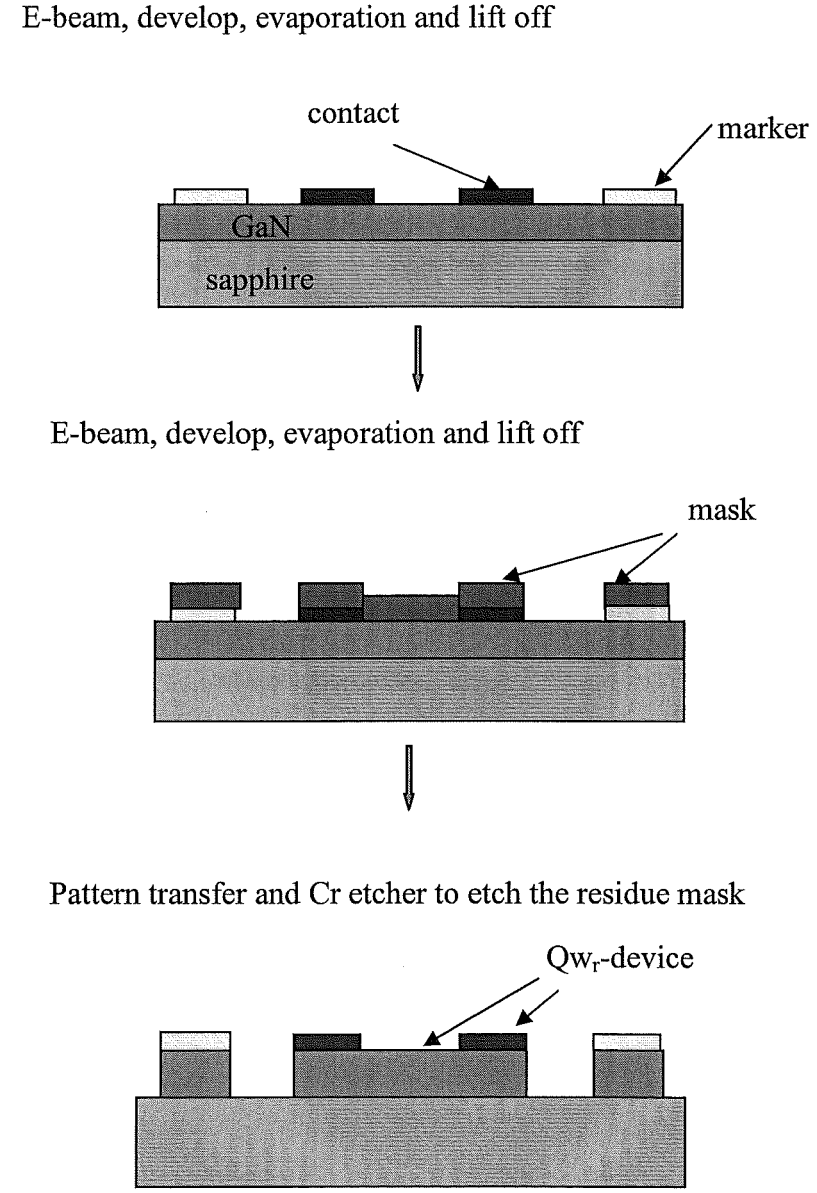

Figure 9. 3 Quantum wire device fabrication process.

The electron beam pattern generator 5 (EBPG5) in DIMES of TUD has been employed to define patterns. After metallization, the mesa level pattern has been transferred through to the substrate by mean of Inductively Coupled Plasma (ICP) etching, which has been illustrated in chapter 2.

The current-voltage (I-V) characteristics of quantum wire devices have been measured at room temperature by a HP 4155 semiconductor parameter analyzer. The two current probes are on contacts 1 and 2, while the voltage has been measured through contacts 3 and 4, or contacts 5 and 6, or contacts 3 and 6, or contacts 4 and 5, as shown in figure 9.2.

9.4 Results and Discussion

9.4.1 Experimental result of sidewall depletion region after fluorine plasma

Wires have been etched in SF_6 : N_2 = 1 : 1 at 250 V dc bias and an etching pressure of 2.9 μBar, ICP source power 1500 W, temperature 25 °C and etching time 9 minutes. Figure 9.4a is a SEM micrograph of the quantum wire device. Figure 9.4b shows preliminary quantum wire conductance vs. wire width data. The cut-off width of around 130nm suggests approximately 65nm sidewall depletion for the given SF_6 + N_2 plasma process. This result is comparable to that of GaAs [79]. Yuda et al reported [208] sidewall damage thickness of 60-90nm on InAlAs by reactive ion etching with a mixture of CH_4 + H_2. This result is comparable to our preliminary result in GaN material. More detailed quantum wire experiments were not possible due to lack of material. See section 9.4.2.4.

Combining with the natural depletion by the surface states etc., the estimated etch induced depletion width is 52 nm. The thickness of the sidewall damage layer is etching time dependent due to accumulative characteristics for the specified etch condition. During the pattern transfer, over etching method has been used to make sure the mesa level transfer through to substrate.

The thick damage layer also could be formed from the scattered ions, which hit the sidewall and cause the damage, redeposition of etch products from the etched

surface, since GaF_X is non-volatile etch product, ion implantation and chemical modification (reaction layer). The ion bombardment, ion implantation and redeposition are cumulative, while chemical modification is self limited. Atomic scale sidewall roughness produced by rf etching is also possible. Although the exact cause and the nature of the damage is unclear at this stage, it is certainly a combination of the above effects that contribute to the presence of such a thickness of damage layer.

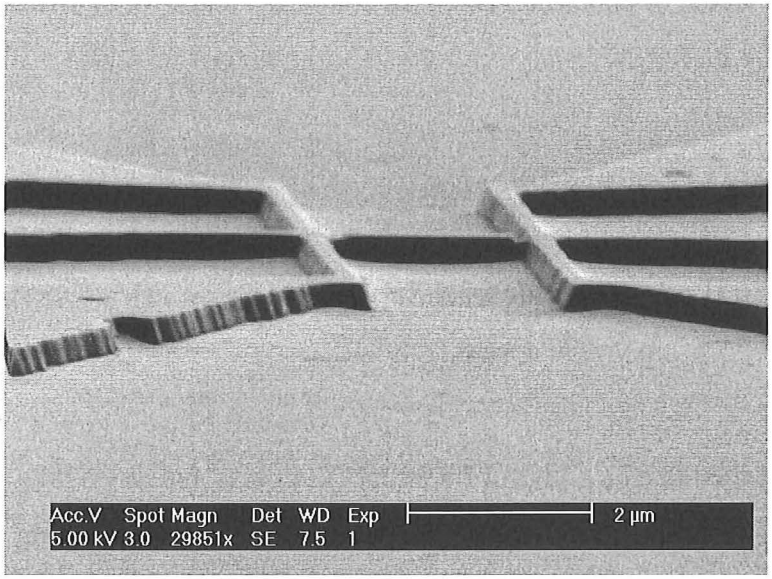

a

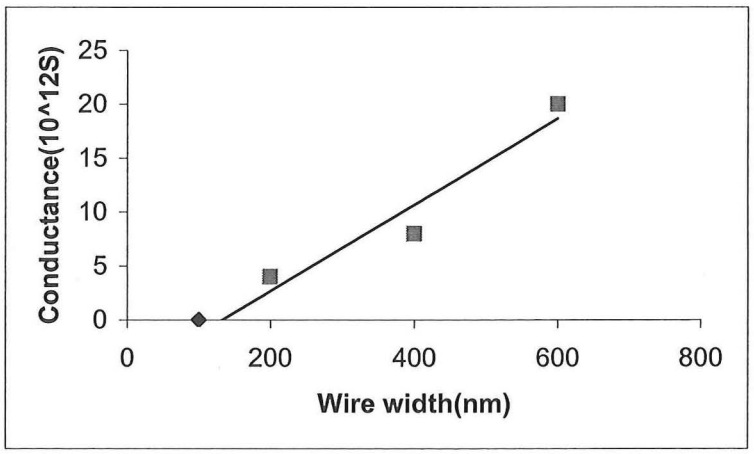

b

Figure 9. 4 a) The SEM image of a wire structure, b) Conductance vs. wire width of quantum wires fabricated in GaN with in SF_6: N_2 = 1 : 1 ICP process. The cut-off width of around 130nm suggests approximately 65 nm sidewall depletion for the given $SF_6 + N_2$ plasma process.

The preliminary result of quantum wire device characterization indicates a typical length scale of depletion region is around 65 nm in GaN we used for this study. This gives an indication of the depth of defects introduced is about 52 nm. However, defects may propagate deeper.

9.4.2 Problems and solutions

Quantum device work is the most interesting part of this thesis. I applied all my knowledge and skills learned previous into this part of the work. Some problems come out in device fabrication. Problems that could be solved have been solved and the others remain out of the control.

9.4.2.1 Material quality problems and suggestions

Figure 9.5a is a SEM image of the top surface of a device pad, which has a thin mask. The holes allocated on the devices degrade the device quality, such as easy break down. Some holes are exactly located on the quantum wire or connection line sees figure 9.5b, which made the device un-workable. There are two possible sources for the existence of these holes. The first possibility is that the holes are original from as grown material. Such holes in GaN thin films down to the substrate have been observed on as grown material. Figure 9.6a is a SEM image of as grown material. This is a material quality problem out of our control.

The other possible reason is due to the fabrication process. Due to a rough GaN surface, the metal pattern after lift off is non-uniform, see figure 9.6b. The mask would be thicker on spikes than that of in valleys due to shadow effect during evaporation. Thinner mask could be etched through during pattern transfer, then etching continues on GaN film, and thus creates holes.

There are two ways to solve these problems. The first way is to improve the material quality to avoid the holes and to smoothen the surface roughness. This is the best option, however, this is out of our control. Another way is to make the metal mask thicker to solve the second problem. A thicker mask can stop the etching

through to substrate material. This technique has been used, and improved the device fabrication process.

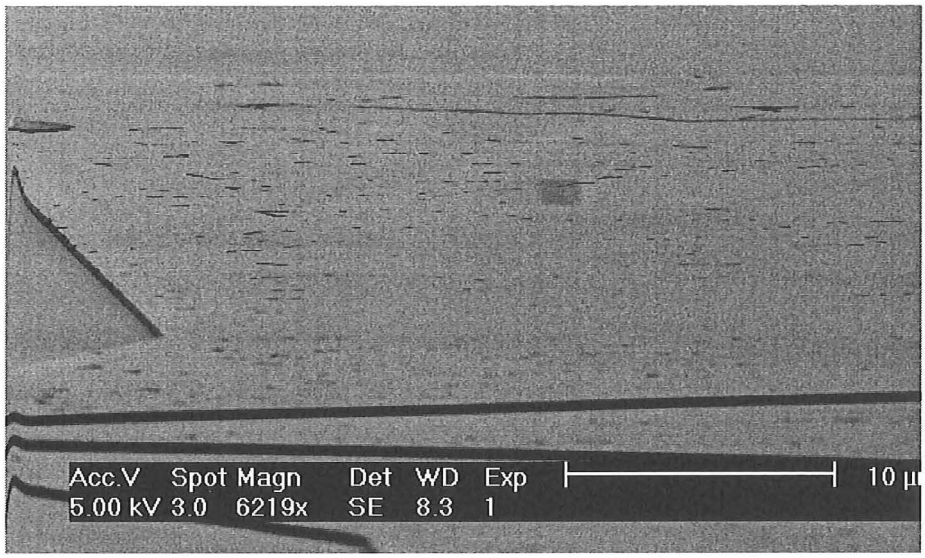

a

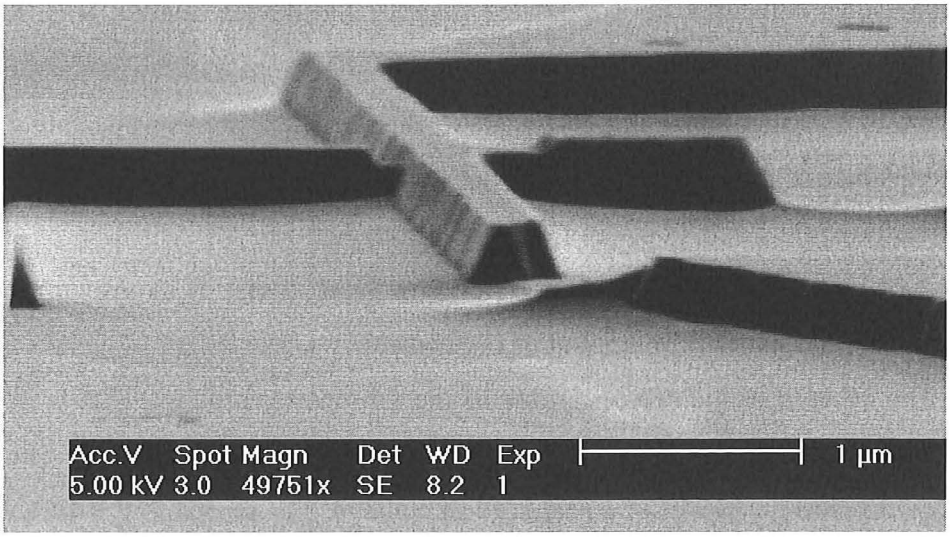

b

Figure 9. 5 a) and b) show the holes on surface of GaN device. There are two sources of these holes. One is original from as grown material. The other possible reason is due to the fabrication process.

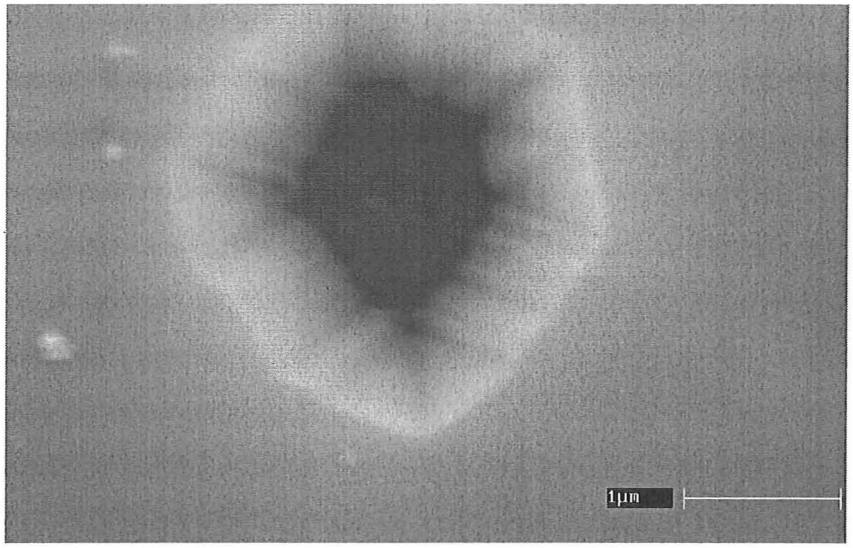

a

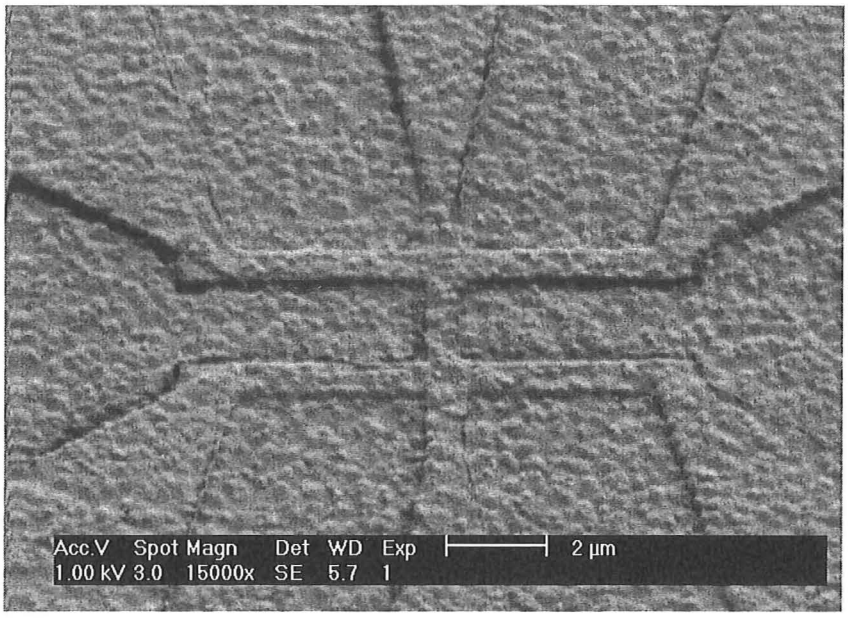

b

Figure 9. 6 a)Hole in as grown GaN material and b) rough metal pattern after lift off.

9.4.2.2 Isolated markers (insulate substrate) and the solution

Technically, from pure processing of device fabrication point of view, the markers should be defined first. Then the mesa level and pattern transfer down to the

substrate afterwards. Then define the contact pads on the top of the mesa. Fabrication process see figure 9.7

Define the markers by E-beam, followed by develop, evaporation and lift off

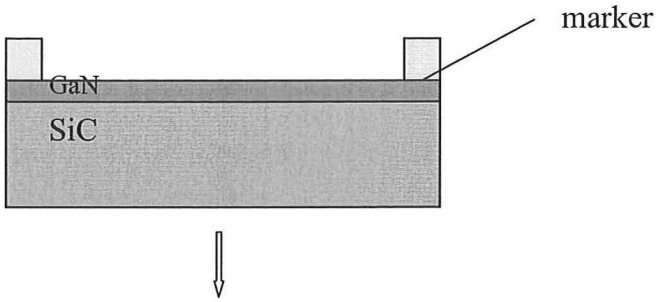

Mesa level pattern definition by e-beam, develop, evaporation, and lift off

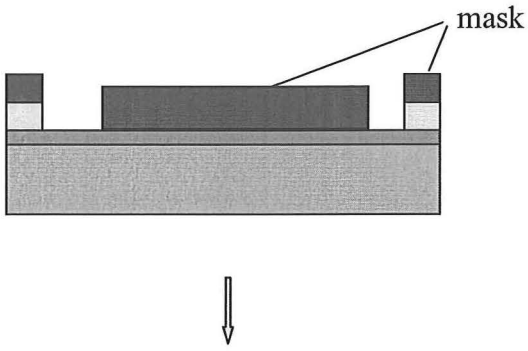

Subtractive pattern transfer and mask wet etching

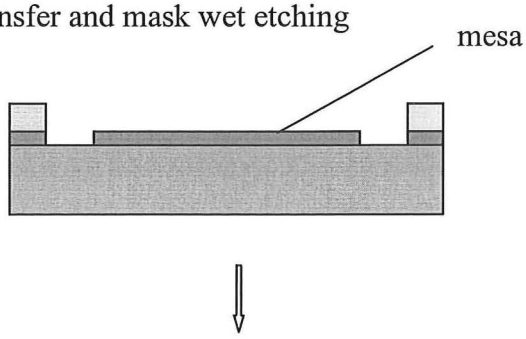

Contact pads fabrication by e-beam, develop, evaporation and lift off

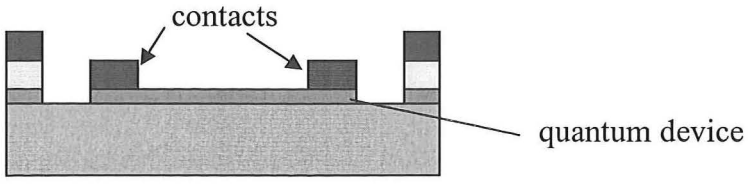

Figure 9. 7 Fabrication process used previously on semi-insulate substrate.

This procedure is reliable on semi-insulate substrate, but it is not workable on insulate substrate (sapphire). Because after marker definition and mesa level transferring, the markers are totally isolated from surrounding GaN and become insulated islands. In the next step, contact pads fabrication, the EBPG5 could not recognize the markers due to electron charging of markers. One option is to use conduction thin film on the top. Theoretically, it is working, but it is not reliable in practice. Thus, we improved the procedure to the previous one, shown in figure 9.3, to solve the isolated marker problem.

9.4.2.3 Etching problem and solution

The third problem is illustrated on figure 9.8. After etching, the wires have been cut from connection lines nearly half by etching trench. Some of them even have been totally isolated. This is a normal etching problem in ion-induced etching. To be able to solve the problem, it is important to recognize the problem and its possibilities of the formation.

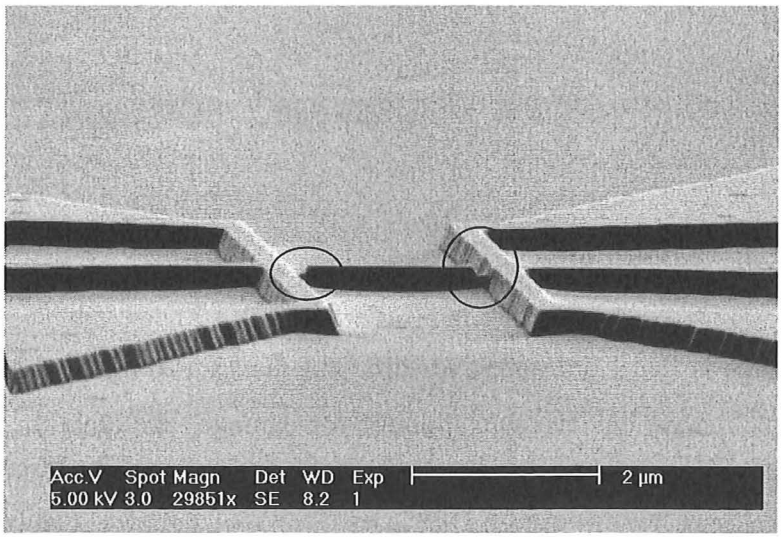

Figure 9. 8 Etching trenches are circled on each sides of quantum wire, which cut off the wire from the connection lines.

In a plasma, ions may come slightly non perpendicular, trench is formed when a sidewall collects these ions. Also when the slope of the sidewall is no longer vertical, some of ions will collide at a glancing angle with the slopping edges before they arrive at the etch surface. This gives a local increase in etch rate leading to trench [95]. The figure 9.9 is schematic drawing of the formation of the trench or ditching due to glancing incidence of ions. The tapered sidewall could be a result from redeposition (chapter 6) or faceting (chapter 3). Since trenching is a small effect, it often goes unnoticed unless thick layers are being etched as it is in this case.

This problem has been solved by thickening the etch mask. See figure 9.3. The quantum wire mask is overlapping the connection line mask. In this case, then mesa level could be perfectly transferred through the GaN thin film up to substrate.

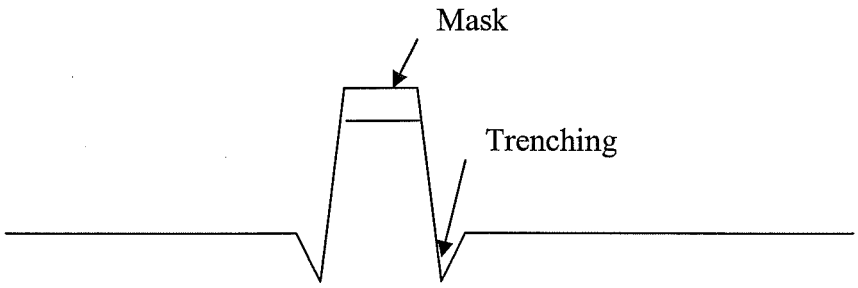

Figure 9. 9 A schematic drawing of the etch trench formation, due to a glancing incidence of ions.

9.4.2.4 Not-sufficient material

The last problem is that I did not have sufficient material to make a full parameter scan for quantum wire devices as a monitor for damage. We have the preliminary result in specified fluorine plasma. Then to verify the ion energy, etching time and temperature dependence will be essential for the recipe to be used in the industry. Ion energy directly affects the ion implantation, as well as enhancement in chemical reaction, while temperature affects the chemical reaction.

Also we already knew that the chlorine plasma has faster etch rate with almost vertical profile, then it would be interesting to see the degree of sidewall damage and compare with F plasma. If all these experiments can be completed, a full picture of fluorine plasma and chlorine plasma etching GaN and its effects on electrical and optical properties will be displayed and will be ready for application in device fabrication.

9.5 Summary

Fabrication processes of quantum wire device on insulated substrates and semi-insulated substrates have been successfully developed and optimized.

During the process development, many problems have been encountered, such as material quality problem, special material demands, and etching problems. Some of the problems have been solved.

The theoretical surface depletion has been calculated as 13 nm.

Preliminary result shows that the overall cut-off width is around 130 nm. This suggests an additional sidewall depletion of approximately 52 nm (65 nm -13 nm) for the given $SF_6 + N_2$ plasma process in given GaN material.

The thicker damage layer is possible from dry etching roughening of the sidewall on atomic scale level, scattered ions hitting the sidewall, redeposition, reaction layer and ion implantation.

The preliminary result of quantum wire device characterization indicates a typical length scale of depletion region is around 65 nm in GaN we used for this study. This gives an indication of the depth of defects introduced is about 52 nm. However, defects may propagate deeper.

Chapter 10

Conclusions and Suggestions

10.1 Conclusion

10.1.1 Nanofabrication and etch mechanism

A procedure that allows the transfer of high-resolution nanometer-scale patterns into GaN by e-beam lithography and reactive ion etching (RIE) has been developed. The developed procedure has been successfully implemented in fabricating nanowire and dots in Si/Si_xN_y super lattice material.

The e-beam dose, for the EBL system at Canterbury University, has been optimised around 2000 $\mu C/cm^2$ to 2500 $\mu C/cm^2$ for 100 nm to 200 nm wires and dots definition for the given double layer PMMA.

The influence of the composition of etch gas mixture on etch rate, profile and microscopic surface roughness has been investigated. The addition of N_2 in $SF_6 + N_2$ gas mixture increases the etch rate, leads to more vertical sidewalls and decreases the microscopic surface roughness in the transfer of nanometre-scale GaN lines and dots in RIE etching. The fastest etch rate in our RIE etching obtained is 13.3 nm/min under the condition of power density 0.45 W/cm^2, etching pressure 15 mTorr, substrate temperature 50 °C, total gas flow rate 40 sccm and gas composition $SF_6 : N_2 = 3 : 1$.

ICP etching of GaN in a $SF_6 + N_2$ plasma is found to be dominated by an ion-induced mechanism. The most efficient etch regime is observed for ICP source power around 1000 W. The fastest etch rate in fluorine plasmas has been achieved is 67 nm/min, which is a factor of 5 increase, compared to RIE etching (13.3 nm/min). The etch condition are gas composition of $SF_6 : N_2 = 1 : 1$, etching pressure of 2.5

μbar, substrate temperature of 25 °C, ICP source power of 1500 W and dc bias of 300 V. The addition of N_2 increases the etch rate without influencing the etch profiles.

Comparison of RIE and ICP fluorine plasmas suggests the etching mechanisms are ion induced, while ICP shows a chemical enhancement.

In chlorine plasma, ion induced etch mechanism in etching GaN has been obtained. The fastest etch rate of 314 nm/min and a vertical profile has been achieved in chlorine based ICP etching of GaN with gas composition of 25% Cl_2 + 75% Ar, total gas flow rate of 100 sccm, etching pressure of 10 μbar, substrate temperature of 25 °C, ICP source power of 500 W and dc bias of 450 V.

Comparison of GaN etch performance in chlorine plasma with fluorine plasma suggests that both of them have ion-induced etching, while chlorine plasma has more chemical enhancement due to volatile reaction product $GaCl_3$, compared with that of fluorine plasma GaF_X.

10.1.2 Electrical aspect

Al + Au ohmic contacts on GaN were successfully fabricated without using an annealing step, due to Al tending to replace Ga and form a mixture layer.

The GaN surface has been found to be smoothened microscopically after an argon bombardment. The specific contact resistance of ohmic contacts fabricated on GaN after argon plasma bombardment for two and a half minutes at 0.03 W/cm^2 are measured and resulted in a decrease by a factor of 6 compared to the unetched surface.

Our results show that gold is the best metal for GaN Schottky contacts in the series of given wafers amongst NiCr, Ti and Pd.

Diodes characterization of pre-etched GaN in RIE shows that 60% N_2 + 40% SF_6 is suitable for low damage dry etch alternative for GaN transistor gate recessing due to N incorporation and smoothening etched surfaces. However, this process is subject to carrier mobility investigation.

High ion energy in SF_6 + N_2 ICP processing, improves the electrical diode properties. Almost ideal diode characteristics are obtained at a dc bias of 300 V. The

XPS and AFM results indicate the diode improvement is a combination of chemical healing, smoothening of a relatively rough surface, removal of surface contamination and incorporation of N in the GaN surface. In contrast, Cl_2 + Ar ICP processing deteriorates the electrical diode properties due to chemical pollution and/or high ion energy dissipation on etched surface.

Chemical aspect of etching induced damage determines the electrical deterioration of diode properties.

That annealing as grown material in nitrogen atmosphere at 1000 K for 1 hour, results in excellent diode characteristics, suggests that material should be annealed before using it for device fabrication.

$SF_6 + N_2$ ICP plasma could be an alternative for electronic device fabrication with reasonable etch rate, smooth surface and good vertical nature of profile. However, it should subject to an investigation of carrier mobility.

10.1.3 Optical aspect

We have used photoluminescence and photoconductivity to study epilayers of GaN on SiC substrates that have been etched with RIE plasma of Ar, N_2, SF_6 and mixed SF_6+N_2 gases. The photoluminescence spectra are dominated by the neutral-donor-bound D^0X emission, while the photoconductivity bands are determined to be intrinsic free-exciton features. The PC signal recorded from the SF_6 + N_2 etched samples, is similar to that recorded from the control sample, while the PC signal recorded from N_2 etched sample is very weak. No PC signal has been detected from the sample etched by SF_6.

ICP and RIE fluorine plasma etching reduces PL intensity dramatically. Among the etched samples, SF_6 + N_2 plasmas are found to cause the least optical damage compared to pure SF_6 and N_2 plasmas. Chlorine plasma etching does not reduce the near band gap PL intensity as fluorine plasma does. The concept of dangling bonds can explain the near band gap PL intensity changes after different plasma etching.

Ion bombardment does not play an important role in creating optical damage in GaN.

There are no saturation effect observed with various incident laser powers on both control and etched samples.

The blue band emission has been investigated. These peaks (3.28 eV, 3.17 eV, and 3.08 eV) are more likely separate defects related. No yellow luminescence has been observed on GaN grown on SiC used for this study. This may suggest yellow luminescence relates to substrate.

A new near-band-gap peak AX, which shows up after Cl etching, is possibly caused by created Ga vacancies. The shifting of all the peaks to higher energy after chlorine plasma etching is possibly due to strain relaxation. Strain can be relaxed by etching away some strain source, such as dislocations.

Annealing of GaN in N_2 atmosphere reduces the emission intensity of the acceptor and donor-bound defect states while etching inhibits the near band-gap luminescence in general.

75% Cl_2 +25% Ar could be used for optical device fabrication, such as laser diode and light emitting diode, with faster etch rate and good vertical nature profile.

10.1.4 Nitrogen role

Nitrogen incorporation on the GaN surfaces exposed to N-containing plasmas has been evidenced by XPS analysis. ICP processing of nitrogen containing plasma causes more N implanted on GaN surface than that of RIE. Chemical healing in SF_6 + N_2 plasma is due to N incorporation and changing the surface to a better stoichiometry and optically clean surface. Chlorine implantation and surface coverage may cause chemical pollution.

Nitrogen adding to SF_6 improves the etch rate, atomic scale surface roughness, and electrical and optical properties. This could be caused by a number of mechanisms. With addition of nitrogen, the presence of N_2 and its associated species may 1) remove the GaF_X efficiently by physical bombardment, 2) react with GaF_X to form volatile NF_X, 3) react with nitrogen atom from GaN to form N_2 molecule, and 4) incorporate N into the nitrogen deficiency surface.

10.1.5 Sidewall damage aspect

Successfully designed quantum wire device and developed processes to fabricate the q-wire device on insulated substrate and on semi-insulated substrate. The preliminary result of quantum wire device characterization shows that the depletion region is about 65 nm with ICP etching condition of 250 V, SF_6 : N_2 = 1 : 1 at 3 μbar, 25 degree for 9 minutes for specified material.

Theoretical calculation of depletion depth is 13 nm without etching damage based on the given assumption. The thicker damage layer may be caused by etch roughening of the sidewall at atomic scale, scattered ions hitting the sidewall, reposition of etch product, ion implantation and chemical surface modification.

The preliminary result of quantum wire device characterization indicates a typical length scale of depletion region is around 65 nm in GaN we used for this study. This gives an indication of the depth of defects introduced is about 52 nm. However, defects may propagate deeper.

10.1.6 Defects nature and characterization techniques

Defects shrink depletion region and cause tunnelling occur to decrease the contact resist and barrier height in electrical properties, while, increase dangling bonds to decrease PL intensity and partially change the strain to broaden the PL peaks in optical properties. A schematic drawing is shown in figure 10.1. Surface roughness has been smoothened after etching.

Defects may respond only to techniques that are able to probe them, and therefore, defects probed by PL and diodes may posses a different nature.

Diode characterization reflects the whole thickness of GaN film in our study; PL detects the information on top 100 nm, while XPS probes top sub-nm.

Evaluating all etch behaviour results, diode and PL characterization, and surface analysis, we make a summary: a mixture of SF_6 + N_2 should be an alternative for fabrication of GaN electronic devices, subject to mobility investigation; a mixture of Ar + Cl_2 is suitable for fabrication of GaN optical devices.

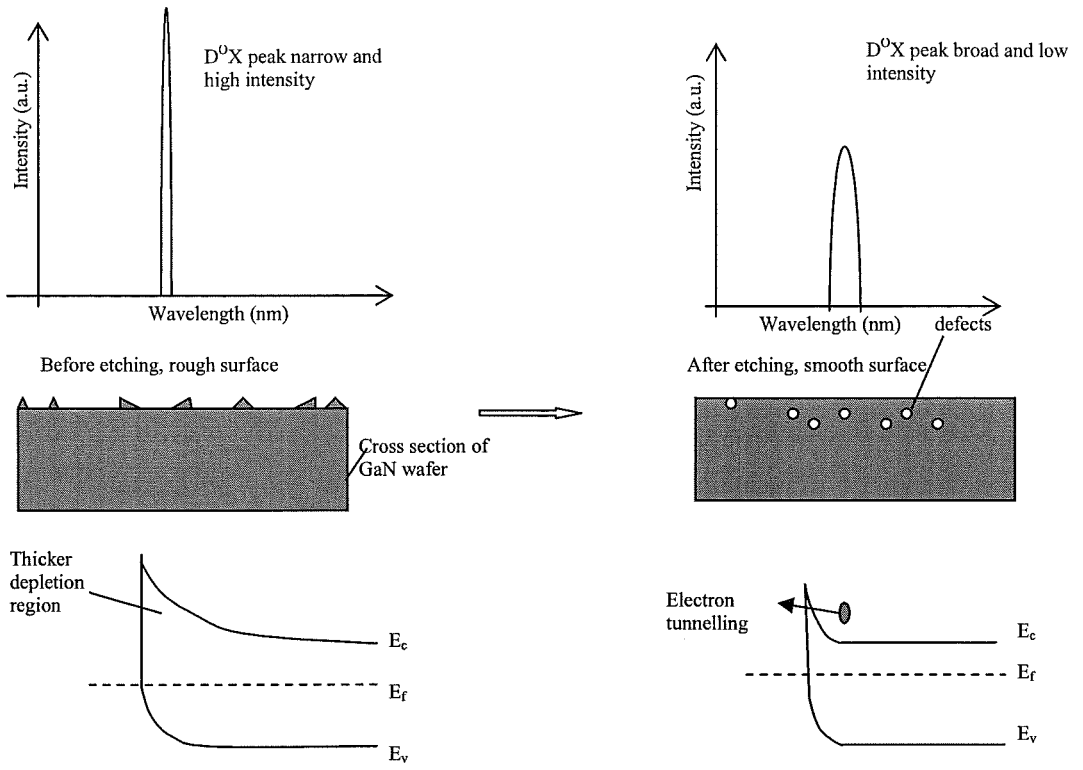

Figure 10 1 A schematic drawing of defects affecting electrical and optical properties. Defects cause PL peaks broaden and reduce PL intensity in optical properties and shrink depletion region and cause tunneling occur and decrease contact resistance and diode barrier height. The surface has been smoothened after etching.

10.2 Further investigation

Based on the present results, the $SF_6 + N_2$ gas composition does not degrade diodes electrical properties, while it increases etch rate and shows good anisotropic profile. Further investigation in effect on carrier mobility will be essential before it can be used for industrial application.

The sidewall damage study has not been completed due to not sufficient material. The suggestions for further investigation in this aspect have been described in 9.4.2.4.

From the damage mechanism aspect consideration, the depth of etch damage is very important for understanding the mechanism of etch-induced damage. The depth of etch-induced defects initially by dry etching could be very shallow [209],

directly from chemical reaction and ion implantation. The depth of ion implantation would be expected to be limited to the top nm, because the maximum of ion energy in plasma etching is around couples of hundreds eV. However, the defects could be propagated deeper by plasma radiation enhanced diffusion and channelling [195-196]. It would be useful to investigate the damage depth and contribution of the different proposed effects for understanding the mechanism and the device performance.

A damage layer induced by dry etch can be removed by wet etching. The depth of etch-induced damage could be estimated by comparing of restoring the electrical and optical properties of etched samples before and after removal of etch damage.

Dry etch effects on optical properties is one part of the thesis. The Hovel's equation has been simplified. Dangling bond concept has been used to explain the PL intensity before and after etching. In the fact, the damage layer could have more complicated effects, such as absorption of the damage layer, mid-gap states recombination, etc. The importance of these effects should be investigated further if possible.

The density of dangling bonds can be verified by electron spin resonance. It would be direct evidence of the accuracy of using bonding band concept.

The etching effects on D^oX intensity were the main content in optical aspect of the thesis. However, etching also affects the peak shape and position, and yellow and blue bands. It would be necessary to investigate these areas systematically for better understanding of etch induced damage effect on optical properties.

In the aspect of the etch effects on electrical properties, the barrier height and ideality factor extracted from I - V characteristics have been used as a monitor. Basically, two methods are used for measure the barrier height, current-voltage (I-V) and capacitor-voltage (C-V). In comparing the etch effects on different plasmas to their control samples, I - V method gives a good indication in relative changes of barrier height and ideality factor, compared to their control samples. However, the barrier height calculated by I-V characteristics is normally lower than the actual barrier height. The barrier height extracted from C-V measurement may give better accuracy of barrier height. In addition, not many C-V measurements have been

reported on GaN after etching until today. Thus, it will be of interesting to do further investigation on C-V characteristics of GaN.

Procedure for Pattern Generating in EBPG5

Step 1 pattern design: ASCII input formats: LDM or TEXTLIB. Then converting pattern data to machine formats: CATS package or CAPROX package.

Step 2 mounting e-beam resist coated samples on a stage. Different size samples (wafers) require different stages. J14 holder, which is designed for the small sample, has been employed in our project.

Step 3 orientating holder and height measurement under alignment microscope. Record the orientation of the sample center for beam writing. To align a pattern with respect to a previous layer, markers are required to measure the translation, rotation and keystone deformation of the wafer. The maximum correction of rotation is 0.2 °. The laser height sensor is calibrated against focus (height table). A reference height plate is used with markers at various heights. At zero reference the height measurement is tilt insensitive. This can be achieved by imaging the surface exactly onto the double diode. The maximum height correction, which can be applied, is +/- 100 μm.

Step 4 loading the holder with samples to chamber and start writing. Detail of computer process to operate the beam writing sees reference [111].

Recipe for Quantum Wire Device Fabrication

1) Clean samples in Aceton, Methanol and IPA, and baked in oven of 95 °C for an half hour.

2) Spin the double layers of PMMA, 2.5% high molecule weight (950 K dissolved in xylene) and 7% low molecule weight (180 K dissolved in chlorobenzene) are spun on the substrate. The spinning speed is 3000 rpm.

3) Bake the samples at 195 °C for 30 minutes.

4) Define the contact pads, its extends, and markers by EBL.

5) Remove exposed resist by a standard develop process.

6) Inspect the sample using optical microscopy to check whether the writing and development is good enough.

7) Apply oxygen plasma to remove the residues. The plasma condition is flow rate of 20 sccm, etching pressure of 10 ubar, dc bias of 180 V, rf power of 30 W (power density 0.11 W/ cm^2) and etching time of 20 seconds.

8) Evaporate 40nm Al and 60nm Au.

9) Standard lift off process has been applied to make the Al/Au ohmic contacts and markers. It is important that marker patterns are perfect and without metal

contamination close by. Otherwise, the EBPG5 will not be able to recognize the markers or mix the unwanted metal with markers.

10) Spin another double layer of PMMA. The same as step 2.

11) Define the mesa level pattern by EBL. It is worth noting that marker alignment procedure has been used here. This is a critical step for the successful fabrication.

11) Standard develop

12) Evaporate mask metal (120 nm Cr or NiCr)

13) Standard lift off processes

14) Transfer the pattern. It is crucial that the patterns are completely transferred up to the sapphire substrate. Otherwise, the residual GaN material will act as a current conducting channel. To make sure the mesa level etching is complete, one could check the devices cross talking by measuring the two pads on two neighbourhood devices and see whether they are conducting.

15) Wet etch the residual mask by standard solution, chromium etch.

Formula for ion yield

GaN molecular number (in 1 cm^2)

=Etch rate x Weight density x Avogradro's number/ molecular weight

$=R_{GaN} \times 6.1 \times 6.022 \times 10^{23} / 83.73$

$=4.39\ R_{GaN} \times 10^{22}\ (s^{-1}cm^{-1})$

Ion number (in 1 cm^2)

=ion density /q

$=I/1.6022 \times 10^{-19}$

$=6.24\ I \times 10^{15}\ (s^{-1}cm^{-1})$

Ion yield

= GaN molecular number in a unit area/ ion number in a unit area

$=7.03 \times 10^{6} \frac{R_{GaN}}{I}$

References

[1] S. Nakamura and G. Fasol, "The blue laser diode-GaN based light emitters and lasers" Springer, New York, (1997), pp1-33

[2] S. J. Pearton 'GaN and related materials-optoelectronic properties of semiconductors and superlattices', Gordon and Breach Science, New York, (1997), pp1-10

[3] B.Gil, "Group III nitride semiconductor compounds physics and applications" Claredon Press, Oxford, (1997), pp1-18

[4] S. Nakamura, Semicond. Sci. Technol. Vol. 14, (1999), R27-R40

[5] Web page, http://www.compoundsemiconductor.net.

[6] S. J. Pearton, R. J. Shul and F. Ren, MRS Internet J. Nitride Semicond. Res. Vol. 5, No.11, (2000)

[7] A. R. Stonas, N. C. MacDonald, K. Turner, S. P. DenBaars and E. L. Hu, the 45th International Conference on Electron, Ion and Photon Beam Technology and Nanofabrication (EIPBN) Washington DC, USA, 29th of May to 2nd of June, (2001)

[8] J. H. Edgar, Properties of group III nitrides, Emis Datareviews Series no.11, Inspec, London, (1994)

[9] J. C. Nipko, C.-K. Loong, C. M. Balkas and R. F. Davis, Appl. Phys. Lett. Vol. 73, No. 1, (1998), pp 34-36

[10] J. W. Orton and C. T. Foxon "Group III nitride semiconductors for short wavelength light-emitting devices" Rep. Prog. Phys. 61, (1998), pp 1-75

[11] H. P. Maruska, J. J. Tietjen, Appl. Phys. Lett. Vol. 15, No. 10, (1969), pp 327-329

[12] M. Mizuta, S. Fujieda, Y. Matsumoto, T. Kawamura, Japan. J. Appl. Phys. Vol. 25, No. 12, (1986), pp L945-L948

[13] A. Munoz, K. Kunc, Phys. Rev. B Vol.44, No. 18, (1991), pp 10372-10373

[14] P. Perlin, C. J. Carillon, J. P. Itie, A. S. Miguel, I.Grzegory, A. Polian, Phys. Rev. B. Vol.45, No. 1, (1992), pp 83-89

[15] Z. Lilental-Weber, M. Benamara, W. Swider, J.Washburn, J. Park, P. A. Grudowski, C. J. Eiting, and R. D. Dupuis MRS Internet J. Nitride Semicond. Res. Vol. 4s1, No. G4.6, (1999)

[16] P. Petroff and R. L. Hartman, J. Appl. Phys.Vol. 45, No. 9, (1974), pp 3899-3903

[17] S. Guha, J. M. DePuydt, M. A.Haase, J. Qiu and H. Cheng, Appl. Phys. Lett. Vol. 63, No. 23, (1993), pp 3107-3109

[18] K. Maeda, M. Sato, A. Kubo and S. Takeuchi, Appl. Phys. Vol. 54, No. 1, (1983), pp161-168

[19] S. D. Lester, F. A. Ponce, M. G. Craford and D. A. Stigerwald, Appl. Phys. Lett. 66, No. 10, (1995), pp 1249-1251

[20] G. D. Chen, M. Smith, J. Y. Lin, H. X. Jiang, S.- H. Wei, M. A. Khan and C. J. Sun, Appl. Phys. Letts. Vol. 68, No. 20, (1996), pp 2784-2786

[21] R. Dingle, D. D. Sell, S. E. Stokowski, M. Ilegems, Phys. Rev. B, Vol. 4, No. 4, (1971), pp 1211-1218

[22] B. Monemar, Phys. Rev. B, Vol. 10, No. 2, (1974), pp 676-681

[23] B. Gil, O. Briot, R. L. Aulombard, Phys. Rev. B, Vol. 52, (1995), R17028-R17031

[24] K. Kim, W. R. L. Lambrecht and B. Segall Phys. Rev. B, Vol. 50, No.3, (1994), pp 1502-1505

[25] G. Martin, S. Stite, A. Botchkarev, A. Agarwal, A. Rockett, H. Morkoc, WRL. Lambrecht and B. Segall, Appl. Phys. Lett. Vol. 65, No.5, (1994), pp 610-612

[26] K. Kim, R. L. Lambrecht and B. Segall, Phys. Rev. B, Vol. 53, No. 24, (1996), pp 16310-16326

[27] O. Lagerstedt and B. Monemar, Phys. Rev. B Vol. 19, No.6, (1979), pp 3064-3070

[28] O. Lagerstedt and B. Monemar, J. Appl. Phys. Vol. 45, No. 5 (1974), pp 2266-2272

[29] B. Monemar, J. P. Bergman, I. A. Buyanova, W. Li, H. Amano, and I. Akasaki, MRS Internet J. Nitride Semicond. Res. Vol. 1, No. 2, (1996)

[30] H. Teisseyre, Gnowak, M. Leszynski, I. Grzegory, M. Bockowski, S. Krukowski, S. Porowski, M. Mayer, A. Pelzmann, M. Kamp, K. J. Ebeling and G. Karczewski, MRS Internet J. Nitride Semicond. Res. Vol. 1, No. 13, (1996)

[31] This thesis, chapter 4 and 5, pp 63-102

[32] B. Rong, R. Cheung, W. Gao and M. kamp, Microelectronic Engineering, Vol. 53(1-4), (2000), pp 419-422

[33] R. Cheung, R. J. Reeves, B. Rong, S A Brown, E J M Fakkeldij, E van der Drift and M. Kamp; J. Vac. Sci. Tech. B Vol. 17, (1999), pp 2759-2763

[34] C. Trager-Cowan, S. McArthur, P. G. Middleton, K. P. O'Donnell, D. Zubia, S. D. Hersee, MRS Internet J. Nitride Semicond. Res. Vol. 3, No.36, (1998)

[35] P. Ruterana, P. Vermaut, G. Nouet, A. Salvador, H. Morkoc, MRS Internet J. Nitride Semicond. Res. Vol. 2, No. 42, (1997)

[36] H. Marchant, N. Zhang, L. Zhao, Y. Golan, S. J. Rosner, G.Girolami, Paul T. Fini, J. P. Ibbetson, S. Keller, S. DenBaars, J. S. Speck and U. K. Mishra, MRS Internet J. Nitride Semicond. Res. Vol. 4, No.2, (1999)

[37] D. M. Follstaedt, J. Han, P. Provencia and J. G. Fleming , MRS Internet J. Nitride Semicond. Res. Vol. 4SI, No.G3.72, (1999)

[38] E. S. Hellman, Z. Liliental-Weber, and D. N.E. Buchanan, MRS Internet J. Nitride Semicond. Res. Vol. 2, No. 30, (1997)

[39] E. S. Hellman, D. N. E. Buchanan, D. Wiesmann and I. Brener, MRS Internet J. Nitride Semicond. Res. Vol. 1, No.16, (1999)

[40] M. Mynbaeva, A. Titkov, A. Kryzhanovski, I.Kotousova, A. S. Zubrilov, V. V. Ratnikov, V. Yu. Davydov, N. I. Kuznetsov, K. Mynbaev, D. V. Tsvetkov, S.

Stepanov, A. Cherenkov, V. A. Dmitriev, MRS Internet J. Nitride Semicond. Res. Vol. 4, No.14, (1999)

[41] S. Nakamura and G. Fasol "Blue laser diode–GaN based emitter lasers" Berlin Springer, (1997), pp 35-77

[42] K. Pakula, J. M. Baranowski, M.Leszcynski, B. Suchanek and M. Wojdak, MRS Internet J. Nitride Semicond. Res. Vol 3, No. 23, (1998)

[43] M. E. Ryan , A. C. Camacho and J. K. Bhardwaj, Phys. Stat. Sol. A, Vol. 176, (1999), pp 743-746

[44] W. V. Schoenfeld, C.-H. Chen, P.M. Petroff, and E. L. Hu, Appl. Phys. Lett. 73, (1998), pp 2935-2937

[45] J. L. Benton, J. Cryst. Growth. Vol. 106, No. 1, (1990), pp 116-126

[46] M. W. Cole, K. K.K Ko and S. W. Pang, J. Appl. Phys. Vol. 78, No. 4, (1995), pp 2712-2715

[47] B. Rong, R. Cheung, W. Gao, M. M. Alkaisi and R. J. Reeves, J. Vac. Sci. Technol. B, Vol. 18, (2000), pp 3467-3470

[48] B. Rong, R. J. Reeves, S. A. Brown, M. M. Alkaisi, E. van der Drift and R. Cheung Microelectron. Eng., Vol. 57/58, (2001), pp 585-591

[49] O. M. Steffson, D. Birkedal, J. Hanberg, O. Albrektson and S. W. Pang, J. Appl. Phys. Vol. 78, No. 3, (1995), pp 1528-1532

[50] S. A. Brown, R. J. Reeves, C. S. Haase, R. Cheung, C. Kirchner and M. Kamp, Appl. Phys. Lett. Vol. 75, (1999), pp 3285-3287

[51] S. A. Brown, R. J. Reeves, B. Rong, R. Cheung, M. Seyboth, C. Kirchner and M. Kamp, Nanotechn. Vol. 11, (2000), pp 263-269

[52] E. L. Hu, proceeding of the SPIE, The international society for optical-engineering, Vol.1361 (1991), pp 512-522

[53] D. Basak, M. Verdu, M. T. Monjo, M. A. Sanchez-Garcia, F. J. Sanchez, E. Munoz and E. Calleja, Semicond. Soci. Techn.Vol. 12, (1997), pp1654-1657

[54] C. R. Eddy Jr, "Etch process of III-V nitrides"J. Nitride Semicond. Res., Vol. 4S1, No. G10.5. (1999)

[55] R. J. Shul, G. B. McClellan, S. J. Pearton, C. R. Abernathy, C. Constantine and C. Barratt, Elec. Lett. Vol. 32, No.15, (1996), pp 1408-1409

[56] S. J. Pearton, C. R. Abernathy, F. Ren, J. R. Lothian, P. W. Wisk and A. Katz, J. Vac. Sci. Technol. A, Vol. 11, No. 4, (1993), pp 1772-1776

[57] W. W. Stoffels, E. Stoffels and K. Tachibana, J, Vac. Sci. Technol. A. Vol. 16, No. 1, (1998), pp 87-95

[58] I. Adesidae, C. Youtsey, A. T. Ping, F. Khan, L. T. Romano and G. Bulman, MRS. Internet J. Nitride Seomcond. Res. Vol. 4S1, No. G1.4, (1999)

[59] J. Fricke, B. Yang, O. Brandt and K. Ploog, Appl. Phys. Lett. Vol. 74, No. 23, (1999), pp 3471-7473

[60] R. Cheung, A. Birnie, J. N. Chapman, S. Thoms and C.D.W. Wilkinson, Micro-electronic Engineering Vol. 11, (1990), pp 591-594

[61] K. T. Sung, S. W. Pang, M. W. Cole and N.Pearce, J.Electrochem. Soc.,Vol. 142, No.1, (1995), pp 206-211

[62] O. J. Glembocki, J. A. Tuchman, K. K. Ko, S. W. Pang, A. Giordana, R. Kaplan and C. E. Stutz, Appl. Phys. Lett. Vol. 66, No. 22, (1995), pp 3054-3056

[63] J.- M. Lee, K. Chang, S. Kim, C. Huh, I. Lee and S. Park, J. Appl. Phys. Vol.87, No.11 (2000), pp 7667-7670

[64] C. D. W. Wilkinson, Superlattices and Microstructure Vol.7, No.4 (1990), pp 381-385

[65] A. T. Ping, I. Adesida and M. Asif Khan, Appl. Phys. Lett. Vol. 67, No. 9, (1995), pp 1250-1252

[66] S. A. Smith, C. A. Wolden, M. D. Bremser, A. D. Hanser, and R. F. Davis. Appl. Phys. Lett., Vol. 71, No. 25, (1997), pp 3631-3633

[67] G. F. Mclane, L. Casas, S. J. Pearton and C. R. Abernathy Appl. Phys. Letts. Vol.66, No. 24, (1996), pp 3328-3330

[68] S. J. Pearton, J. W. Lee, J. D. Mackenzie, C. R. Abernathy and R. J. Shul, Appl. Phys. Lett. Vol.67, No. 16, (1995), pp 2329-2331

[69] H. Cho, Y. B. Hahn, D. C. Hays, K. B. Jung, S. M. Donovan, C. R. Abernathy, S. J. Pearton and R. J. Shul, MRS Internet J. Nitride Semicond. Res., Vol. 4S1, No. G6.56, (1999)

[70] Y. H. Lee, Y. J. Sung, Y. Yeom, J. W. Lee and T. I. Kim, J. Vac. Sci. Technol. A Vol. 18, No. 4, (2000), pp1390-1394

[71] F. A. Khan, L. Zhou, V. Kumar and I. Adesida, the 45th international conference on electron, ion and photo beam technology and nanofabrication, Washington DC May 29 to June 1, (2001)

[72] X. Tang, Q. Wang, D. and M. Manos, J. Vac. Sci. Technol. B Vol. 18, No. 3 (2000), pp 1262-1267

[73] C. T. Gabriel and Y. Melaku, J. Vac. Sci. Technol. B Vol. 12 No. 454, (1994), pp 454-460

[74] H. Kim, W. Nam, G. Yeom, H. Lee, J. Kim and K. Whang, J. Vac. Sci. Technol. A. Vol. 14, No. 1062, (1996), pp1062-1066

[75] X. A. Cao, H. Cho, S. J. Pearton, G. T. Dang, A. P. Zhang, F. Ren, R. J. Shul, L. Zhang, R. Hickman and M. van Hove, Appl. Phys. Lett. Vol. 75, No. 2, (1999), pp 232-234

[76] R. G. van Veen, M. J. Teepen, E. van der Drift. T. Zijlstra, E. J. M. Fakkeldij, K. Wener, A. H. Verbruggen and S. Radelaar, Microelectron. Eng. Vol. 35, (1997), pp55-58

[77] R. Cheung. R. J. Reeves, S. A. Brown, E. van. der. Drift and M. Kamp, J. Appl. Phys. Vol. 88. No.12. (2000), pp 7110-7114

[78] S. Thoms (III), S. W. Pang, "Diagnostic technique for semiconductor materials processing" Symposium Mater. Res. Ptttsburgh, PA, USA, (1994), pp 421-426

[79] R. Cheung, Y. H. Lee, C. M. Knoedler, K. Y. Lee, T. P. Smith III, and D. P. Kern, Appl. Phys. Lett Vol. 54. No. 21, (1989), pp 2130-2132

[80] M. Yuda, S. Kondo, Y. Noguchi and K. Kishi, Jpn J. Appl. Phys. Vol. 37, pp 4624-4626, 1998

[81] S. M. Sze, " Physics of semiconductor devices" Second edition, John Wiley &Sons, Inc, (1981), pp 304-308

[82] D. Qiao and Z. F. Guan, Appl. Phys. Lett. Vol. 74, No. 18, (1999), pp2652-2654

[83] B. P. Luther, J. M. Delucca, S. E. Mohney and R. F. Karlicek, Jr, Appl. Phys. Lett. Vol. 71, No. 26, (1997), pp 3859-3861

[84] S. Ruvimov, Z. Liliental-Weber, J. Washburm, K. J. Duxstad, E. E. Haller, Z.-F. Fan, S. N. Mohammad, W. Kim, A. E. Botchkarev and H. morkoc, Appl. Phys. Lett. Vol. 69, No. 11, (1996), pp 1556-1558

[85] L. F. Lester, J. M. Brown, J. C. Ramer, L.Zhang, S. D. Hersee and J. C. Zolper, Appl. Phys. Lett. Vol. 69, No. 18, (1996), pp 2737-2739

[86] Z.-F. Fan, S. Noor Mohammad, Wook Kim, Ozgur Aktas, Andrei E. Botchkarev and Hadis Morkoc, Appl. Phys. Lett. Vol. 68, No. 12, (1996), pp 1672-1674

[87] B. P. Luther, S. E. Mohney, T. N. Jackson, M Asif Khan, Q. Chen and J. W. Yang, Appl. Phys. Lett. Vol. 70, No. 1, (1997), pp 57-59

[88] E. H. Rhoderick "Metal-semiconductor contacts" Oxford science publication, Monographs in electrical and electronic engineering (1980)

[89] F. D. Auret, S. A. Goodman, F. K. Koschnick, J.-M. Spaeth, B. Beaumont and P. Gibart, MRS Internet J. Nitride Semicond., Vol. 4S1, No. G6.13, (1999)

[90] D. K. Schroder "contact resistance, Schottky barrier and electromigration" of "Semiconductor metal and device characterization" Second edition, John-Wiley& Sons, Inc. (1998) pp134-199

[91] W. E. Spicer, I. Lindau, P. R. Skeath and C. Y Su, Appl. Surf. Sci. Vol. 9, No. 1-4, (1981), pp 83-91

[92] C. Y. Su, I. Lindan, P. W. Chye, S. J. Oh and W. E. Spicer, J. Electron Spectroscopy and related phenomena, Vo. 31, No. 3, (1983), pp 221-259

[93] A. P. Zhang, G. Dang, F. Ren, X. A. Cao, H. Cho, E. S. Lambers, S. J. Pearton, R. J. Shul, L. Zhang, A. G. Baca, R. Hickman and J. M. van Hovel, J. Electrochem. Soc. Vol. 147, No. 2, (2000), pp 719-722

[94] D. Mistele, J. Aderhold, H. Klausing, R. Rotter, O. Semchinova, J. Stemmer, D. Uffman, J. Graul, F. Eberhard, M. Mayer, M. Schauler, M. Kamp and C. Ahrens, Semicond. Sci. Technol. Vol. 14, No. 7, (1999), pp 637-641

[95] M. Madou "Pattern transfer with dry etching techniques" of "Fundamentals of microfabrication" CRC Press, Boca Raton, London, New York, Washington, D. C (1991), pp53-87

[96] F. C. Chen, "Introduction to plasma physics" Plenum press, New York (1977)

[97] D. J. Oostra, PhD thesis "Sputtering in a reactive environment" Technical University of Delft, Netherlands, (1987), pp14

[98] N. St. J. Braithwaite, Plasma Source Sci. Technol. Vol. 9, No. 4, (2000), pp 517-527

[99] A. J. van Roosmalen, J. A. G. Baggerman and S. J. H.Brader, chapter 4 "gas and surface process" of "Dry etching for VLSI" Plenum Press, New York and London (1991)

[100] W. J. Goedheer, Plasma Source Sci. Technol. Vol. 9. No. 4, (2000), pp 507-516

[101] T. D. Mantei, Technical notes, Department of Electrical and Computer Enigineering, University of Cincinnati, Cincinnati, Ohio, (1983)

[102] A. Manenschijn PhD thesis "Ion bombardment and ion-assisted etching in rf discharges" Technology University of Delft, (1991), pp1-4

[103] Alcatel, User's manual –Micromachine Etch Tool (MET Lab)(1995)

[104] O. Auciello and D. L.Flamm, "Preface" of Plasma diagnostics" Academic Press, Inc. (London) Ltd. Harcourt Brace Jovanovich, (1989)

[105] V. M. Donnelly "optical diagnostic techniques for low pressure plasma and plasma processing" of "Plasma diagnostics", edited by O. Auciello and D. L. Flamm, Academic Press, Inc. (London) Ltd. Harcourt Brace Jovanovich, (1989), pp1-46

[106] Scientific system Ltd., Smart probe instruction and maintance manual (1997)

[107] J. W. Coburn and M. Chen, J. Appl. Phys. Vol. 51, No. 6, (1980), pp 3134-3136

[108] G. R. Brewer ed. "Electron-beam Technology in Microelectronics Fabriaction" Academic Press, New York, (1980)

[109] R. D. Allen, W. E. Conley and R. R. Kunz, "Deep- UV resist technology" of hand-book "Microlithography, micromachining and microfabrication" Vol. 1, Microlithography, edited by P. Rai-Choudhury, the institution of electrical engineers, London, UK, (1997), pp 321-376

[110] F. Cerrina, "X-ray lithography" of hand-book "Micro-lithography, micro-machining and micro-fabrication" Vol. 1, edited by P. Rai-Choudhury, The institution of electrical engineers, London, UK, (1997), pp 251-320

[111] Web address: http://www.nanofacility/dimes/tudelft/nl

[112] Y. Tarui, "VLSI Technology, Fundamentals and Applications" Springer series in electrophysics 12, Springer-Verlag, Berlin, (1986).

[113] M. A. McCord and M. J. Rooks, "Electron Beam Lithography" of hand-book of "Microlithography, Micromachining, and Microfabrication" edited by P. Chai-Choudhury, Vol. 1:Microlithography, the institution of electrical engineers, London, UK, (1997), pp 139-250

[114] Tencor, instrument "Alpha-step 500 surface profiler user manual" (1994)

[115] N. W. Ashcroft and N. D. Mermin, "Solid state physics" Saunders College Pub. USA, (1976)

[116] Web page, http://www.park.com

[117] Park scientific instruments part 1: "learning to use auto-probe: contact AFM" (1993)

[118] J. F. Muth, J. D. Brown, M. A. L. Johnson, Z. Yu, R. M. Kolbas, J. W. Cook, Jr and J. F. Schetzina, MRS Internet J. Nitride Semicond. Res. 4S1, G5.2(1999)

[119] H. J. Hovel, Semicond. Sci. Technol. Vol. 7, (1992), A1-A9

[120] G. S. Oehrlein, J. F. Rembetski and E. H. Payne, J. Vac. Sci. Technol. B, Vol. 8, (1990), pp1199-1203

[121] E. van der Drift, T. Zijlstra, E. J. M. Fakkeldij, R. Cheung, K. Werner and S. Radelaar, Microelecrton. Eng. Vol. 27, (1995), pp 481-485

[122] H. Lee, D. B. Oberman, J. S. Harris Jr. Appl. Phys. Lett. Vol. 67, No. 12, (1995), pp1754-1756

[123] G. Sullivan, Nitride Semicond. Res., Vol. 4S1, No. G1.4. (1999)

[124] H. I. Smith, "Submicron and nanometer-structures technology" lecture notes for course 6.781 in Massachusetts institute of technology, 1999.

[125] Y. X. Li, P. J. French and R. F. Wolffenbuttel, J. Vac. Sci. Technol. B, Vol. 13, No. 5, (1995), pp 2008-2012

[126] R. A. Gottscho, R. H. Burton, D. L. Flamm, V. M. Donnelly and G. P. Davis, J. Appl. Phys. Vol. 55, (1984), pp 2707-2709

[127] Z. H. Lu, D. J. Lockwood and J. -M. Baribeau, Nature Vol. 378, (1995), pp 258

[128] B. T. Sullivan, D. J. Lockwood, H. J. Labbe and Z. H. Lu, Appl. Phys. Lett. Vol. 69, No. 21, (1996), pp 3149-3151

[129] K. Saotume, A. Matsutani, T. Shirasawa, M. Mori, T. Honda, T. Sakaguchi, F. Koyama and K. Iga, Mater. Res. Soc. Symp. Proc. Vol. 449, (1997), pp 1029-1033

[130] C. - H. Chen, S. Keller, E. D. Habere, L. Zhang, S. P. Denbaars, E. L. Hu, U. K. Mishra and Y. Wu, J. Vac. Sci. Technol. B, Vol. 17, No. 6, (1999), pp 2755-2758

[131] R. T. Tung, Appl. Phys. Lett. Vol. 58, No. 24, (1991), pp 2821-2823

[132] P. Skeath, I. Lindau, C. Y. Su and W. E. Spicer, Phys. Rev. B, Vol. 28, No. 12, (1983), pp 7051-7057

[133] S. Oktyabrsky, K. Dovidenko, A. K. Sharma, V. Joshkin and J. Narayan, MRS Internet J. Nitride Semicond. Res. Vol. 4S1, No. G6.43, (1999)

[134] A. S. Usikov, W. V. Lundin, U. I. Ushakov, B. V. Pushnyi, N.M. Schmidt, Yu. M. Zadiranov and T. V. Shubina, Proceedings of the second symposium on III-V nitride materials and processes. Electrochem. Soc.Pennington, NJ, USA, (1998), pp 57-62

[135] J. A. Hay, third professional year project "ohmic contact on SiC", Electronic and Electrical Engineering Department, Canterbury University, (1999), pp 4

[136] E. Hu. Private communication in Santa Barbara, L.A., U.S.A., on June 4, (2001)

[137] T. Saitoh and H. Kanbe, Jpn. J. Appl. Phys., Part 2, Vol. 35, No. 1, (1996), pp L60-L62

[138] B. Y. Yoo, S. J. Park and K. H. Park, J. Vac. Sci. Technol. A, Vol. 13, No. 3, (1995), pp 931-934

[139] B. Molnar, C. R. Eddy, Jr. and K. Doverspike, J. Appl. Phys. Vol. 78, No. 10, (1995), pp 6132-6134

[140] R. Cheung, private communication, Email on 3-August-2001

[141] R. Cheung, S. Withanage, R. J. Reeves, S. A. Brown, I. Ben-Yaacov, C. Kirchner and M. Kamp, Appl. Phys. Lett. Vol. 74, No. 21, (1999), pp 3185-3187

[142] G. Popovici, H. Morkoc and S. N. Mohammad, "Deposition and properties of group III nitrides by molecular beam epitaxy" of "Group III nitride semiconductor compounds" edited by B. Gil, Oxford Science, New York, (1998), pp 53

[143] J. Neugebauer and C. G. van der Walle, Phys. Rev. B. Vol. 50, No. 11, (1994), pp 8067-8070

[144] P. Perlin, T. Suski, H. Teisseyre, M. Leszczynski, I. Grzegory, J. Jun, S. Porowski, P. Boguslawski, J. Bernholc, J. C. Chervin, A. Oloian and T. D. Moustakas, Phys. Rev. Lett. Vol. 75, No. 2, (1995), pp 296-299

[145] Y. C. Chang, A. E. Oberhofer, J. F. Muth, R. M. Kolbas and R. F. Davis, Appl. Phys. Letts. Vol.79, No. 3, (2001), pp 281-283

[146] G. Yu, G. Wang, H. Ishikawa, H. Umeno, M. Soga, T. Egawa, J. Watanabe, and T. Jimbo, Appl. Phys. Lett. Vol. 71, No. 24, (1996), pp 3209-3211

[147] O. Dickie, Photoconductivity Experiments report, Physics and Astronomy Department, Canterbury University, New Zealand, (2000)

[148] D. K. Schroder "Semiconductor Material and Device Characterisation" John Wiley & Sons Inc., Second Edition, (1998), pp 623-627

[149] X. A. Cao, S. J. Pearton, A. P. Zhang, G. T. Dang, F. Ren, R.J. Shul, L. Zhang, R. Hickman and J. M. Van Hove, Appl. Phys. Lett. Vol. 75, No. 2, (1999), pp 2569-2571

[150] E. D. Haberer, C.-H. Chen, A. Abara, M. Hansen, L. Coldren, S. DenBarrs, U. Mishra, E. L. Hu, Appl. Phys. Lett. Vol. 76, No. 26, (2000), pp 3941-3943

[151] P. Boguslawski, E. L. Briggs and J. Bernholc, Phys. Rev. B Vol. 51, No. 23 (1995), pp17255-17258

[152] P. Boguslawski, K. Rapcewicz, J. J. Bernholc, Phys. Rev. B, Vol. 61, No. 16, (2000), pp10820-10826

[153] I. A. Buyanova, J. P. Bergman, B. Monemar and I. Amano, Appl. Phys. Lett. Vol. 69, No. 78, (1996), pp 3959-3961

[154] D. Nel'son, Yu. V. Mel'nik, A. V. Sel'kin, M. A. Yakobson and V. A. Dmitriev, Phys. Sol. State Vol. 38, (1996), pp 455-457

[155] M. DeVittorio, G. Coli, R. Rinaldi, G. Gigli, R. Cingolani, D. De Salvador, M. Berti, A. Drigo, F. Fucillo, T. Ligonzo, V. Augelli, A. Rizzi, R. Lantier, D. Freundt, H. Luth, B. Neubauer and D. Gerthsen: Solid-State Electron. Vol. 44, (2000), No. 3, pp 465-470

[156] M. Tchounkeu, O. Briot, B. Gil, J. P. Alexis and R-L. Aulombard: J. Appl. Phys. Vol. 80, No. 9, (1996), pp 5352-5360

[157] W. Shan, B. D. Little, A. J. Fischer, J. J. Song, B. Goldenberg, W. G. Perry, M. D. Bremser and R. F. Davis: Phys. Rev. B Vol. 54, No. 23, (1996), pp16369-16372

[158] R. J. Reeves, O. Dickie, B. Rong, R. Cheung and S. A. Brown, Proc. Int. Workshop on Nitride Semiconductors (IPAP) CS1, (2000), pp 774-777

[159] W. Shan, A. J. Fischer, J. J. Song, G. E. Bulman, H. S. Kong, M. T. Leonard, W. G. Perry, M. D. Bremser and R. F. Davis: Appl. Phys. Lett. Vol. 69, No. 6, (1996), pp 740-742

[160] R. J. Reeves, Data Collection, (2001)

[161] C. I. Harris, B. Monemar, H. Amano, I. Akasaki, Appl. Phys. Letts. Vol. 67, No. 6, (1996), pp 840-842

[162] S. Strite and H. Morkoc, J. Vac. Sci. Technol. B, Vol. 10, No. 4, (1992), pp 1237-1266

[163] K. Naniwae, S. Itoh, H. Amano, K. Itoh, K. Hiramatsu and I. Akasaki, J. Cryst. Growth Vol. 99, No. 1-4, (1990), pp 381-384

[164] N. V. Edwards, A. D. Batchelor, I. A. Buyanova, L. D. Madsen, M. D. Bremsetr, R. F. Davis, D. E. Aspnes and B. Monemar, MRS Internet J. Nitride Semicond. Res. Vol. 4S1, No. G3.78, (1999)

[165] F. J. Sanchez, D Basak, M. A. Sanchez-Garcia, E. Calleja, E. Munoz, I. Izpura, F. Calle, J. M. G. Tijero, B. Beaumont, P. Lorenzini, P. Gibart, T. S. Cheng, C. T. Foxon and J. W. Orton, MRS Internet J. nitride Semicond. Res. Vol. 1, No. 7, (1996)

[166] F. J. Sanchez, F. Calle, D. Basak, J. M. G. Tijero, M. A. Sanchez-Garcia, E. Monroy, E. Calleja, E. Munoz, B. Beaumont, P. Gibart, J. J. Serrano and J. M. Blanco, MRS Internet J. Nitride Semicond. Res. Vol.2, No. 28, (1997)

[167] B. K. Meyer, A. Hoffmann and P. Thurian, "Defects spectroscopy in the nitrides" of " Group III nitride semiconductor compounds physics and applications" edited by B. Gil, Oxford science, (1998), pp 205-306

[168] M. Leroux, B. Beaumont, N. Grandjean, C. Golivet, P. Gibart, J. Massies, J. Leymarie, A. Vasson and A. M. Vasson "Comparative optical characterization of GaN grown by metal-organic vapor phase epitaxy, gas source molecular beam epitaxy and hilde vapor epitaxy", Proc. EMRS-96, Strasboug, France (1996)

[169] M. Leroux, B. Beaumont, N. Grandjean, P. Gibart, J. Massies and J. P. Faurie, MRS Internet J. Nitride Semiconduct. Res. Vol. 1, No. 25, (1995)

[170] C. Trager-Cowan, S. McArthur, P. G. Middleton, K. P. O'Donnell, D. Zubia and S. D. Hersee, MRS Internet J. Nitride Semicond. Res. Vol. 3, No. 36, (1998)

[171] S. J. Pearton, C. R. Abernathy and F. Ren, Electron. Lett. Vol 30, No. 23, (1994), pp 1985-1986

[172] H. S. Venugopalan and S. E. Mohney, Appl. Phys. Lett., Vol. 73, No. 9, (1998), pp 1242-1244

[173] L. Wang, M. I. Nathan, T. -H. Lim, M. A. Khan and Q. Chen, Appl. Phys. Lett. Vol. 68, (1966), pp 1267-1269

[174] S. J. Pearton and R. J. Shul " Gallium nitride" of "Semiconductor and semimetals series, Vol. 50" Edited by I. J. Pankove, T. D. Moustakas, Acad. Press, New York, (1998)

[175] Y. Yau, R. F. W. Pease, A. Iranmanesh, and K. Polasko, *J. Vac. Sci. Technol.* Vol. 19, No. 4, (1981), pp 1048-1051

[176] This thesis, chpter 3, 4 and 5 pp 45-102

[177] A. P. Zhang, G. Dang, F. Ren, X. A. Cao, H. Cho, E. S. Lambers, S. J. Pearton, R. J. Shul, L. Zhang, A. G. Baca, R. Hickman and J. M. Van Hove, MRS Internet J. Nitride Semicond. Res. Vol. 5S1, No.W11.66 (2000)

[178] V. M. Donnelly, D. L. Flamm, W. C. Dautermont-Smith and D. J. Werder, J. Appl. Phys. Vol. 55, No.1, (1984), pp 242-252

[179] B. E. E. Kastenmeier, P. J. Matsuo, J. J. Beulens and G. S. Oehrlein, J. Vac. Sci. Technol. A, Vol. 14, No. 5, (1996), pp 2802-2813

[180] A. E. Wickenden, D. K. Gaskill, D. D. Koleske, K. Doverspike, D. S. Simons and P. H. Chi, Mater. Res. Soc, Pittsburgh, PA, USA, (1996) pp 679-683

[181] K. Usami, T. Saegusa and S. Yamanaka, Reports of university of electro-communication, Vol. 27, No. 1, (1976) pp 23-31

[182] F. Eberhard, M. Schayler, E. Deichsel, C. Kirchner and P. Unger, Microelectron. Eng. Vol. 46, No. 1-4, (1999), pp 323-326

[183] C. Seidel, B. Gotsmann, H. Kopf, K. Reihs and H. Fuchs, Surface and Interface analysis, Vol. 26, (1998), pp 306-315

[184] M. V. Malyshev, N. C. M. Fuller, K. H. A. Bogart and V. M. Donnelly, Appl. Phys. Lett. Vol. 74, No. 12, (1999), pp 1666-1666

[185] M. S. P. Andriesse, T. Zijlstra and E. van der Drift, J. Vac. Sci. Technol. B, Vol. 18, No. 6, (2000), pp 3462-3466

[186] L. A. D'Asaro, J. L. DiLorenzo and H. Fukui, IEEE Trans. Electron Devices, ED-25, (1981), pp 5218

[187] R. J. Shul, "Inductively coupled plasma etching of III-V nitrides" of "GaN and related material" II, edited by S. J. Pearton, Gordon and breach science, (2000), pp 621-622

[188] A. Manenschijn, "Ion bombardment and ion assisted etching in RF discharge" Ph.D thesis, Technical University of Delft, Netherlands, (1991)

[189] Landolt-Bornstein, Zahlenwerte und funktionen aus naturwissenschaften und technik, Neue serie, group 2, atomic physics, Berlin Gottingen, Heidelberg, Springer-Verlag, (1960)

[190] R. Cheung, B. Rong, W. Gao and M. kamp, Electron New Zealand, national conference proceeding in Auckland, New Zealand, (1999)

[191] This thesis, chapter 6 pp 103-122

[192] R. J. Shul, L. Zhang, A.G. Baca, C. G. Willison, J. Han, S. J. Pearton, K. P. Lee and F. Ren, Solid –State Electronics. Vol. 45, pp 13-17, 2001

[193] K. Naniwae, S. Itoh, H. Amano, K. Itoh, K. Hiramatsu and I. Akasaki, J. Cryst. Growth 99, (1999)

[194] M. Ohring, "The material science of thin films" Academic Press, USA, (1992), pp 10-13

[195] M. Rahman, J. Appl.Phys. Vol.82, No.5, (1997), pp2215-2224

[196] E. L. Hu and C.-H. Chen, Microelectron. Eng. Vol. 35, (1997), pp 23-28

[197] P. Emanuelsson, I. Maximov, H. Linke, P. Omling, L. Samuelson and B. K. Meyer, Mater. Sci, Forum. Vol. 143-147. pt. 3, (1994), pp 1541-1545

[198] T. Chevolleau, P. Y. Tessier, C. Cardinaud and G. Turban, J. Voc. Sci. Technol. A, Vol. 15, No. 5, (1997), pp 2661-2669

[199] D. P. Kern, K. Y. Lee S. A. Rishton and S. J. Wind, Jpn. J. Appl. Phys. Vol. 32, (1992), pp 4496-4500

[200] S. W. Pang, J. Electrochem. Soc. Vol. 133, No. 4 (1986), pp 784-788

[201] S. W. Pang, W. D. Goodhue and T. M. Lyszczarz, J. Vac. Sci. Technol. B. Vol. 6, No. 6, (1988), pp 1916-1920

[202]C. D. W. Wilkinson, Superlattice and Microstructure, Vol. 7, No 4, (1990), pp 381-385

[203] S. Q. Gu, X. Lin, M. Covington, E. Reuter, H. Chang, R. Panepucci, I. Adesida, S. G. Bishop, C.C. Aneau and Bishop, Appl. Phys. Vol. 75, No. 12, (1994), pp 8071-8074

[204] A. Forchel, A. Mensenig. B. E. Maile. H. Leter, and R. Germar Sci. Technol. B, Vol. 9, (1991), pp 444-448

[205] S. Thoms. P. Beaumont, C. D. W. Wilkinson, J. Frost and C. R. Stanley, Microelectron. Eng. (1986), pp 249-256

[206] A. R. Long, M. Rahman, I. K. MacDonald, M. Kinsler, S. P. Beaumont, C. D. W. Wilkinson and C. R. Stanley, Semicond. Sci. Technol. Vol. 8, (1993), pp 39-44

[207] J. H. Davies, Semicond. Sci. Technol. Vol. 3, No 10, (1988), pp 995-1009

[208] M. Yuda, S. Kondo, Y. Noguchi, K. Kishi, Jpn. J. Appl. Phys. Vol. 37, No. 8, (1998), pp 4624-4626

[209] S. O. Kucheyev, J. S. Williams and S. J. Pearton, Mater. Sci. Eng. Vol. R33, (2001), pp 51-107